The University of Adelaide

Department of Mechanical Engineering

A Study of the Transmission of Vibration in Structures Characteristic of Naval Ships

Yan TSO

Thesis submitted for the Degree of Doctor of Philosophy

May 1996

CONTENTS

ABSTRACT

Naval surface ships and submarines have to meet stringent noise and vibration requirements to minimise the risk of detection and the interference with on-board equipment. As part of an effort to control the acoustic signatures of naval vessels, the present study examined, both theoretically and experimentally, the transmission of vibration in a number of structures characteristic of naval ships. The main areas of work are divided into four parts as presented in Chapters 2 - 5 of this thesis. The first part consists of a detailed analytical study of the transmission of vibratory power through structural junctions including plate elements coupled to a thin rectangular beam, three-dimensional beam junctions and cylinder/plate junctions. Particular attention is paid to the effect of cross sectional deformation of stiffening elements in a junction due to vibration. The study also accounts for the effects of mode conversion at a junction, together with the coupling between different types of waves in an element. Calculations were performed on a number of example junctions to demonstrate such effects on vibratory power transmission.

In part 2 of this thesis, the transmission of vibration through a periodic structure in the form of a plate with periodic beam stiffeners is investigated. The Bloch theorem was used for the analysis to relate the wave solutions in adjacent bays of the periodic structure. It is found that the band pass nature of the periodic structure is a function of the wave heading angle and the frequency, in addition to the physical properties of the structure. The study then investigates the transmission of vibration through coupled periodic structures using an example junction which consists of a plate with periodic stiffeners, coupled to a uniform plate. The travelling wave method of analysis as described in Chapter 2 is used to evaluate the transmission efficiency of the junction.

Part 3 of this thesis deals with the analysis of the transmission of vibration through complex built-up structures by using the method of Statistical Energy Analysis (SEA). Methods for the evaluation of SEA parameters including modal density, internal loss factors and coupling loss factors are discussed. The coupling loss factors for a cylinder/plate structure and a coupled

periodic structure are derived and calculations on some numerical examples are performed to illustrate the method.

The final part of this thesis describes an experimental program to verify the coupling loss factor for the cylinder/plate structure and coupled periodic structure. Results from the measurements of input power and vibrational energy are used in a numerical procedure to determined the internal loss factors and coupling loss factors. The experimental results show good agreement with theoretical predictions and confirm the validity of the present formulation of coupling loss factors.

STATEMENT OF ORIGINALITY

This thesis contains no material which has been accepted for the award of any other degree or diploma in any university and, to the best of my knowledge and belief, contains no material previously published or written by another person, except where due reference has been made in the text.

I give consent to this copy of my thesis, when deposited in the University Library, being available for loan and photocopying.

Yan Kit TSO

17 May 1996

ACKNOWLEDGEMENTS

I would like to express my sincere thanks to my project supervisor, Dr C. H. Hansen, for his help, guidance and encouragement throughout the duration of this research. In particular, his constructive criticisms and comments on this thesis are very much appreciated. He has made this project an enjoyable and valuable learning experience for me.

I would also like to give a special thanks to Dr. J. C. Ritter, my co-supervisor at the Aeronautical and Maritime Research Laboratory, Defence Science and Technology Organisation (AMRL, DSTO), for creating this opportunity for me to pursue my post-graduate study. His guidance, unfailing support and encouragement will not be forgotten. It has been a pleasure and privilege for me to work under the guidance of my project supervisors, Dr. Hansen and Dr. Ritter.

To my friends at the DSTO and the Department of Mechanical Engineering, the University of Adelaide, their generous help and support are deeply appreciated. In particular, I would like to thank Mr. Peter Climas of the DSTO for his help in the preparation of drawings and graphs.

The DSTO has provided me with study leave and financial assistance to carry out the research, for which I gratefully acknowledge.

Last but not least, I would like to thank my wife Veronica and my daughters Jessica and Emily for their patience and understanding, especially during the difficult times when I was away from home to pursue my study in Adelaide.

LIST OF SYMBOLS

a	mean radius of cylindrical shell
A	area
A_a	acceleration measured by the accelerometer
A_h	acceleration measured by the impedance head
A_S, A_S'	wave amplitudes of the travelling and decaying waves in the source plate respectively
A_u	acceleration of the structure with correction for the effect of mass loading of the accelerometer
$A_1 \ldots A_6, A'_1 \ldots A'_4$	unknown constants representing the wave amplitudes of an elastic element in out-of-plane motion
b	distance between the centroid and shear centre of a beam element measured along the z_p axis
$B_1 \ldots B_6, B'_1 \ldots B'_4$	unknown constants representing the wave amplitudes of an elastic element in in-plane motion
B	coefficient matrix for the wave amplitudes of a beam element
c	wave speed
c_g	group velocity
C	coefficient matrix that relates the local and reference displacements of a beam

d	distance between the shear centre and attachment point of a beam element measured along the y_p axis
d,d'	vectors for the local and reference translational beam displacements respectively
D	flexural rigidity
D	coefficient matrix that accounts for the moments at the attachment point of a beam element due to junction forces
e	distance between the shear centre and attachment point of a beam element measured along the z_p axis
$<e_n>$	time-averaged energy density for the n^{th} circumferential mode
E	elastic modulus
$<E>$	time-averaged energy
E	coefficient matrix that accounts for the translational motions at the attachment point due to beam rotation
f	frequency
f_k	natural frequency of a circular plate with two nodal diameters and k nodal circles
F	junction force per unit length of plate or cylinder
F_b	beam junction force
F_h	force measured by the impedance head

g	distance between the centroid and shear centre of a beam element measured along the y_p axis
G	shear modulus
$\mathbf{G}_i$	coefficient matrix that relates the reference displacements between beam i and beam 1
h	thickness of plate or cylinder
$\mathrm{H}_n^{(2)}$	Hankel function of the second kind of order n
i	element number or bay number of a periodic system
I_c, I_s	second moment of inertia per unit length of beam about the centroid and shear centre respectively
I_x, I_y, I_z	second moment of area of beam about the x, y and z axes respectively
I_n	modified Bessel function of the first kind of order n
j	complex number $\sqrt{-1}$
J	torsional constant of beam
J_n	Bessel function of the first kind of order n
k	wave number
k_m	root of the dispersion equation
K	constant
K_p	number of elements in a periodic system

K_y, K_z	shear factors
K_n	modified Bessel function of the second kind of order n
l	length of element
l_c	coupling line length
$\mathbf{L}$	matrix differential operator of the Donnell-Mushtari equation
L	element of the matrix L
m_a	mass of accelerometer
m_s	mass of structure
M	junction bending moment per unit length of plate or cylinder
M_b	beam junction moment
n	circumferential mode number or number of standing waves
$n(\omega)$	modal density
$\mathbf{P}$	force vector
$\mathbf{Q}$	moment vector
r	radius
r_1, r_2	inner and outer radii of an annular plate respectively
$\mathbf{r}, \mathbf{r}'$	vectors for the local and reference rotational beam displacements respectively
t	time
T_{60}	reverberation time

u, v, w	displacements of an element in the x, y and z directions respectively; they also correspond to the longitudinal, circumferential and radial displacements of a cylindrical shell respectively
u_p, v_p, w_p	displacements of a circular plate in the radial, circumferential and out-of-plane directions respectively
U, V, W	displacement amplitudes in the x, y and z directions respectively; they also correspond to the displacement amplitudes in the longitudinal, circumferential and radial directions of a cylindrical shell respectively
x, y, z	system of co-ordinates
x_r, y_r, z_r	reference axes of a beam element
x_p, y_p, z_p	principal axes of a beam element
Y	mobility
Y_n	Bessel function of the second kind of order n
Z	impedance
α	wave heading angle
β	angle between the reference and principal axes
χ	real part of wave number
Δ	experimental errors in power and energy measurement
ϕ	angular displacement of an elastic element

γ	wave angle of reflected/transmitted waves
Γ	sum of squared errors
η	internal loss factor
η_i	internal loss factor of element *i*
η_{ij}	coupling loss factor between elements *i* and *j*
η_m	generalised notation for internal loss factors and coupling loss factors
φ	parameter defined by equations (A1.4), (A1.5) and (A3.13)
ϑ	amplitude of φ
λ	propagation constant
Λ	system matrix for a plate with periodic stiffeners
μ	Poisson's ratio
π	3.1415926.....
Π	power
$\Pi(\alpha)$	power due to an incident wave at an angle α
Π_{inc}	incident wave power
$<\Pi>$	time-averaged power
θ	polar co-ordinate
$\theta_x, \theta_y, \theta_z$	angular displacement of beam element about the *x*, *y* and *z* axes respectively

Θ_x, Θ_y, Θ_z	amplitudes of angular beam displacements about the x, y and z axes respectively
ρ	density
ρ_A	mass per unit area of element
$\tau(\alpha)$	transmission efficiency at a wave angle α
τ_{ij}	transmission efficiency between elements i and j
τ	mean transmission efficiency
ϖ	parameter defined by equations (A1.4), (A1.5) and (A3.14)
ς	amplitude of ϖ
ω	circular frequency
Ω	frequency parameter
ξ_i	angle between elements i and 1 measured on the x - y plane
ψ_i	angle between elements i and 1 measured on the x - z plane
ζ	imaginary part of wave number
∇^2	Laplacian operator which may be expressed as $\{\partial^2/\partial x^2 + \partial^2/\partial y^2\}$ in Cartesian co-ordinates or $\{\partial^2/\partial r^2 + (1/r)\ \partial/\partial r + (1/r^2)\ \partial^2/\partial\theta^2\}$ in polar co-ordinates

Subscripts

b	beam
B	bending wave

c	cylinder or centroid
i	element number or bay number of a periodic structure
j	element number
K	total number of elements in the structure of interest
L	longitudinal wave
m	eigensolution number
n	circumferential mode number, number of standing waves or order of Bessel functions
N	number of circumferential modes
p	plate
r	reference axis or receiving plate
s	source plate
S	transverse shear due to bending
T	shear or torsional wave
x, y, z	direction of forces, displacements or wave power

CHAPTER 1

INTRODUCTION

1.1 General Introduction

This thesis is concerned with the transmission and distribution of vibratory power in built-up structures, and in particular, structures characteristic of naval ships.

The study of noise and vibration in ships has received considerable attention in the past few decades as a result of stringent ship noise legislation introduced by many countries (see, for example, Conn, 1976). Such legislation aims to provide a safe and comfortable working environment for crew members by specifying a maximum allowable sound pressure level in various ship compartments. The ability for the designer to predict noise level in ship compartments at the design stage is therefore highly desirable and several empirical and analytical studies on ship noise prediction have been reported (for example, Janssen and Buiten, 1973; Nilsson, 1977; Ødegaard Jensen, 1976; Plunt, 1980a, b and Hynnä *et al.*, 1995).

Naval surface ships and submarines require additional noise and vibration control measures to minimise the risk of detection and the interference with on-board equipment (for example, sonar and weapon systems). Furthermore, the extensive use of periodically stiffened plates and shells in naval ships increases the structural complexity for noise and vibration analysis. It has long been recognised (Brillouin, 1946) that vibration waves in a periodic structure can only propagate in certain frequency bands (pass bands) and this phenomenon has a significant effect on vibration transmission. Clearly, the control of acoustic signatures of naval ships is a complex task that requires a thorough understanding of the mechanism of noise and vibration transmission. The present study is directed at contributing to the knowledge needed to successfully predict vibration transmission through naval ship structures.

Due to the complexity of naval ship structures and the high frequency range of interest (up to 20 kHz for torpedo homing devices), a deterministic analysis of all the resonant modes of vibration is usually not practical. A powerful tool for predicting the high frequency response of complex systems is Statistical Energy Analysis (SEA) which deals with the time-averaged flow of vibrational energy between groups of similar modes (Lyon 1975). The vibrational energy of the mode groups (or SEA elements) is determined from the power applied to the elements, together with the SEA parameters known as modal density, internal loss factor and coupling loss factor.

The evaluation of coupling loss factors is one of the most difficult aspects in applying SEA to the study of noise and vibration problems. Although some progress has been made in the experimental techniques for measuring this parameter (see, for example, Bies and Hamid, 1980), the most commonly used method to determine coupling loss factors is based on wave transmission analysis. The present study therefore consists of a detailed investigation of the wave transmission properties of structural junctions, followed by an analysis of the wave propagation through plates with periodic stiffeners. The results of these investigations are then used to develop SEA models for the prediction of vibration levels in structures characteristic of naval ships.

A review of previous work on wave transmission through structural junctions, as well as studies on periodic structures and the applications of SEA, is given in the following section.

1.2 Review of Previous Work

Naval ship structures may be considered as an assembly of beam, plate and shell elements. These elements are coupled together at junctions throughout the entire ship structure. As a first step towards understanding the transmission of vibration in a complex naval ship structure, it is perhaps logical to review some of the earlier work conducted on the transmission of vibration waves through individual junctions that consist of structural elements of semi-infinite extent.

Cremer (1948) carried out an investigation on the wave transmission of a right-angled two-plate junction subjected to an oblique incident bending wave. In this approach, the evaluation of complex wave amplitudes and hence wave powers is based on the boundary conditions at the junction (i.e., compatibility of wave motion and the equilibrium of forces and moments).

Other authors (Swift, 1977; Craven and Gibbs, 1981 and Wöhle *et al.*, 1981) have extended Cremer's method to four-plate cross junctions and presented detailed analyses of the in-plane waves generated at the junctions. Lyon (1986) reported on the contribution of in-plane waves to structure-borne noise. The wave transmission properties of a number of plate-beam junctions have been investigated by Heckl (1961) and Cremer *et al.* (1988). A more general approach to the study of wave transmission was presented by Langley and Heron (1990). They investigated structural junctions with an arbitrary number of plate elements which were either coupled to a beam or directly coupled along a line. The beam model studied by these authors has taken into account the effects of shear deformation, rotary inertia and warping.

In all the studies reviewed so far involving wave transmission through plate-beam junctions, the stiffening beam was modelled using conventional beam theory and the effect of beam cross sectional deformation due to vibration was ignored. While this approach may be valid for thick heavy beams, there are situations where elastic vibrations of the beam have to be considered. For example, in plate/beam structures typical of naval ship constructions, the beam web thickness may be of the same order as that of the plate and hence the web vibrations have to be accounted for. Lu *et al.* (1992) presented an analysis of a plate/beam junction which considered the effect of elastic vibrations of the stiffening beam. However, their method in general does not satisfy the condition for conservation of vibratory power transmission through the junction.

The transmission of vibration through beam networks has also received considerable attention. Sablik (1982) studied the wave transmission through a right-angled beam junction in which the generation of torsional waves in the source and receiving beams due to an out-

of-plane bending wave was analysed. A theoretical and experimental study of the vibrational energy transmission at a corner junction was reported by Gibbs and Tattersall (1987). More recently, Moore (1990a) and Horner (1993) also conducted analyses on the transmission of vibration in general two-dimensional beam junctions. However, neither of these studies has accounted for the coupling between torsional and bending waves due to the offset between the shear centre and the beam centroid. This type of coupling often exists in thin-walled open section beams which are commonly used in naval ship structures. Moreover, the results of these studies are not readily applicable to three-dimensional engineering structures (for example, the framework for shipboard machine foundations).

Wave propagation in cylindrical shells with a finite region of structural discontinuity has been studied by Harari (1977) and Fuller (1981). The structural discontinuity analysed by Harari was in the form of a ring stiffener while Fuller treated the discontinuity as a step change in shell wall thickness. By comparison with the structural discontinuities found in submarine hulls, a typical stiffener or bulkhead may have approximately the same thickness as the hull plate. Hence the stiffeners and bulkheads are subjected to bending and in-plane vibrations and their effects on wave transmission have yet to be investigated.

The literature review up to this point indicates that some important studies have been conducted on structural junctions that consist of beam, plate and shell elements. In particular, the early work of Cremer (1948) formed the basis of many subsequent studies. However, as discussed in the preceding paragraphs, there still appears to be a lack of research effort concerning the analysis of structural junctions typical of naval ship constructions. Section 1.3 outlines the objectives of the present study to address these shortcomings. It includes a detailed investigation of the wave transmission through typical naval ship structural junctions. The results of this investigation are used later in Chapter 4 for the evaluation of coupling loss factors for SEA studies.

Another area of concern in this thesis is the wave transmission through periodically stiffened plate and shell elements which are commonly used in naval ships (for example, bulkheads,

decks and hulls). A periodic structure freely transmits vibration waves in certain frequency bands (pass bands) and attenuates waves in other frequency bands (stop bands). An extensive study on the wave motion of a number of periodic systems such as crystals, atoms and transmission lines was given by Brillouin (1946).

Heckl (1964) studied the wave transmission properties of two intersecting beams and applied the results to investigate the vibration of a beam grillage which is in effect a two-dimensional periodic structure that consists of beams intersecting one another at right angles. He accounted for the propagation of different wave types in the grillage but neglected the effect of near-field bending waves on the assumption that the beam spacing was larger than a bending wavelength.

More recently, Mead (1973) presented a general theory of wave propagation in one-dimensional periodic systems with multiple couplings between elements. The relationship between the bounding frequencies of the pass bands and the natural modes of a single element in the periodic system was further investigated and reported by Mead (1975a, b).

Mead and Bardell (1986, 1987) used a variational approach to study the wave propagation in cylindrical shells with periodic axial and circumferential stiffeners respectively. However, the cylindrical shells investigated by these authors were more typical of aircraft fuselage structures than ship structures and the cross sectional deformation of the stiffener due to vibration was not included in the analysis.

Hodges *et al.* (1985a, b) also used a variational approach to study wave propagation in a periodic ring stiffened cylinder. They allowed for the cross sectional deformation of the stiffeners and obtained good agreement with experimental results. However, it should be noted that the ring stiffener model used in this study was only applicable at low frequencies in that the mode shape of the stiffeners was approximated by a cubic expression and the effect of in-plane vibration was not considered. The validity of this model at high frequencies (i.e., above three times the ring frequency) has yet to be verified.

Progress in this area was accelerated recently by Langley (1991) who presented an elastic wave technique for the analysis of free vibrations of periodic plate assemblies. This technique is based on the wave transmission properties of structural junctions. Neither the effect of near-field bending waves nor the effect of in-plane waves was considered in the analysis.

So far, the literature review has been confined to the study of wave transmission through idealised structures (for example, individual junctions that consist of elements of semi-infinite extent and periodic structures that are not coupled to other elements). While these studies provide the basic tools for the analysis of simple structures and are fundamental to the understanding of this subject, much effort is required to tackle complex built-up structures, such as naval ships.

Due to the complexity of ship structures, it is clear that a rigorous analysis based on the 'classical' approach (for example, wave theory; transfer matrix) would be difficult. Nilsson (1977, 1978) presented a simplified analytical method based on a grillage model which was made up of two parallel hull frames and the associated plate elements. He considered that the frames would act as wave guides for the transmission of vibration from the hull to the superstructure. The plate elements used in Nilsson's analysis were assumed to be uniform and this approach may not be suitable for the analysis of structures with horizontal stringers between the frames that are typical of naval ship structures. A further restriction of this method is that it is essentially a two-dimensional model and is not readily applicable to the general analysis of vibration transmission in ships.

The Finite Element Method (FEM) may be used to model the response of complex structures. However, in the frequency range of interest for structure-borne noise studies (i.e., up to the several kHz range), the number of elements required would probably be too large for the practical analysis of a substantial part of a ship's structure, even with the help of modern computer technology and software packages. Furthermore, at high frequencies where the wavelength is much smaller than the overall dimensions of the structure, FEM would become very sensitive to the system parameters and may lead to incorrect prediction of the

structural response. Hence FEM is normally restricted to the vibration analysis of ship structures at low frequencies.

A number of empirical studies (Janssen and Buiten, 1973; Buiten, 1976 and Plunt, 1980a) have been reported for ship noise predictions. These studies were mainly based on measurements and data taken on board merchant ships. In general, empirical methods are valuable tools in the analysis of a generic type of ship, especially at the design stage where limited information is available. These methods become less attractive in situations where a detailed analysis is required on different types of ships (for example, naval surface ships and submarines).

Statistical Energy Analysis (SEA) is a framework of study for the forced response of systems, and is based on the power balance between individual elements of a system (Lyon, 1975). It provides a basis for the prediction of average vibration and noise levels in complex structures, particularly in the high frequency regions.

Sawley (1969) demonstrated that SEA can be used successfully to investigate the noise transmission paths of a motor vessel. Ødegaard Jensen (1976) studied the distribution of vibratory power in a 1:5 scale ship section and also investigated the effects of damping on vibration transmission. Good agreement between calculated and measured results was obtained for the lightly damped case but the agreement was poor for the heavily damped case and Jensen attributed the discrepancy to the effect of in-plane waves acting as flanking transmission paths for the vibratory power.

Other authors (Irie and Takagi, 1978; Fukuzawa and Yasuda, 1979 and Hynnä *et al.*, 1995) also reported on the application of SEA to the study of vibration transmission in ships. A more detailed treatment of this subject was given by Plunt (1980b) where he investigated the rear section of a cargo ship and found reasonable agreement with experimental results.

A common feature of the SEA studies reviewed so far is that the ship structures were modelled as an assembly of plate elements subjected to bending waves except for Plunt (1980b) where longitudinal waves were also considered.

Tratch (1985) investigated the transmission of vibration in a 1:2.5 scale model of the machinery foundation of a ship bottom structure using SEA. He also modelled the structure as plate elements but considered all the possible wave types generated at the junction (i.e., bending, longitudinal and shear). Good agreement between calculated and experimental results was reported.

Naval ship structures often make use of shell elements coupled to various types of plate element (for example, submarine hull/bulkhead coupled structure). The transmission of vibration through coupled cylinder/plate structures has been investigated by a number of researchers. Hwang and Pi (1973) conducted an experimental investigation on a cylindrical shell welded onto a base plate and concluded that the SEA method was not capable of reaching any intelligent prediction of the coupling loss factor due to the strong interaction at the cylinder/plate interface. Blakemore *et al.* (1992) studied a number of flange-connected cylindrical shells and found considerable discrepancy between measurement and SEA predictions. They attributed the discrepancy to internal acoustic coupling, non-equipartition of energy between modes in a cylindrical shell element and low modal overlap. Pollard (1992) also investigated experimentally the coupling loss factors of two cylinder/plate structures (one with a long thin cylinder and the other with a short squat cylinder) and found conflicting results although the short cylinder showed good agreement between the theoretical and experimental results. Recently, Schlesinger (1995) presented a theoretical analysis of the transmission of vibration through a cylinder/plate coupled structure based on an arbitrary distribution of the wave energies in the radial, circumferential and longitudinal directions. The theory is supported by a limited amount of experimental data but further work is needed to show that this method satisfies the reciprocity requirement of SEA. Thus the study of

cylinder/plate coupled structures using SEA has been less successful compared with plate/plate structures and further research effort is required to address this shortcoming.

Another type of structure often used in naval engineering constructions is a plate or shell element reinforced with periodic stiffeners. The application of conventional SEA through successive elements of this type of structure can significantly overestimate the transmission loss (see, for example, Blackmore *et al.*, 1992). This is a matter of concern and has been the subject of criticism (Fahy, 1994). Clearly, the band pass nature of a periodic structure has to be considered in SEA modelling since it has a strong influence on the transmission of vibratory power.

Keane and Price (1989) applied the theory of periodic structures to enhance a one-dimensional SEA model. They investigated a point spring coupled, multi-modal system and compared the results obtained from 'exact' modal analysis with the normal and enhanced SEA model. A significant improvement in results was obtained by using the enhanced SEA model rather than the normal model. However, the model studied by these authors was made up of highly idealised one-dimensional elements and therefore the analysis may not be readily applicable to ship structures such as hull plates and bulkheads. Langley (1994b) also studied the modal characteristics of periodic structures and derived modal density expressions for one- and two-dimensional structures. He further studied the forced response of a damped one-dimensional periodic structure based on vibratory energy flow and compared the effect of material damping with the effect of damping caused by structural irregularity on vibration attenuation (Langley, 1994c). On the subject of 'near' periodic structures, Langley (1995) investigated the wave transmission through a randomly disordered one-dimensional periodic structure and discussed the occurrence of frequencies of perfect transmission.

From the preceding discussion, it can be concluded that SEA is a useful tool for the prediction of vibration transmission through complex built-up structures, especially in situations where the structure can be modelled as an assembly of plate elements. However, a number of areas have to be addressed before this method can be applied successfully to naval

ship structures. Notably, the evaluation of coupling loss factors for junctions characteristic of naval ship structures and the modelling of periodic structures as SEA elements. The above-mentioned studies on periodic structures, together with the work on wave transmission through junctions, provide the basis for further development of SEA models for predicting noise and vibration transmission in naval ships.

1.3 Objectives

An initial objective of this thesis is to investigate the wave transmission properties of junctions typical of naval ship structures. In particular, the effects of structural details on wave transmission such as the cross sectional deformation of stiffeners due to vibration, and the coupling between different wave types in an elastic element, are to be fully investigated.

A second objective is to identify pass and stop bands of periodic structures typical of naval ship constructions, and to investigate the effects of these bands on vibratory power transmission through coupling with other structural elements.

A third objective is to develop SEA models for naval ship structures, based on the results of analyses of junctions and periodic structures, and to conduct experiments to verify the models.

In view of the objectives outlined in the preceding paragraphs, the present study may be regarded as a step forward in the development and refinement of the necessary tools for the identification and quantification of vibration transmission paths in built-up structures, such as naval ships. It is hoped that the results of this study will contribute to the understanding of vibration transmission and lead to an improvement in the prediction of noise and vibration levels in such structures.

CHAPTER 2

WAVE PROPAGATION THROUGH STRUCTURAL JUNCTIONS

2.1 Introduction

A complex built-up structure may be considered as an assembly of structural elements such as plates, beams and shells. These elements are coupled together at junctions which may be regarded as a series of structural discontinuities. If an incident wave impinges on a structural junction or discontinuity, it will be partially transmitted and partially reflected at the junction according to the boundary conditions and this phenomenon has a strong influence on the propagation of waves. A commonly used method to characterise the wave transmission properties of a structural junction involves evaluating the wave powers of the structural elements. This leads to the determination of transmission efficiency which is defined as the ratio between the transmitted wave power and the incident wave power. The transmission efficiency is an important parameter in the study of structure-borne noise since it provides the basis for the identification and quantification of vibration transmission paths through a junction. This information is useful for the application of appropriate vibration control techniques. As well as being a parameter of intrinsic importance, the transmission efficiency may also be used to evaluate the coupling loss factors for the purpose of predicting the vibration of complex structures using SEA which is discussed in Chapter 4 of this thesis.

One of the early attempts to evaluate the transmission efficiency was carried out by Cremer (1948). His work included right-angled plate junctions subjected to oblique incident bending waves. In Cremer's analysis, expressions for the plate displacements were developed from the wave equations in terms of complex wave amplitudes. The wave amplitudes and hence wave powers were then evaluated by considering the boundary conditions at the junction (i.e., compatibility of wave motion and equilibrium of forces and moments). This method of analysis formed the basis of many subsequent investigations (see, for example, Craven and

Gibbs, 1981; Wöhle *et al.*, 1981; Fuller, 1981 and Langley and Heron, 1990) where junctions with plate, beam and shell elements were analysed. Although the subject of wave propagation through junctions has received considerable attention in the past, there seems to be a lack of research effort regarding structural junctions that are characteristic of naval ship constructions. For example, the plate and shell elements of naval ships are often reinforced by thin-walled stiffeners with a thickness approximately the same as that of the plate or shell elements. The vibrations of stiffeners would therefore have a significant effect on structure-borne noise transmission and this problem has not been adequately addressed.

The work described in this chapter was designed to complement existing studies on wave propagation through junctions and in particular, the modelling of structures characteristic of naval ships. Although the approach is similar to that of Cremer's analysis, the present study considers the modelling of structural details such as the cross-sectional deformation of stiffeners due to vibration and the coupling between different types of waves in structural elements.

The structural junctions covered in this chapter include:

- Uniform semi-infinite thin plates coupled to a thin rectangular section beam.
- Three-dimensional beam junctions that consist of semi-infinite beam elements with bending and torsional wave coupling due to the offset between the shear centre and beam centroid.
- Semi-infinite thin cylindrical shells coupled to various types of plate element including annular, circular and infinite plates.

Figure 2.1 shows these structural junctions schematically. In the following sections, equations of motion for the structural elements of these junctions are given. The solutions to these equations are represented by complex wave amplitudes and by using the appropriate boundary conditions at the junctions (i.e., the compatibility of displacements and the

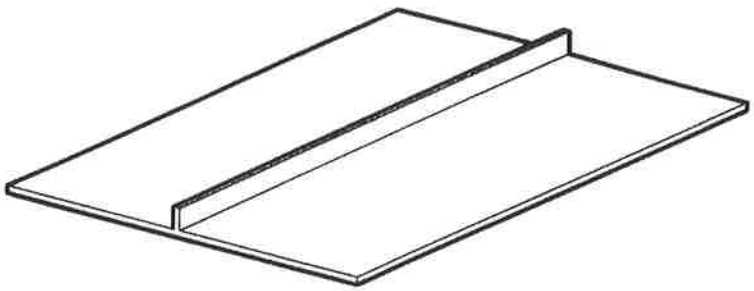

(a) Plate / beam junction

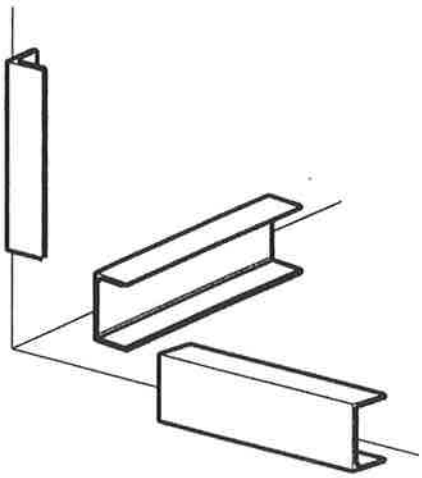

(b) Beam junction

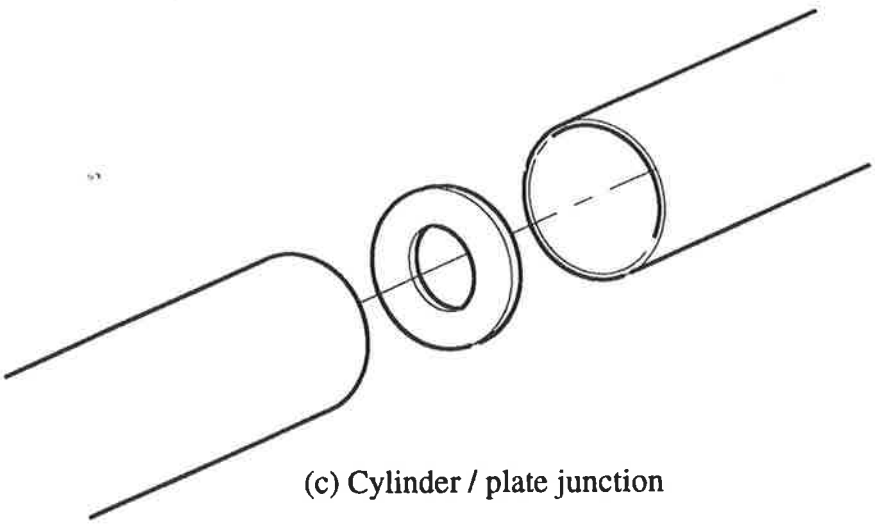

(c) Cylinder / plate junction

Figure 2.1 Examples of structural junctions.

equilibrium of forces and moments), the wave amplitudes and hence the transmission efficiency can be determined (detailed derivations are given in Appendices 1 - 4).

2.2 Plate/beam Junction

Figure 2.2a shows a schematic diagram of a junction which consists of a number of semi-infinite plates. The source plate (plate 1) is subjected to an oblique incident wave at angle α to the x_1 - axis. The incident wave may be a bending, longitudinal or shear wave and when it impinges on the line junction, it is partially transmitted and partially reflected as bending, longitudinal and shear waves as shown. To study the wave transmission mechanism of the junction, one may first consider the displacements due to the transmitted or reflected waves in an arbitrary plate as shown in Figure 2.2b. The equations of motion for bending and in-plane displacements of the plate may be written in the following form (see, for example, Love, 1927):

$$\nabla^4 w + [12\rho(1-\mu^2)/Eh^2]\partial^2 w/\partial t^2 = 0, \tag{2.1a}$$

$$\partial^2 u/\partial x^2 + [(1-\mu)/2]\partial^2 u/\partial y^2 + [(1+\mu)/2]\partial^2 v/\partial x\partial y - [\rho(1-\mu^2)/E]\partial^2 v/\partial t^2 = 0, \tag{2.1b}$$

$$\partial^2 v/\partial y^2 + [(1-\mu)/2]\partial^2 v/\partial x^2 + [(1+\mu)/2]\partial^2 u/\partial x\partial y - [\rho(1-\mu^2)/E]\partial^2 u/\partial t^2 = 0, \tag{2.1c}$$

where ∇^2 is the Laplacian operator in Cartesian co-ordinates; u, v and w are the plate displacements in the x, y and z directions respectively; E, h, ρ and μ are the elastic modulus, thickness, density and Poisson's ratio of plate respectively.

Solutions of equation (2.1) lead to four unknown complex wave amplitudes for one direction of wave propagation. These wave amplitudes represent the longitudinal and shear waves, as well as the travelling and decaying bending waves. Details of the mathematical solutions are given in Appendix 1.

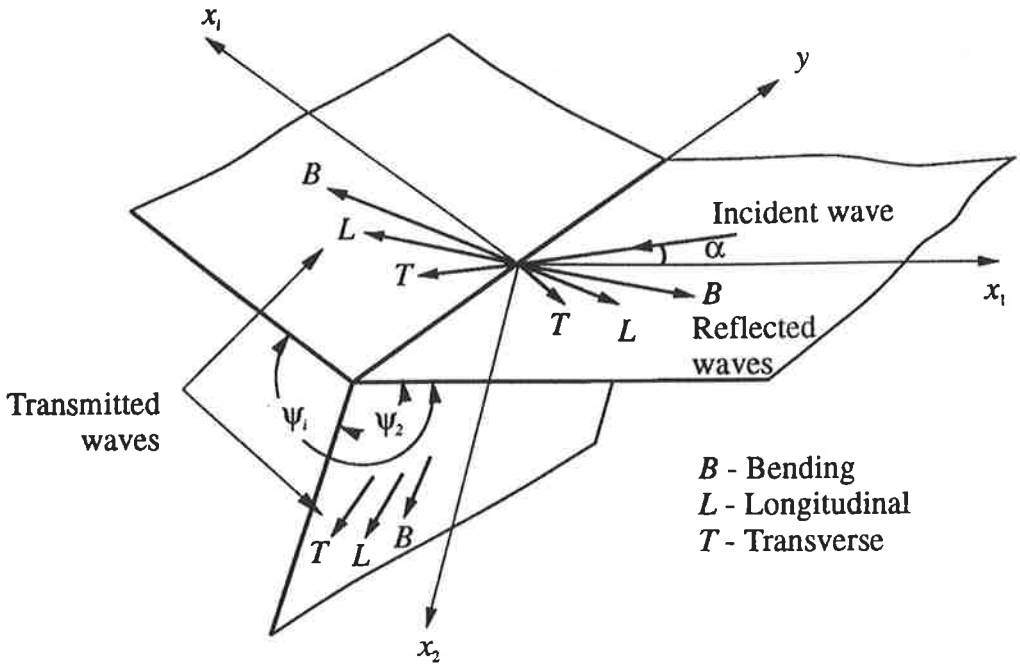

(a) Schematic diagram of junction.

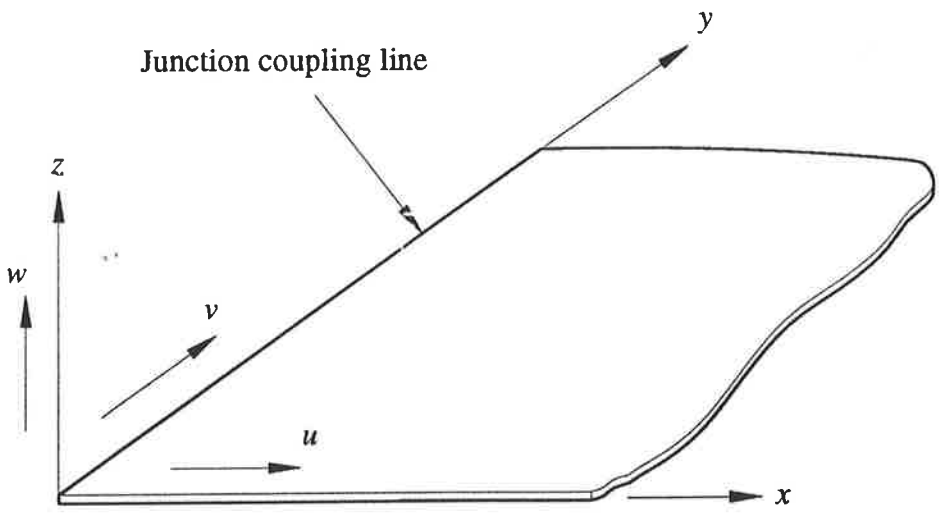

(b) Displacements and co-ordinate system of an arbitrary plate.

Figure 2.2 A plate / plate junction.

For junctions that consist of a number of semi-infinite plates coupled along a line or coupled to a thick beam, the source plate carries the incident and reflected waves and the receiving plates carry the transmitted waves. The displacements of the source plate therefore consist of the incident and reflected wave components. For the purpose of calculating the transmission and reflection efficiencies, the incident component may be regarded as a wave of unit amplitude. The unknown reflected and transmitted wave amplitudes may be determined by consideration of the boundary conditions at the junction. Detailed studies on these junctions have been reported by and Langley and Heron (1990) and will not be considered here.

For a structural junction with a number of semi-infinite plates coupled to a thin rectangular beam, the beam is subjected to bending and in-plane waves and the analysis may be carried out by assuming that the thin beam behaves as a finite plate with waves travelling in both the positive and negative x - directions as shown in Figure 2.3. The solutions to wave motion of a finite plate therefore consist of eight unknown complex wave amplitudes (four amplitudes for the positive x - direction of wave propagation and four amplitudes for the negative x - direction) and the solutions for plate deformations are described in Appendix 1. Four additional boundary conditions are required in this case. These boundary conditions may be obtained by equating the forces and moment to zero at the free edge of the finite plate. Combined with the boundary conditions at the junction, they provide sufficient information for the solution of all complex wave amplitudes.

2.3 Three - dimensional Beam Junction

An arbitrary beam section is shown in Figure 2.4. The shear centre, centroid and attachment point of the beam are denoted by S, C, and P respectively. Two fixed co-ordinate systems are attached to the beam element. The axes x_r, y_r and z_r are defined as the reference axes of the beam with the axis x_r passing through the attachment point in the longitudinal direction. The principal axes of the beam are denoted by x_p, y_p and z_p with axis x_p parallel to x_r and passing

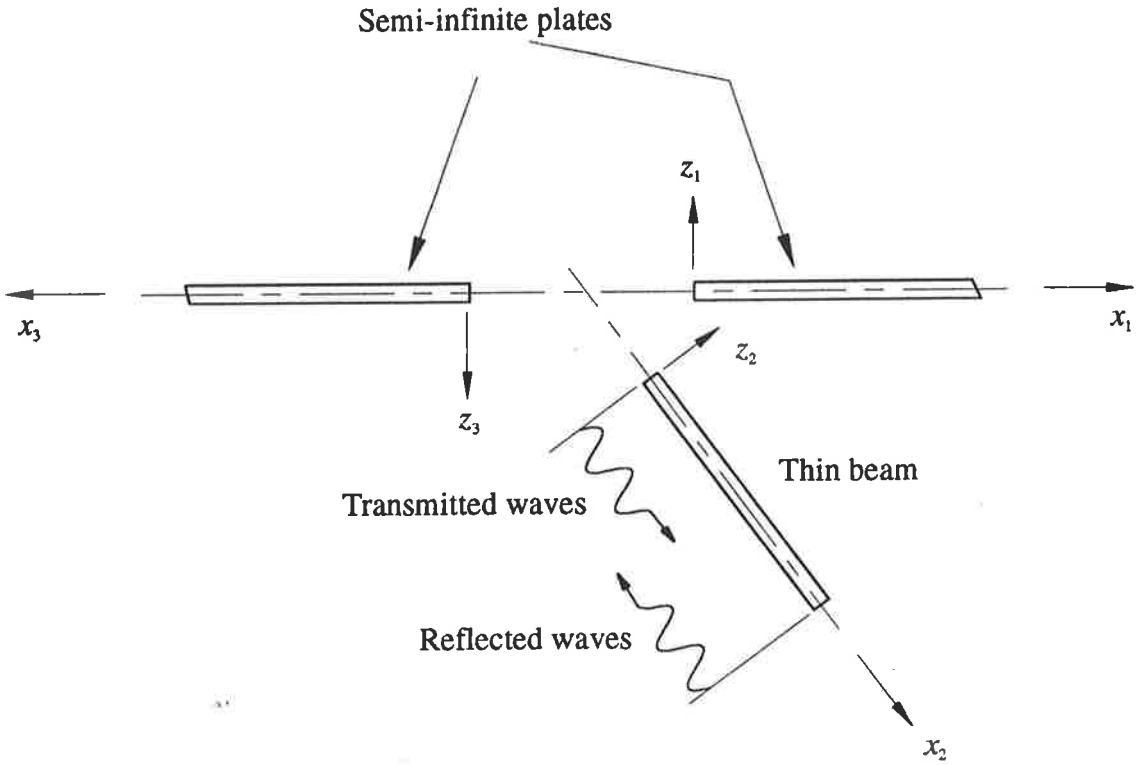

Figure 2.3 A plate / thin beam junction.

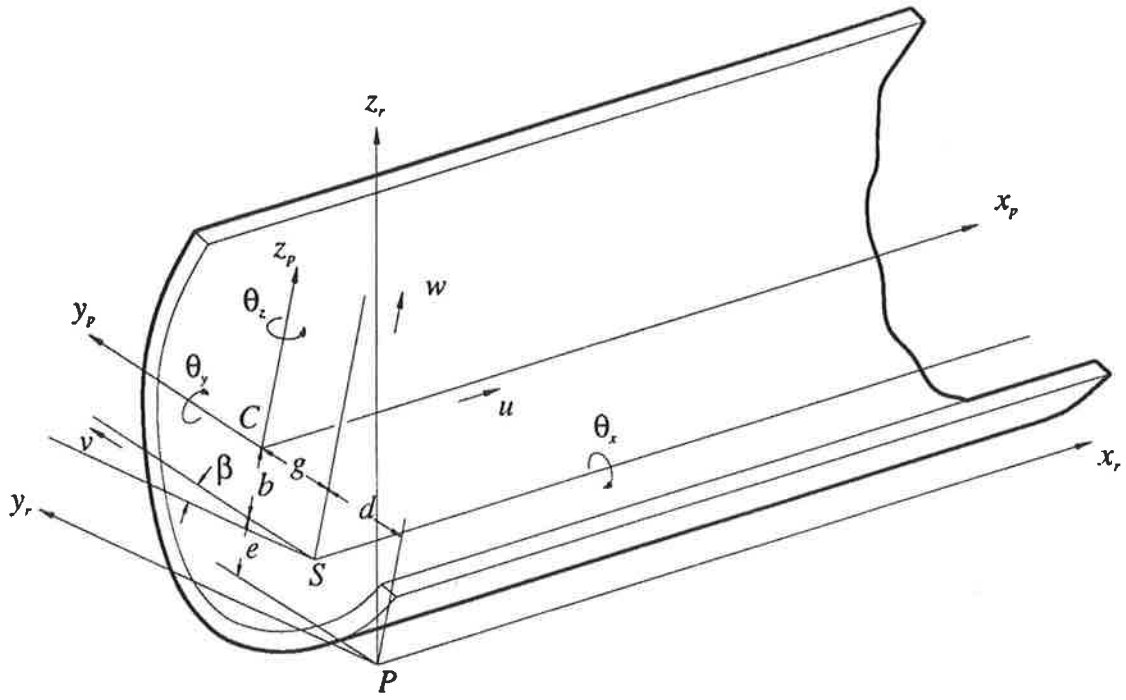

Figure 2.4 An arbitrary beam element.

through the beam centroid. The beam displacements v, w and θ_x are related to the shear centre, while u, θ_y and θ_z are related to the centroid.

The equations of motion of the beam, taking into account the effects of shear deformation and rotary inertia, may be derived by considering an element of unit length and the associated forces, moments and inertias (see, for example, Timoshenko *et al.*, 1972),

$$GAK_z(\partial\theta_y/\partial x_p + \partial^2 w/\partial x_p^2) = \rho A(g\,\partial^2\theta_x/\partial t^2 + \partial^2 w/\partial t^2), \tag{2.2a}$$

$$EI_y\,\partial^2\theta_y/\partial x_p^2 - GAK_z(\theta_y + \partial w/\partial x_p) = I_y\rho\,\partial^2\theta_y/\partial t^2, \tag{2.2b}$$

$$GAK_y(\partial^2 v/\partial x_p^2 - \partial\theta_z/\partial x_p) = \rho A(\partial^2 v/\partial t^2 - b\,\partial^2\theta_x/\partial t^2), \tag{2.2c}$$

$$EI_z\,\partial^2\theta_z/\partial x_p^2 - GAK_y(\partial v/\partial x_p - \theta_z) = I_z\rho\,\partial^2\theta_z/\partial t^2, \tag{2.2d}$$

$$GJ\,\partial\theta_x/\partial x_p = I_s\,\partial^2\theta_x/\partial t^2 - \rho Ab\,\partial^2 v/\partial t^2 + \rho Ag\,\partial^2 w/\partial t^2, \tag{2.2e}$$

$$EA\,\partial^2 u/\partial x_p^2 = \rho A\,\partial^2 u/\partial t^2, \tag{2.2f}$$

where I_y, I_z are the second moment of area of beam about the y_p and z_p axes respectively; K_y, K_z are the shear factors in the y_p and z_p directions respectively, J is the torsional constant of beam, I_s is the second moment of inertia per unit length of beam about the shear centre, A is the cross-sectional area of beam, G is the shear modulus and b, g represent the offset between the shear centre and beam centroid as shown in Figure 2.4.

Due to the offset between the shear centre and the centroid, the bending and torsional motions of the beam are coupled as can be seen in equations (2.2a) - (2.2e). Equation (2.2f) represents the longitudinal mode and is independent of the bending and torsional modes. Solutions of equations (2.2a) - (2.2e) may be obtained by evaluating the roots of the

dispersion equation and this leads to five wave numbers for one direction of wave propagation. There are altogether six unknown complex wave amplitudes in the beam element. Detailed derivations of the solutions to equation (2.2), as well as the consideration of boundary conditions at a three-dimensional beam junction, are shown in Appendix 2.

2.4 Cylinder/plate Junction

The dynamics of thin cylindrical shells have been studied extensively (see, for example, Leissa, 1973). Of prime importance to the present study is the nature of the waves in a thin cylinder and this will be reviewed briefly in this section. Figure 2.5 shows the co-ordinate system and displacements in the axial, circumferential and radial directions (u, v and w) of a thin cylinder. The shell motion may be described by the Donnell-Mushtari system of equations which is given by (Leissa, 1973) :

$$\mathbf{L} \begin{bmatrix} u \\ v \\ w \end{bmatrix} = 0, \tag{2.3}$$

where **L** is a matrix differential operator (see Appendix 3 for elements of the operator). For a particular circumferential mode number n, the solution to equation (2.3) may be obtained by evaluation of the dispersion equation, leading to four unknown wave amplitudes for one direction of wave propagation. The nature of the waves generated in a thin cylinder is important to the study of vibratory power transmission. From the dispersion equation (see Appendix 3), one obtains the axial wave numbers which can be real, imaginary or complex. The real roots represent the travelling waves which propagate energy from the junction. A plot of the wave number of the travelling waves against the non-dimensional frequency Ω (Ω is sometimes referred to as the ring frequency ratio and is given by $\omega a/c_L$, where ω is the circular frequency, a is the cylinder mean radius and c_L is the longitudinal wave speed) of a steel cylinder with thickness h = 0.02 m, radius a = 1 m, Poisson's ratio μ = 0.3, and

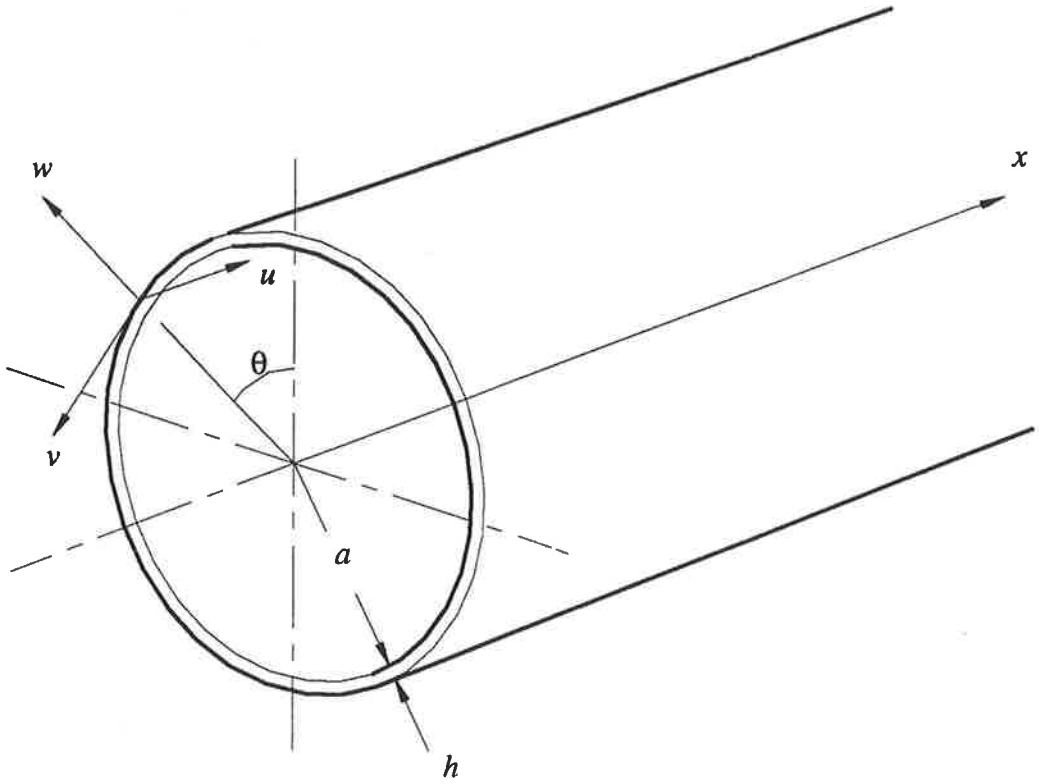

Figure 2.5 Co-ordinate system of cylindrical shell.

circumferential mode number $n = 2$, is shown in Figure 2.6. Also shown in Figure 2.6 are the wave numbers of a flat plate in bending, longitudinal and transverse shear motions k_B, k_L and k_T respectively. Three travelling waves can be observed in the figure. These waves are labelled as Type I, II and III and at high frequencies, their wave numbers approach the values of k_B, k_T and k_L respectively. The fourth root of the dispersion equation can be recognised as the near field bending wave solution for a flat plate at high frequencies. The low frequency behaviour of these waves has been discussed in detail by Smith (1955) and Fuller (1981).

For circular and infinite plates, it is more convenient to express the plate equation (equation (2.1)) in terms of the polar co-ordinates,

$$\nabla^4 w_p + [12\rho(1 - \mu^2)/Eh^2]\partial^2 w_p/\partial t^2 = 0, \tag{2.4a}$$

$$\partial/\partial r\{\partial u_p/\partial r + u_p/r + (1/r)\,\partial v_p/\partial\theta\} - \{(1-\mu)/2r\}\partial/\partial\theta\{\partial v_p\partial r + v_p/r - (1/r)\partial u_p/\partial\theta\}$$

$$- \{\rho(1-\mu^2)/E\}\partial^2 u_p/\partial t^2 = 0, \tag{2.4b}$$

$$(1/r)\partial/\partial\theta\{\partial u_p/\partial r + u_p/r + (1/r)\partial v_p/\partial\theta\} + \{(1-\mu)/2\}\partial/\partial r\{\partial v_p/\partial r + v_p/r - (1/r)\partial u_p/\partial\theta\}$$

$$- \{\rho(1-\mu^2)/E\}\partial^2 v_p/\partial t^2 = 0, \tag{2.4c}$$

where ∇^2 is the Laplacian operator in polar co-ordinates, u_p and v_p are the plate displacements in the r and θ directions respectively and w_p is the out-of-plane displacement of the plate.

Solutions to these equations may be obtained in terms of the Bessel functions for circular and annular plates, and Hankel functions for an infinite plate as shown in Appendix 3. Depending on the types of cylinder/plate coupled structure, the solutions to equation (2.4) may be used in conjunction with equation (2.3) to satisfy the boundary conditions of the junction and lead to the determination of wave amplitudes.

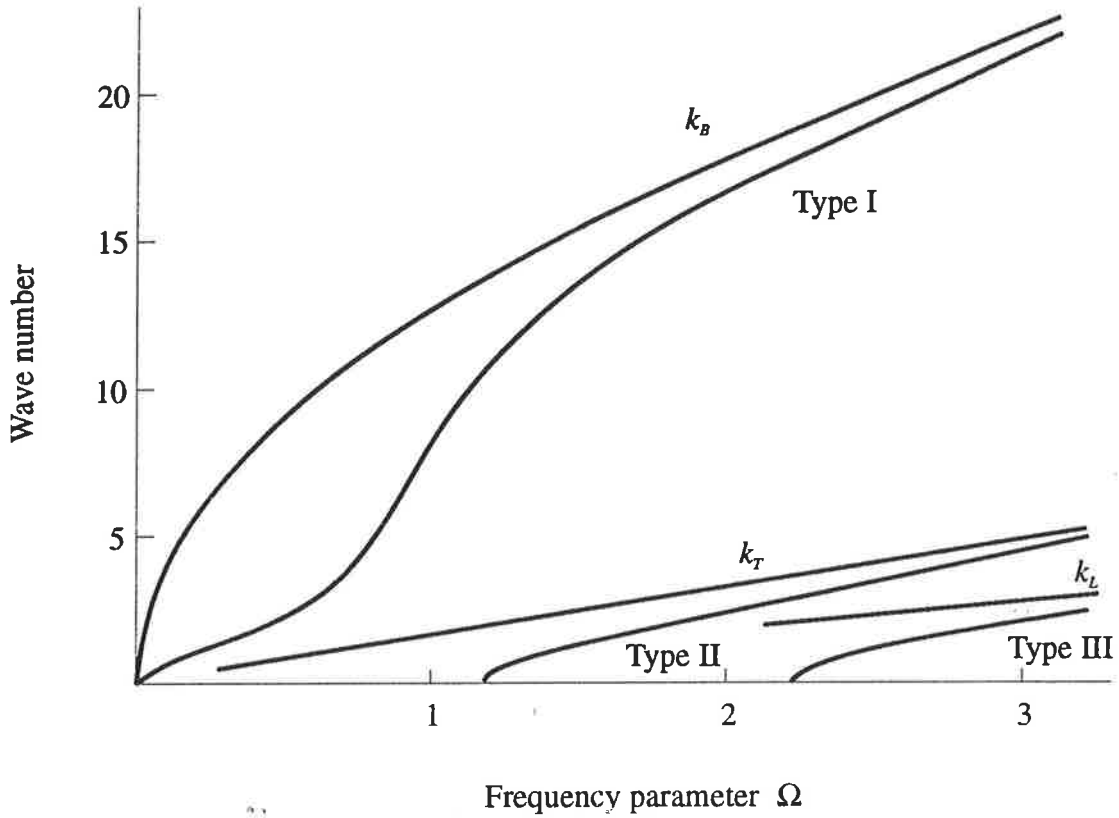

Figure 2.6 Travelling waves in a cylindrical shell.

2.5 Evaluation of Wave Powers and Transmission Efficiency

The power for a particular travelling wave in a semi-infinite structural element may be determined from the junction forces and displacements. For plate/beam junctions, the bending, longitudinal and shear wave powers may be expressed as:

$$\Pi_B = \tfrac{1}{2}\,\mathrm{Re}\{M\dot{\phi}^* + F_z\dot{w}^*\}, \tag{2.5a}$$

$$\Pi_L = \tfrac{1}{2}\,\mathrm{Re}\{F_x\dot{u}^*\}, \tag{2.5b}$$

$$\Pi_T = \tfrac{1}{2}\,\mathrm{Re}\{F_y\dot{v}^*\}, \tag{2.5c}$$

where $\cdot$ and * denote the derivative with respect to time and the complex conjugate respectively, F_x, F_y and F_z are the plate forces in the x, y and z directions respectively, M is the bending moment and ϕ is the plate rotation about the y-axis. Similar expressions for wave powers may be obtained for beam junctions. For cylinder/plate junctions, the above wave power expressions have to be integrated around the circumference of the cylinder to obtain the total wave power. Detailed expressions for wave powers of cylinder/plate junctions are shown in Appendix 4.

The transmission / reflection efficiency is defined as the ratio between the transmitted / reflected wave power and the incident wave power. For plate junctions subjected to an oblique incident wave, the efficiency is a function of the incident wave angle. If one assumes that the source plate carries a diffuse vibration field, one may average the efficiency from an incident angle α of $-\pi/2$ to $\pi/2$ radians and obtain the mean transmission / reflection efficiency which is defined as (Cremer *et al.*, 1988):

$$\tau = \tfrac{1}{2}\int_{-\pi/2}^{\pi/2} \tau(\alpha)\cos\alpha\, d\alpha\,,$$

$$= \int_0^1 \tau(\alpha)\, d \sin\alpha \,. \qquad (2.6)$$

This is a more meaningful parameter to characterise the wave transmission properties of plate elements subjected to a diffuse incident vibration field as can be seen in Section 4.1.5 of Chapter 4 where the derivation of coupling loss factors are presented.

Throughout the preceding analysis, it has been assumed that the material loss factor of all structural elements is equal to zero. From the principle of conservation of energy, it can be deduced that the sum of the transmitted and reflected wave powers is equal to the incident wave power. Material damping in the structural elements may be accounted for by replacing the elastic modulus E in the analysis by $E\ (1 + j\eta)$, where η is the material loss factor. However, with the introduction of damping, there will be no definitive distinction between the travelling and evanescent waves and that raises the problem in the definition of wave power. The effects of material damping on wave transmission have been discussed by Craven and Gibbs (1981) and will not be considered any further in the present study. For lightly damped structures, the assumption of zero damping gives a good estimation of the transmission efficiency (see, for example, the book by Cremer *et al.*, 1988 where theoretical and experimental results of the transmission efficiency of a right-angled structural junction are presented and discussed).

2.6 Numerical Examples

2.6.1. Plate-beam junctions

Figure 2.7 shows a plate/beam junction that consists of two semi-infinite plates coupled to a thin rectangular beam with one of the plates subjected to a diffuse incident bending wave field. The method of analysis outlined in Section 2.2 and Appendix 1 which involves treating the thin beam as a finite plate (thin beam model) was used to determine the mean transmission efficiency of the junction and the results are shown in Figure 2.8. The effect of

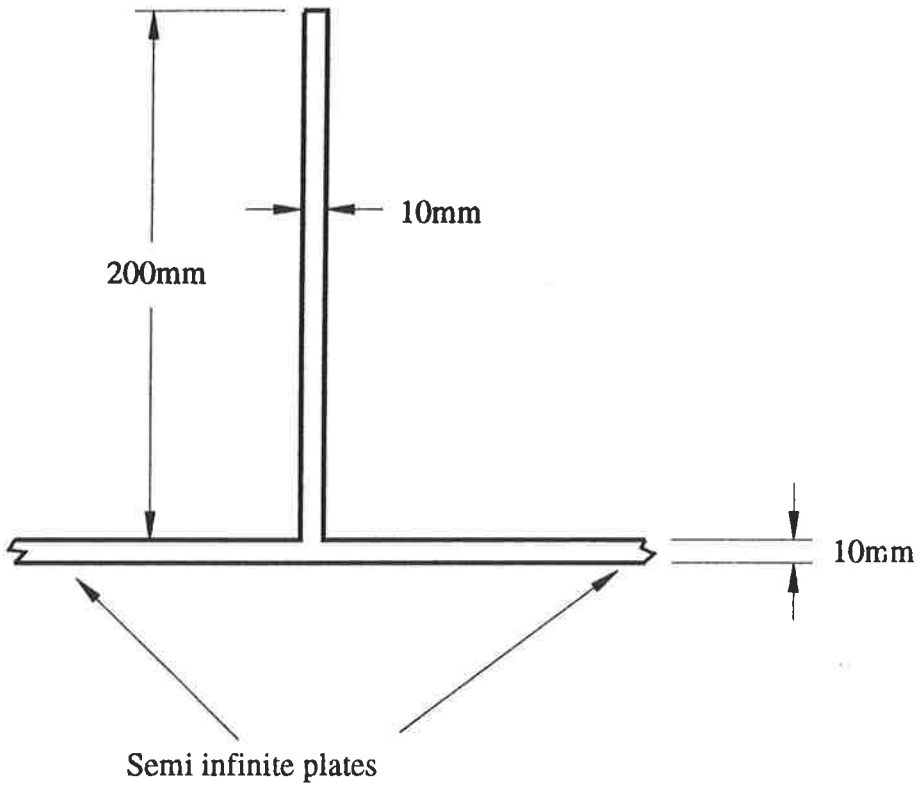

Figure 2.7 Example of a plate / thin beam junction.

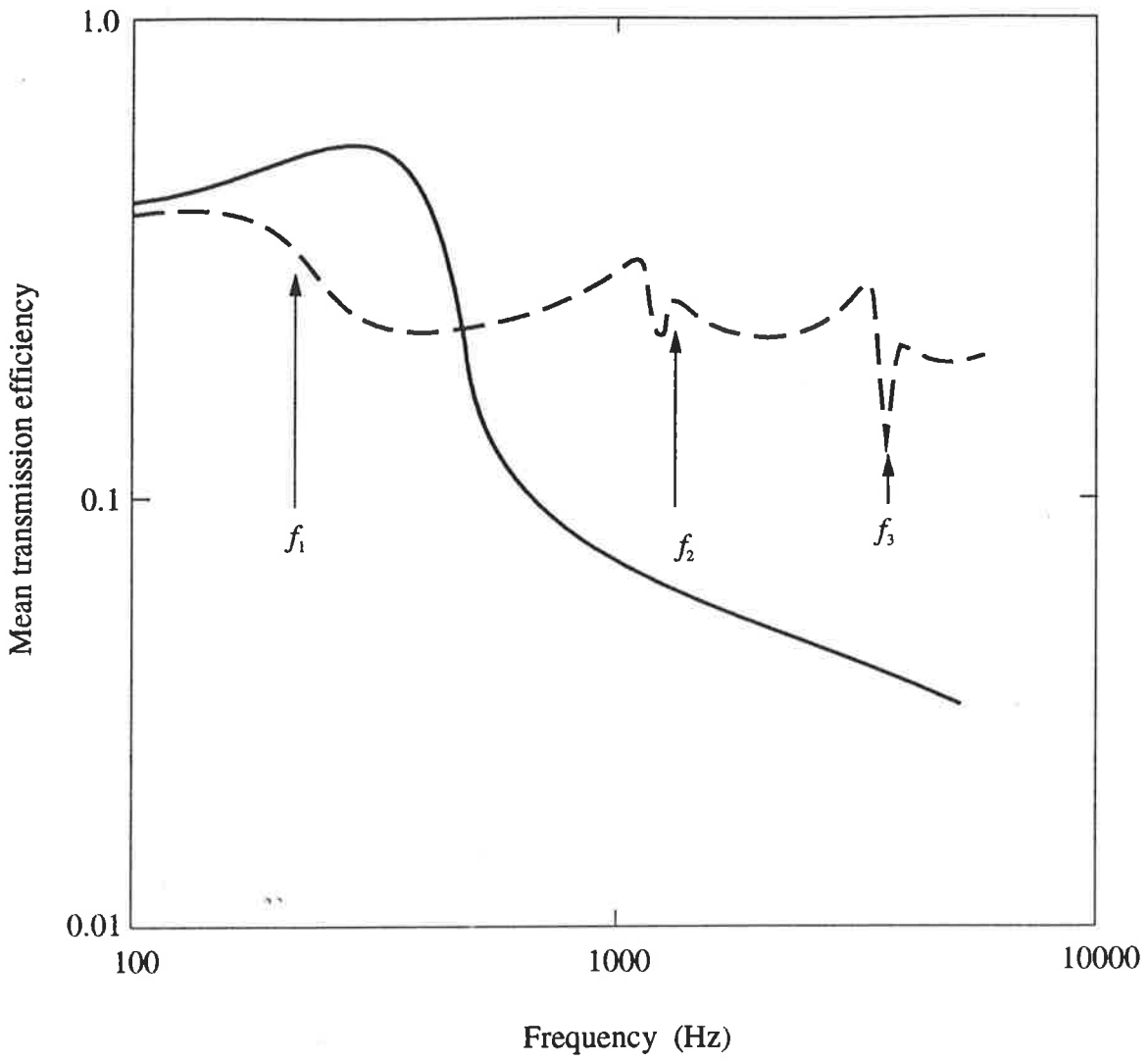

Figure 2.8 Bending wave transmission for a plate / thin beam junction.

———— , thick beam theory ;

— — — — , thin beam theory ;

f_1 , f_2 and f_3 are the bending resonance frequencies of the beam.

bending resonance frequencies of the thin beam on wave transmission can be observed. A detailed discussion of the relationship between the natural frequencies of a junction element and wave transmission has been presented by Allwright *et al.*, 1994. To demonstrate the effect of beam vibration on wave transmission, a second set of calculations was performed on the same junction but with the beam vibration ignored in the analysis (thick beam model). This method is based on the work reported by Cremer (1948) and the results are also plotted in Figure 2.8 for comparison. As the beam thickness in this example is the same as that of the plates, it is reasonable to assume that the thin beam model would give a more accurate prediction of the transmission efficiency. Figure 2.8 shows that the thick beam model predicts a low pass characteristic of the plate/beam junction and underestimates the transmission efficiency at frequencies above 500 Hz.

As a second example, the beam thickness of the previous example was doubled and calculations based on the thin beam and thick beam models were performed. Figure 2.9 shows the calculated mean transmission efficiency. Below a frequency of 1 kHz, the results between the thick beam and thin beam models are in reasonable agreement. At higher frequencies, the thin beam model predicts a higher transmission efficiency, possibly due to the effect of beam resonance. It should be noted that the mathematical models used in this thesis are based on thin plate theory and the assumption that the boundary conditions can be applied on the plate/beam centreline. These assumptions may not be justified at high frequencies where the cross sectional dimensions of the junction is not negligible compared with the bending wavelength. Cremer *et al.* (1988) suggested that thin plate theory may be used if the bending wavelength is longer than six times the plate thickness. For the present examples, this occurs at a frequency of approximately 26 kHz which thus represents the upper frequency limit of the analysis. The effect of plate offset from the centreline of a thick beam may be considered by modifying the compatibility and equilibrium equations. This approach has been carried out and reported by Langley and Heron (1990).

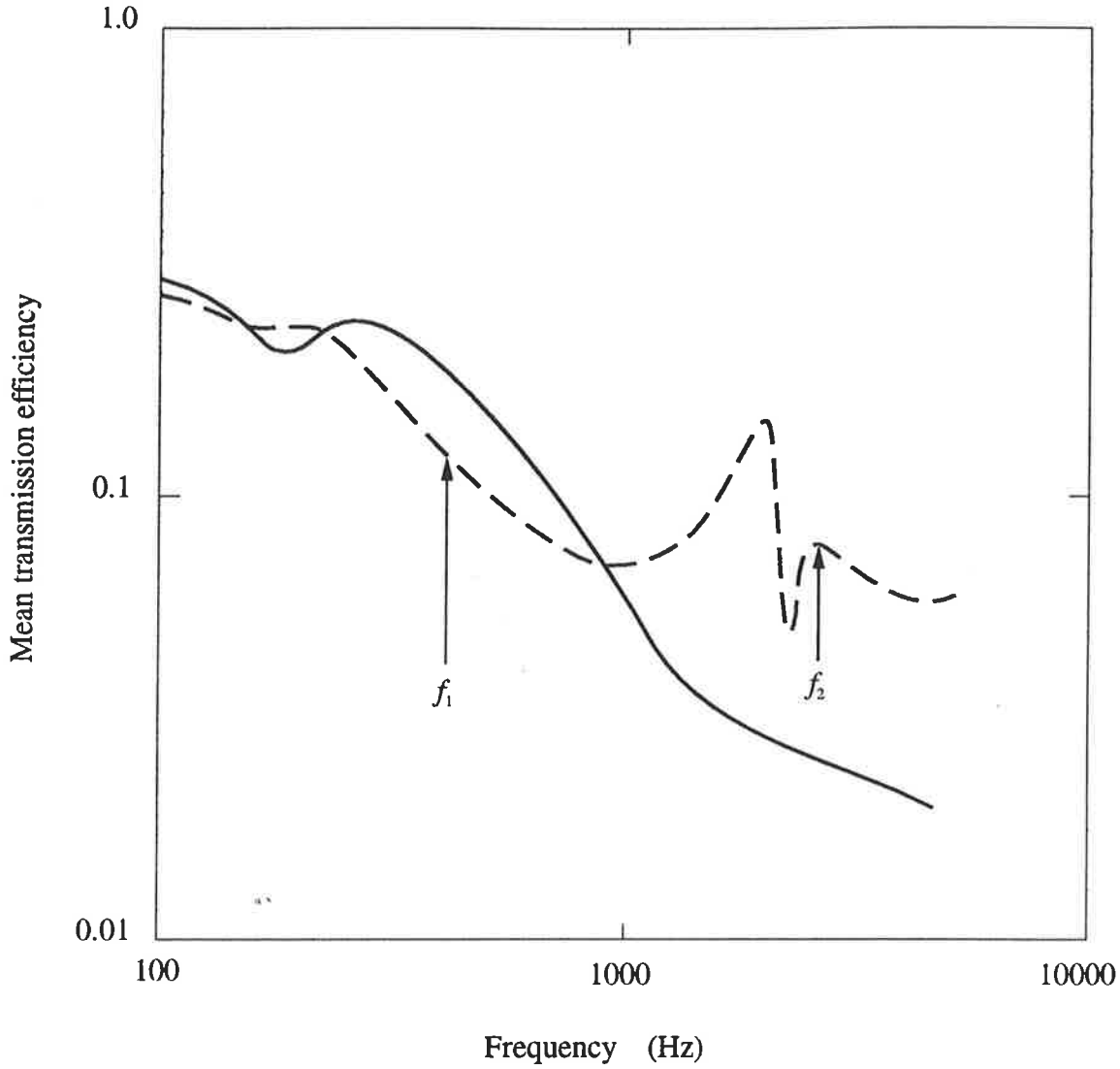

Figure 2.9 Bending wave transmission for a plate / thick beam junction.

——— , thick beam theory;

— — — , thin beam theory;

f_1 and f_2 are the bending resonance frequencies of the beam.

2.6.2 Symmetrical T-junction

Figure 2.10 shows three identical I-section beams in a symmetrical T-junction about the x-y plane. The beam parameters are shown in Table 2.1. This example is chosen to coincide with an example discussed by Moore (1990) who used the Euler-Bernoulli theory to describe the beam motion. Beam 1 carries an out-of-plane bending wave which transmits into torsional and out-of-plane bending waves in beams 2 and 3. Due to the symmetrical nature of the junction, the transmission efficiencies of beams 2 and 3 must be equal. To account for the shear deformation of the beam elements, it is required to determine the shear factors K_y and K_z which are defined as the ratio between the average shear strain and the local shear strain at which the equivalent shear force acts. Expressions for shear factors of some beam sections commonly found in engineering applications are given by Cowper (1966). However, for the purpose of illustrating the present method of analysis, it is assumed in the following beam examples that plane sections remain plane during bending, i.e., the shear factors are equal to unity. To demonstrate the effects of shear deformation and rotary inertia on vibration transmission, a second set of calculations was carried out using the Euler-Bernoulli beam theory. This can be achieved in the present analysis by ignoring the rotary inertia terms (the terms in the right hand side of equations (2.2b) and (2.2d)) and putting the shear factors equal to infinity. Figure 2.11 shows the bending and torsional transmission efficiencies of beams 2 and 3. With shear deformation and rotary inertia ignored in the analysis, the results are identical to those given by Moore (1990). The transmission of torsional wave power is due to a rotation of beam 1 about the y - axis while the transmission of bending power results from the motion of beam 1 in the z direction. As expected, the effects of shear deformation and rotary inertia become more significant as the frequency increases. Below a frequency of approximately 200 Hz, such effects on wave transmission are negligible. At higher frequencies, shear deformation and rotary inertia reduce the transmission of torsional waves while at the same time increasing the transmission of bending waves.

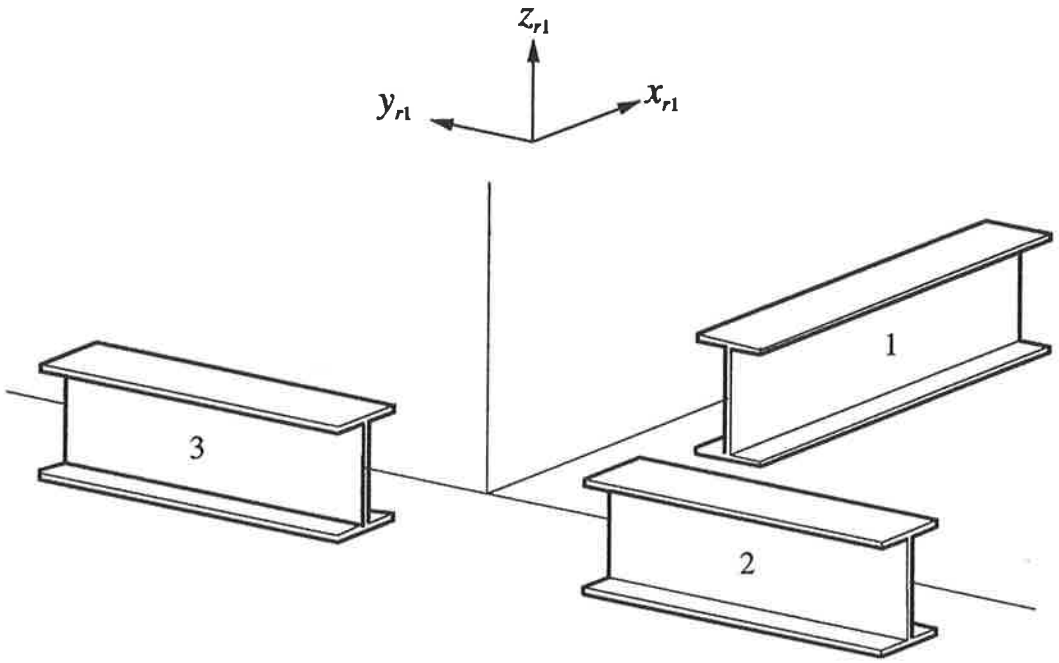

Figure 2.10 A symmetrical T-junction.

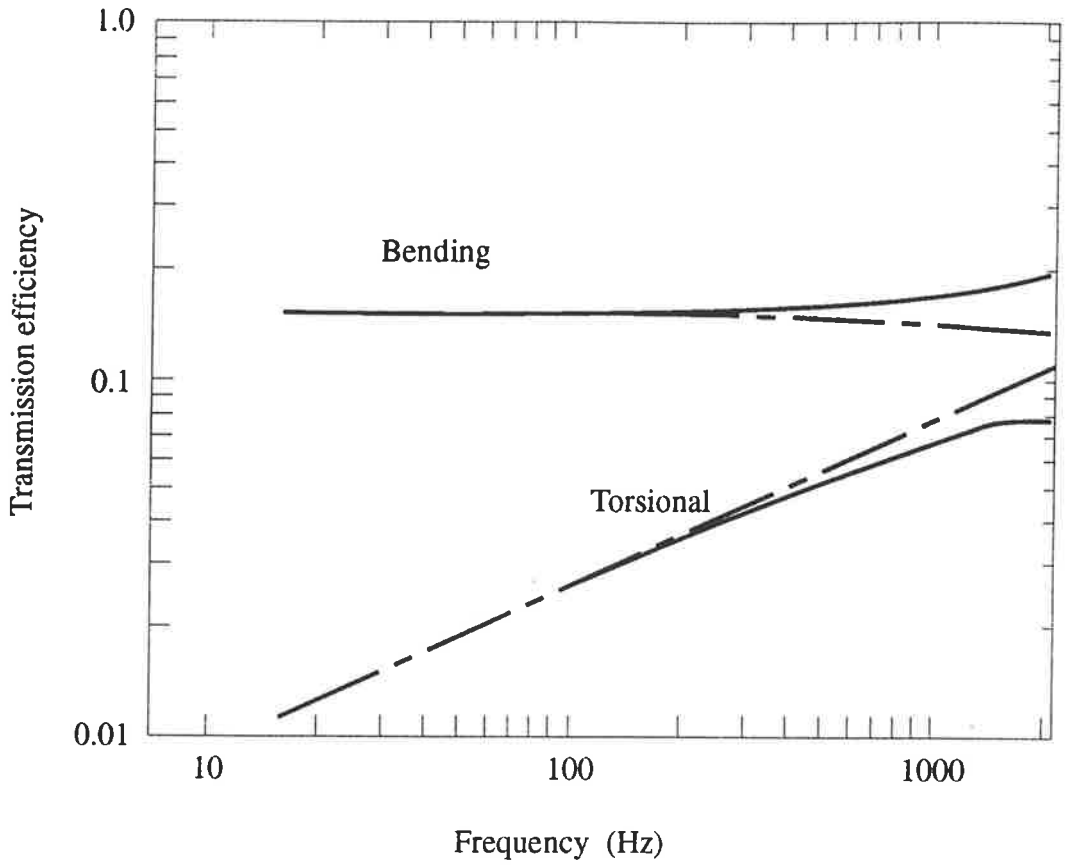

Figure 2.11 Transmission efficiency of beams 2 and 3 for an incident bending wave in beam 1.

———— , results with the effects of shear deformation and rotary inertia included in the calculation;

— — — , results calculated without the effects of shear deformation and rotary inertia.

Table 2.1

Parameters of beam element
$E = 7.2 \times 10^{10}$ N/m^2 ; $\rho = 2.71 \times 10^3$ kg/m^3 ; $G = 2.69 \times 10^{10}$ N/m^3
$A = 4 \times 10^{-4}$ m^2 ; $I_y = 2.8 \times 10^{-6}$ m^4 ; $I_z = 3.48 \times 10^{-8}$ m^4
$GJ = 3.5 \times 10^3$ Nm^2

2.6.3 Three-beam orthogonal junction

A structural junction which consists of three orthogonal steel beams is shown in Figure 2.12. Beam 1 carries a predominantly bending incident wave in the x_{r1} - z_{r1} plane. The bending and torsional vibration modes of these beams are coupled and as a result, the incident wave is partially reflected and partially transmitted as bending, longitudinal and torsional waves. For beams 1 and 2, the attachment point is offset from the shear centre and this has an effect on the coupled torsional and bending modes as can be seen later in the results.

The bending incident wave in beam 1 produces torsional and out-of-plane bending waves (in the z_{p2} - x_{p2} plane) in beam 2 with the transmission efficiency increasing with frequency (see Figure 2.13). Both the longitudinal and in-plane wave powers are negligible within the frequency range considered in this example. Figure 2.14 shows the transmission efficiencies of beam 3. Significant longitudinal power is transmitted to this beam due to the incident wave motion of beam 1 in the z_{r1} - direction. The rotation of beam 1 about the y_{r1} - axis also transmits into bending motion in beam 3 about its principal axes. The torsional wave in beam 3 is due to the coupling effect caused by the offset between the shear centre and beam centroid. Figure 2.15 shows the reflection efficiencies of beam 1. The reflected wave power is predominantly bending in the x_{r1} - z_{r1} plane.

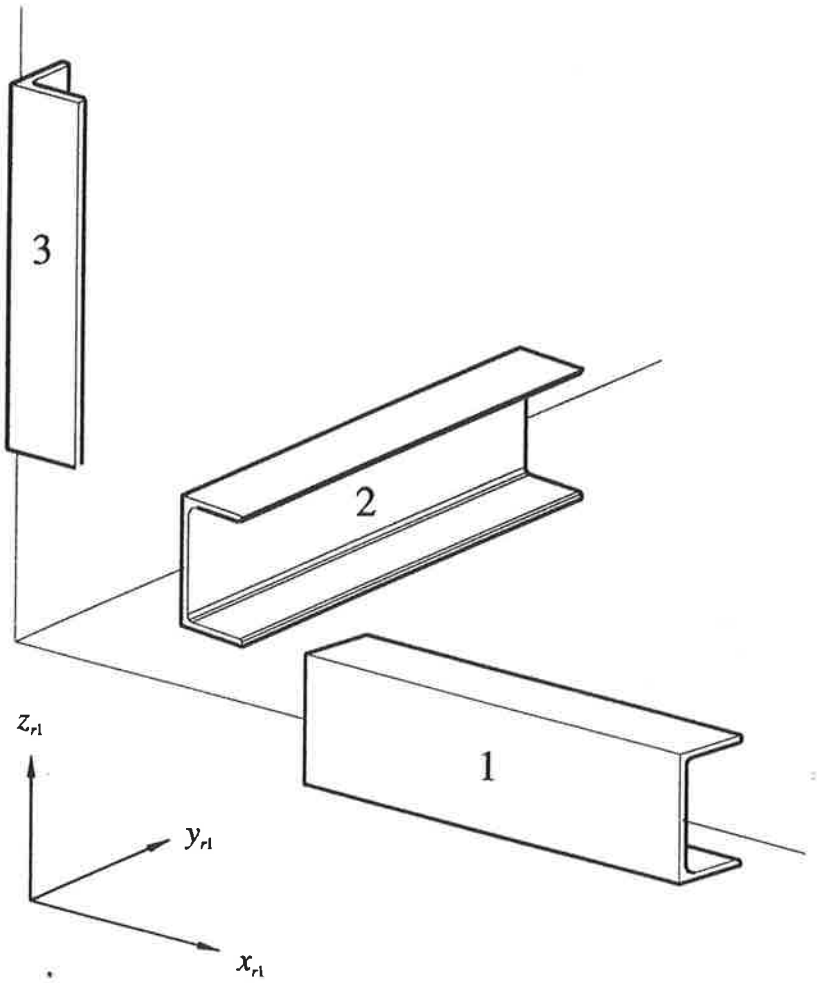

Figure 2.12 A three-beam orthoganol junction.

Cross sectional dimensions of beams 1 and 2 are
160mm x 80mm x 10mm thick.

Cross sectional dimensions of beam 3 are
80mm x 80mm x 10mm thick.

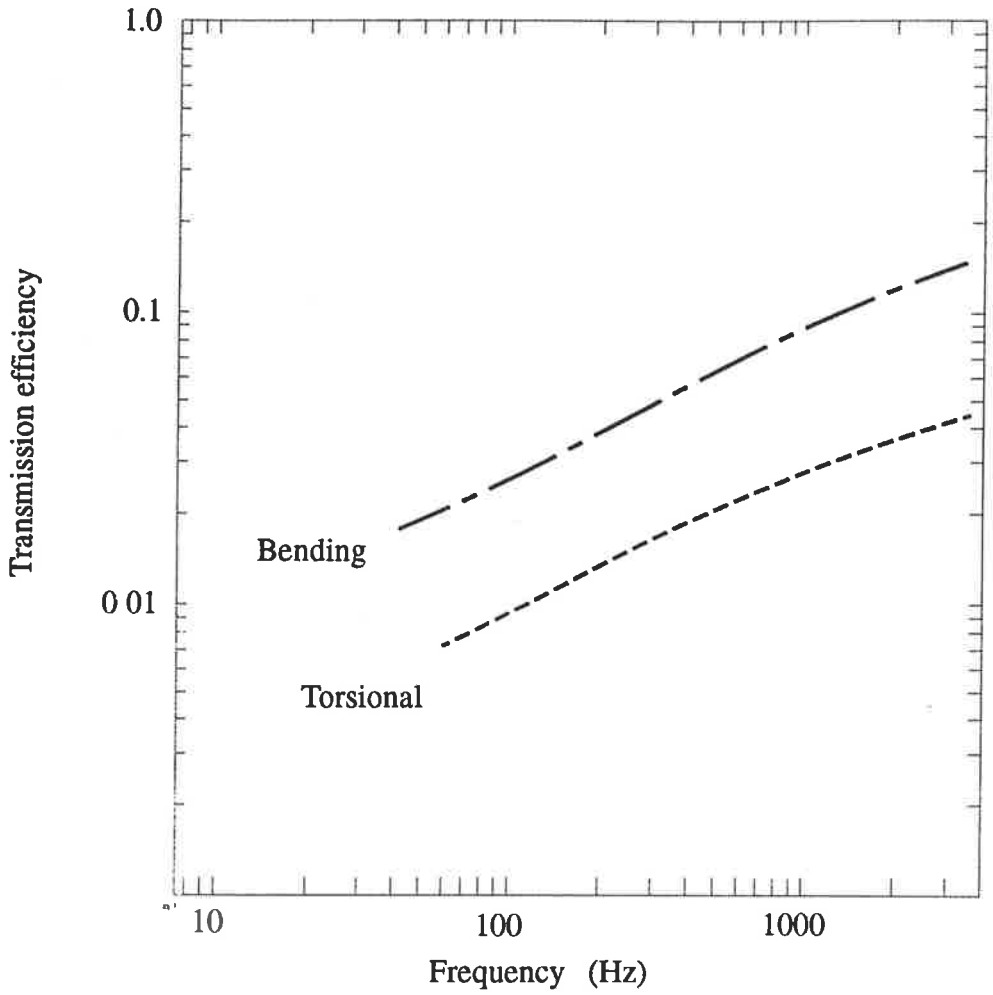

Figure 2.13 Transmission efficiency of beam 2 for an incident bending wave in beam 1.

— – — , bending wave in the z_p- x_p plane;

- - - - - - - , torsional wave.

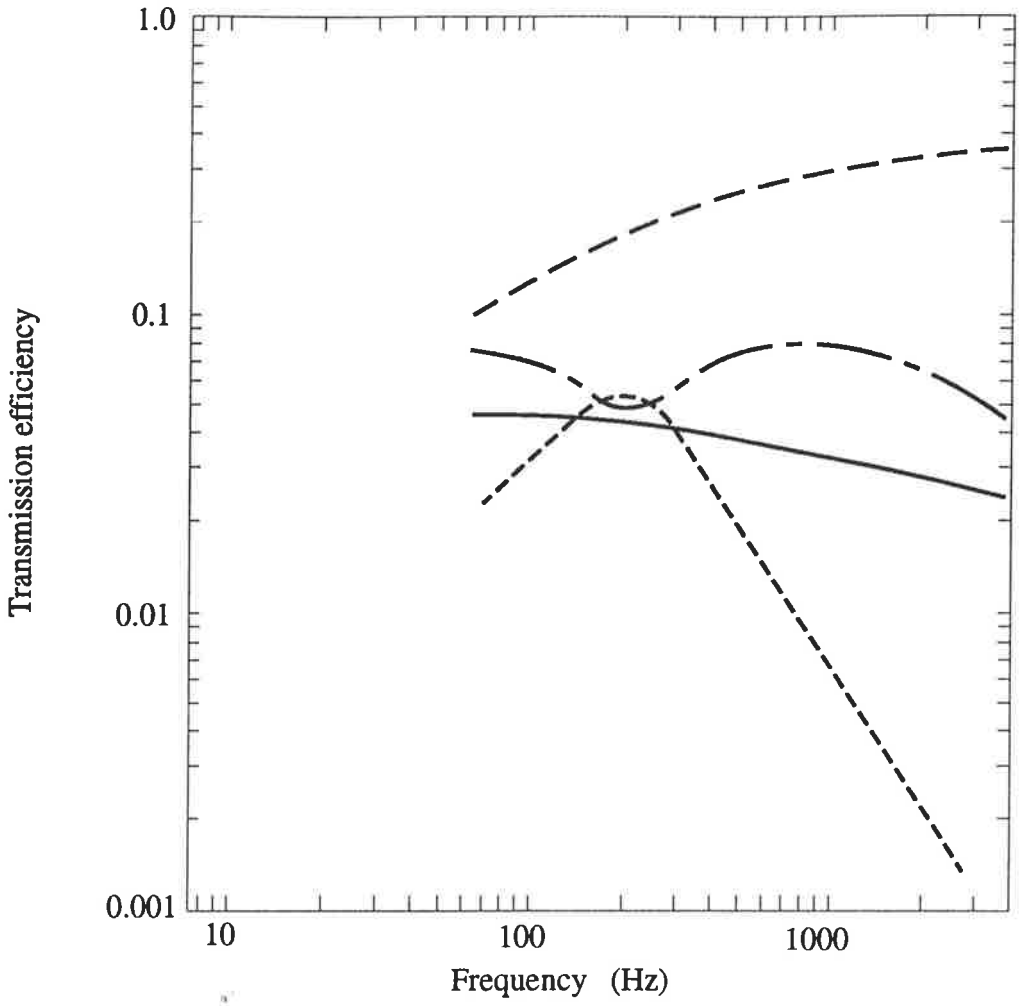

Figure 2.14 Transmission efficiency of beam 3 for an incident bending wave in beam 1.

———— , bending wave in the y_p - x_p plane;

— – — , bending wave in the z_p - x_p plane;

– — – — , longitudinal wave;

------- , torsional wave.

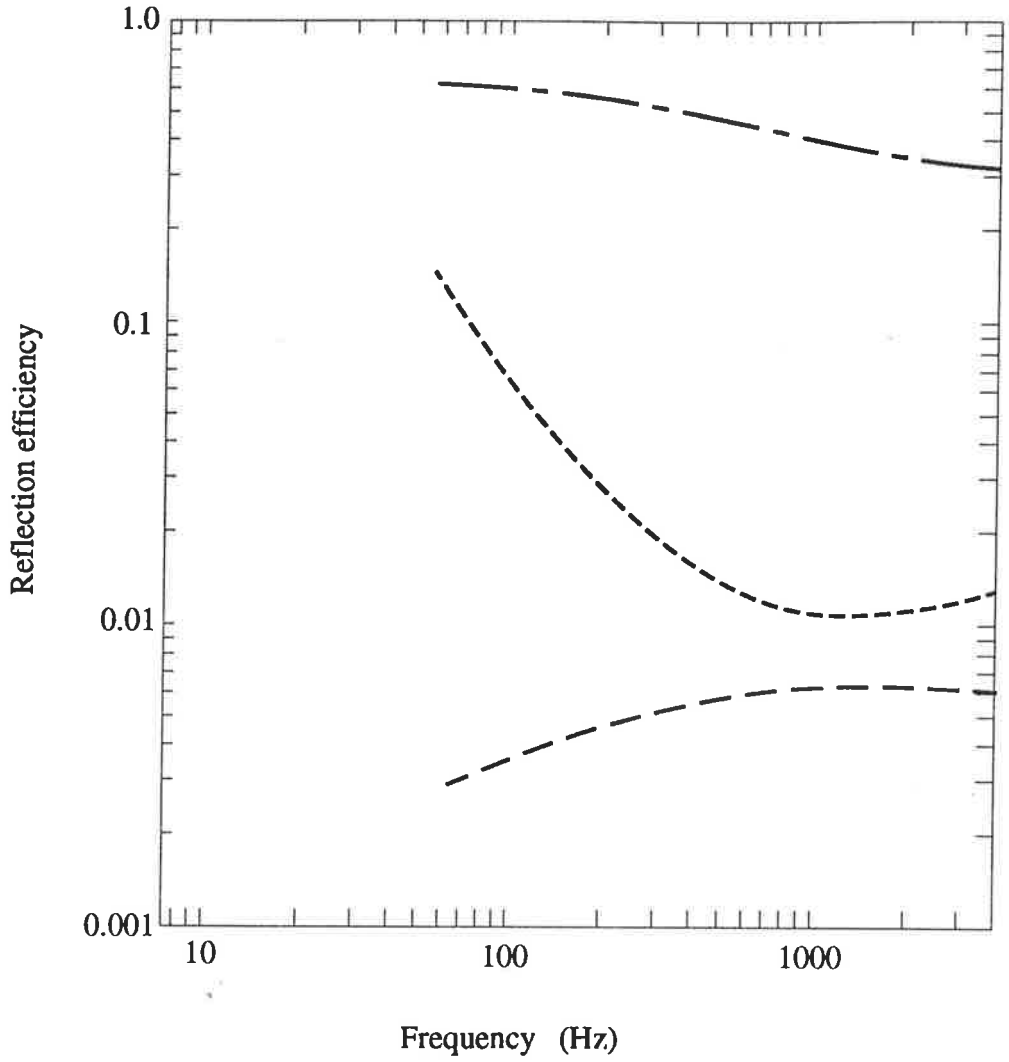

Figure 2.15 Reflection efficiency of beam 1 for an incident bending wave.

——— - ——— , bending wave in the z_p - x_p plane;

— — — — , longitudinal wave;

------- , torsional wave.

To demonstrate the effect of bending - torsional mode coupling, as well as the offset of the attachment point from the shear centre, two additional sets of calculations were performed on this beam junction. First, the centroid of all beam elements was assumed to coincide with the shear centre while all other beam parameters remain unchanged. Second, the attachment point of all beam elements was assumed to coincide with the shear centre, again with all other beam parameters unchanged. A discussion of such effects on wave transmission of bending waves in beam 1 to bending waves in beam 2 is presented here. While the discussion is based on this particular example, it is hoped that it may shed some light on the wave transmission mechanism of general beam junctions. Figure 2.16 shows the bending wave transmission efficiency in the z_r - x_r plane of beam 2 due to an incident bending wave in beam 1. To explain how the offsets of the centroid and attachment point from the shear centre affect the transmission of bending waves, it should be noted that the bending wave in beam 2 is strongly influenced by the torsional component of the incident wave in beam 1. This torsional component consists of two parts, the first part is due to the coupled bending - torsional mode while the second part is due to the offset between the attachment point and the shear centre. With the beam centroid coincident with the shear centre, there is no coupling between the bending and torsional modes in the incident wave. The reduction in the torsional component of the incident wave results in a decrease in the transmission of bending waves to beam 2. In the second case, a shift of the attachment point to the shear centre has a similar effect and for this particular example, it is more significant for bending wave transmission.

2.6.4 Cylinder/annular plate junction

Figure 2.17 shows two semi-infinite thin cylinders coupled rigidly to a finite annular plate at the inside of the cylinders. This example is chosen to coincide with an example discussed by Harari (1977) who treated the discontinuity as a ring stiffener. The physical parameters characterising the cylinders are the same as those of the example considered in Section 2.4. The thickness of the stiffening plate is twice that of the shell and the width of the plate is eight times the thickness of shell. A Type I (see Section 2.4 for a discussion of the types of

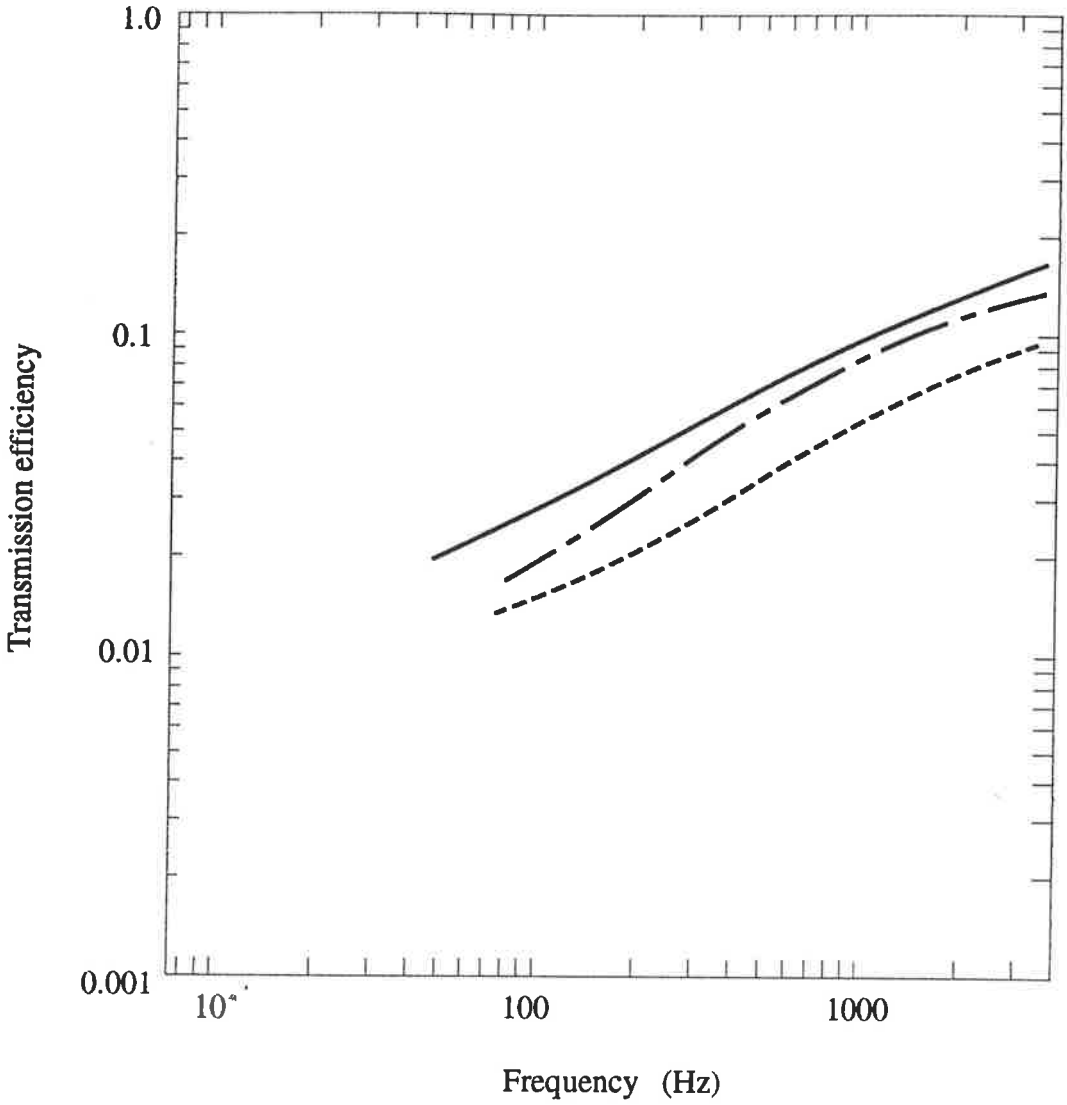

Figure 2.16 Bending wave transmission efficiency of beam 2 for an incident bending wave in beam 1.

———— , transmission efficiency from Figure 2.13;

— - — , centroid coincident with shear centre;

- - - - - - - - , attachment point coincident with shear centre.

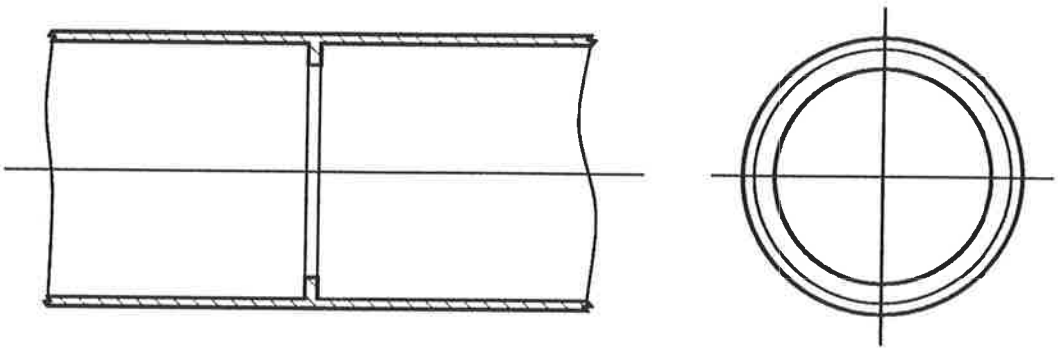

Figure 2.17 Cylinder / annular plate junction.

waves in a cylinder) incident wave is applied to one of the cylinders. Figure 2.18 shows the total transmission efficiency at a circumferential mode number $n = 2$ due to all admissible propagating waves in bending, longitudinal and torsional motions. Despite the difference in approach in calculating the transmission efficiency, the results obtained by using the present method of analysis are in close agreement with those obtained by Harari (1977) who also discussed the effects of the resonance frequencies of the stiffener on vibration transmission. The major discrepancy occurs at the region of total transmission ($\Omega = 0.6 \sim 0.8$) which is likely to be caused by the difference in resonance frequencies between the ring stiffener (the model used by Harari) and the annular plate.

At high frequencies ($\Omega > 1$) where the wavelength is small compared with the radius, a cylindrical shell vibrates in approximately the same way as a flat plate. This is demonstrated in Figure 2.18 where the total transmission efficiency of a beam stiffened plate is calculated and plotted against the frequency parameter. The plate has a width of $2\pi a$ in the y direction and is infinite in both the positive and negative x-directions (see Figure 2.19). It can be thought of as equivalent to a cylinder/annular plate system that is cut along a line parallel to the axis and then flattened so that the junction is a straight line. The incident wave consists of a component 'standing' in the y-direction with two wave cycles (corresponding to a circumferential mode number $n = 2$ in the cylinder) and a component 'propagating' in the positive x-direction. The wave heading angle α is given by :

$$\alpha = \sin^{-1} [n/(a\, k_{pB})], \tag{2.6}$$

where n is the circumferential mode number, a is the mean cylinder radius and k_{pB} is the bending wave number of the equivalent plate. The transmission efficiency of the plate/beam system is calculated according to the method outlined in Section 2.1. It should be noted that the wave heading angle α decreases as the frequency increases.

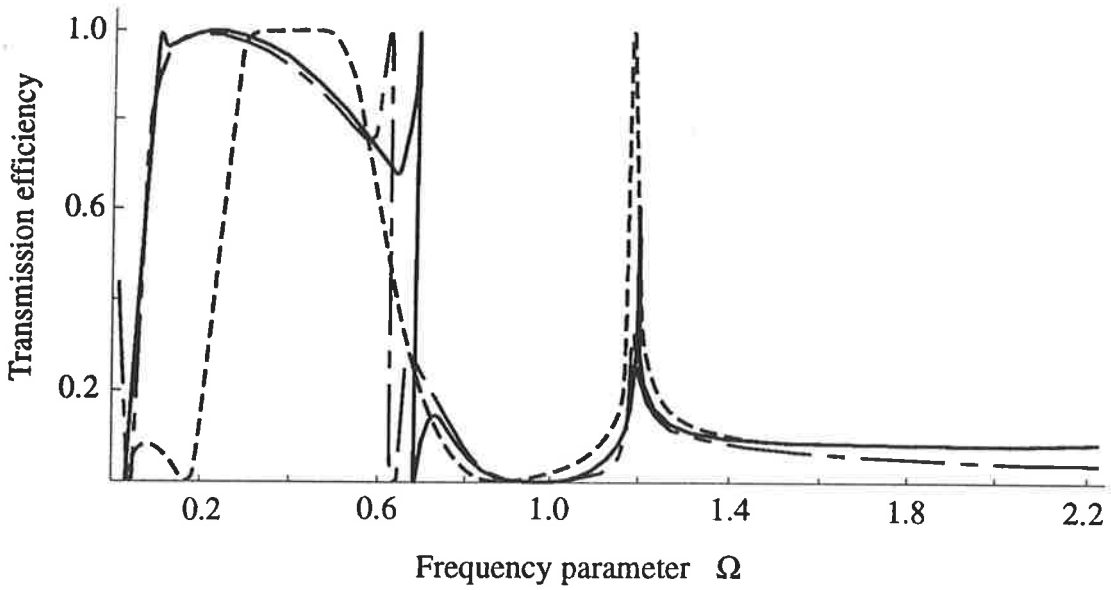

Figure 2.18 Total transmission efficiency due to an incident type I wave.

——————— , cylinder / annular plate junction;

- - - - - - - - , equivalent plate / beam junction;

——— - ——— , Harari (1977).

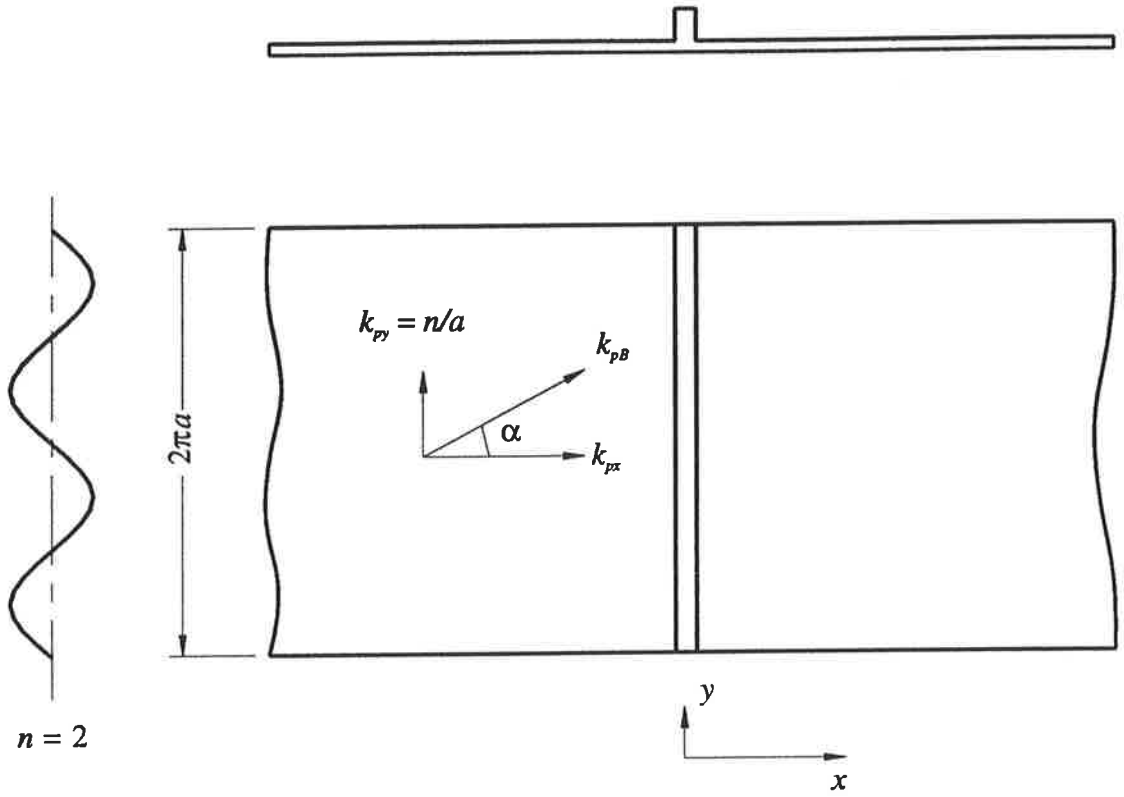

Figure 2.19 Equivalent plate / beam junction.

From Figure 2.18, it can be seen that the plate/beam system shows a region of total transmission between a frequency parameter Ω of approximately 0.3 ~ 0.5, followed by a point of total reflection at $\Omega = 0.9$. As the frequency increases, the shear wave cuts on at $\Omega = 1.183$ and results in a sudden increase in the transmission efficiency. A similar behaviour can be observed in Figure 2.18 for the cylindrical shell where the Type II wave cuts on at approximately the same frequency. Above a frequency parameter Ω of 1.4, there is no significant difference between the total transmission efficiency of the cylinder and flat plate.

2.6.5 Cylinder/circular plate junction

This example consists of a thin solid circular plate coupled to the inside of two semi-infinite cylinders (as for Figure 2.17 but with the annular plate replaced by a solid circular plate). The cylinder parameters are the same as for the previous example and the thickness of plate is the same as that of the shell. Figure 2.20 shows the total transmission efficiency for an incident Type I wave and circumferential mode number $n = 2$. Regions of peak transmission efficiency due to the resonance effects of the circular plate can be observed. The bending resonance frequencies of the plate with two nodal diameters and various nodal circles were calculated and plotted in Figure 2.20 as f_k (k = number of nodal circles). It can be seen that the regions of peak transmission efficiency are closely related to the plate resonance frequencies above a nodal circle of three (see Allwright *et al.*, 1994, for a detailed discussion of the relationship between the plate resonance frequencies and wave transmission).

2.6.6 Cylinder/infinite plate junction

As a final example, transmission efficiency calculations were performed for a semi-infinite cylinder coupled to an infinite plate at the outside of the cylinder. Figure 2.21 shows the transmission efficiencies due to bending, longitudinal and shear motions of the plate with a circumferential mode number $n = 2$ and an incident Type I wave in the cylinder. It can be observed from Figure 2.21a that a significant amount of shear power is transmitted below the

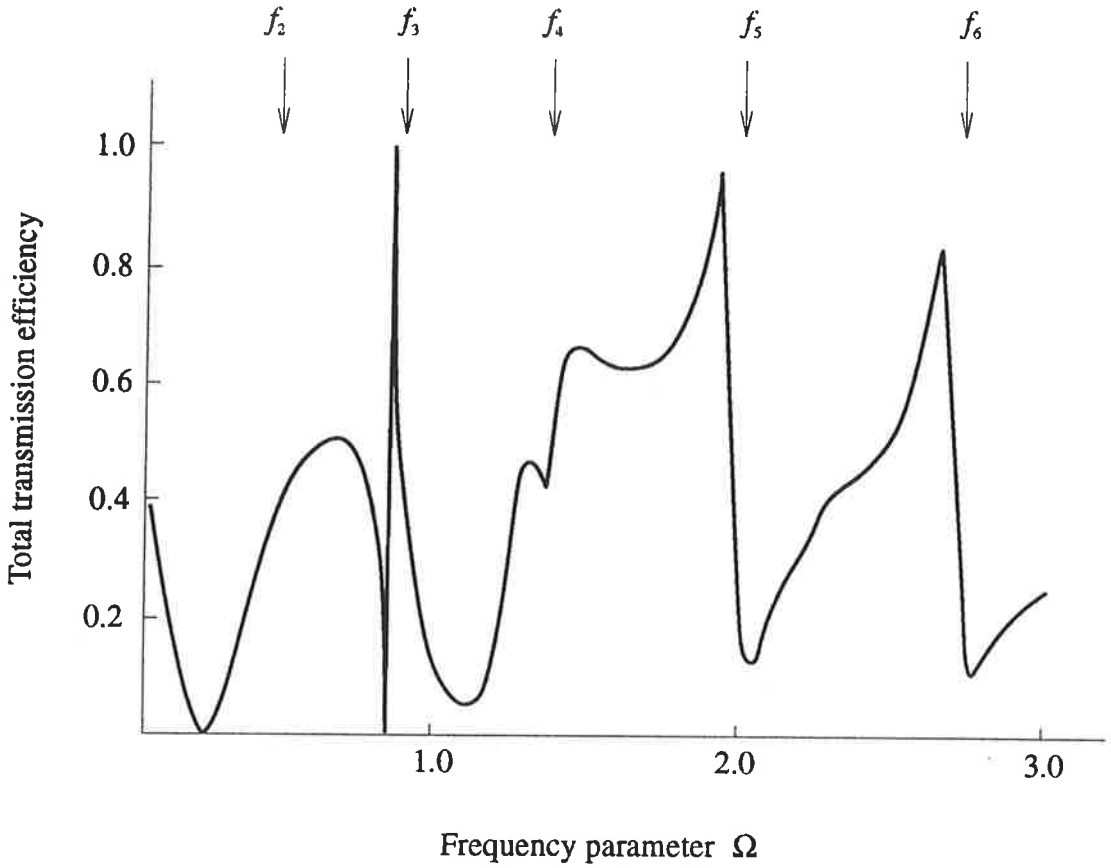

Figure 2.20 Total transmission efficiency of a cylinder / circular plate junction. f_2 ..... f_6 are the bending resonance frequencies of the circular plate.

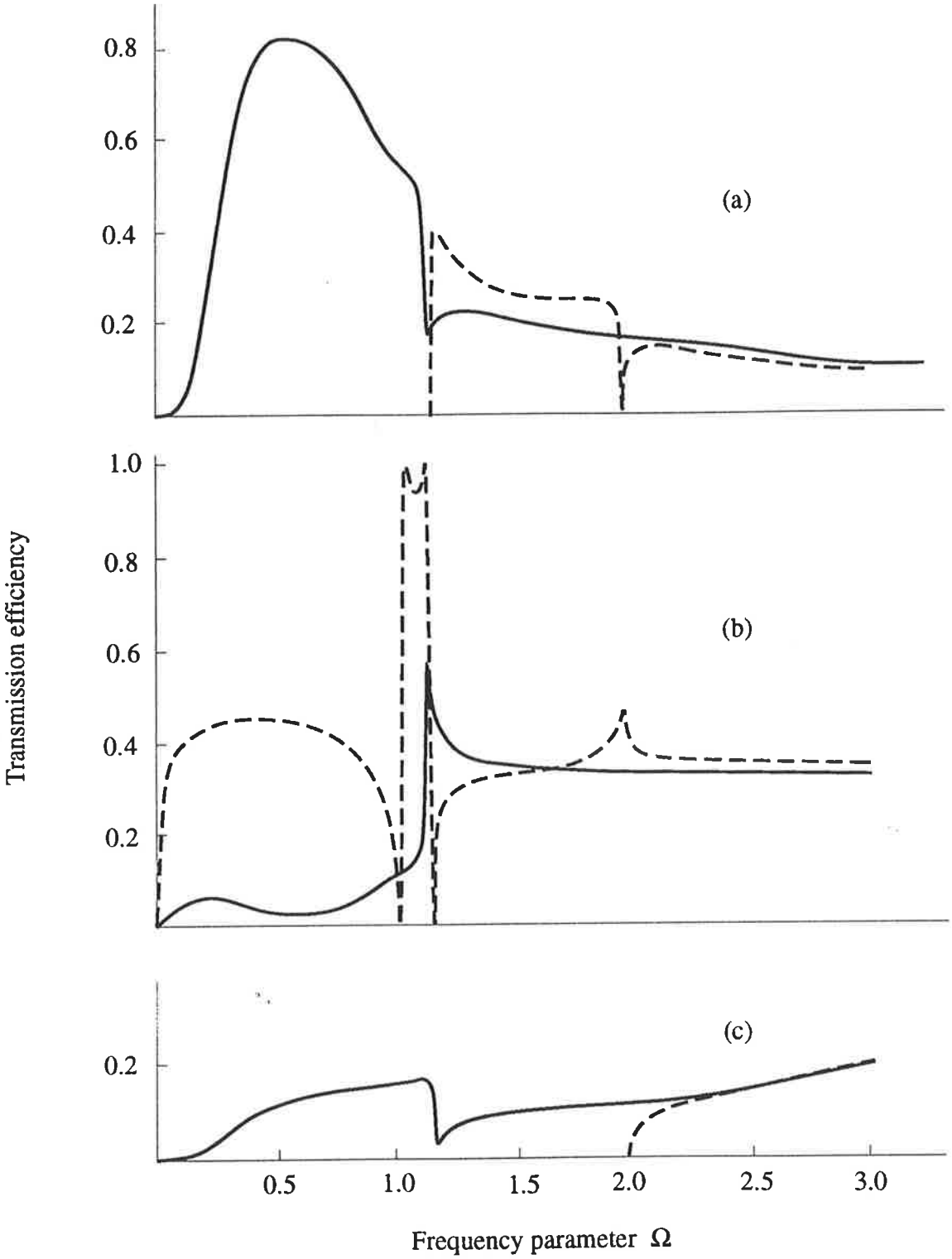

Figure 2.21 Transmission efficiency for (a) shear, (b) bending and (c) longitudinal wave motion in the plate subjected to a type I incident wave in the cylinder with a circumferential mode number n=2.

———— , cylinder / infinite plate junction;

- - - - - - , equivalent plate / plate junction.

cut-on frequency of the Type II wave ($\Omega < 1.18$). This is due to the component of circumferential motion in the Type I wave, coupled with the fact that the plate has a much higher shear rigidity than bending, so that a moderate value of circumferential wave amplitude will result in a considerable amount of shear power being transmitted. The cut-on of the Type II wave is followed by a sharp increase in bending power (see Figure 2.21b) because the Type II wave has a large axial component at low frequencies that is readily transmitted into bending motion in the plate.

As a comparison, the transmission efficiencies of a right angled two plate junction in bending, longitudinal and shear motions were calculated and plotted in Figure 2.21. The source plate has a width equal to the circumference of the cylinder and the receiving plate is semi-infinite. The source plate is subjected to an incident bending wave with the heading angle α given by equation (2.6). The shear wave and longitudinal wave can propagate only in the plates above a cut-on frequency which is related to the wave heading angle by (see Cremer *et al.*, 1988):

$$k_{pT}/k_{pB} = \sin\alpha\,; \quad k_{pL}/k_{pB} = \sin\alpha\,, \tag{2.7a, b}$$

where k_{pL} and k_{pT} are the wave numbers for longitudinal and shear waves in the plate respectively. The cut-on frequencies correspond to a frequency parameter $\Omega = 1.183$ and 2.0 for the shear wave and longitudinal wave respectively. After the cut-on of the longitudinal wave, the wave transmission properties of the cylinder are approximately the same as those of a flat plate.

The transmission efficiencies of the same cylinder/plate and plate/plate junctions with a circumferential mode number $n = 1$ are shown in Figure 2.22. The cut-on frequencies of the longitudinal and shear waves now occur at half the values as those of the previous case. However, the general shapes of the transmission efficiency plots for the two cases are similar. Both the cylinder/plate and plate/plate junctions show approximately the same transmission efficiency at high frequencies after the cut-on of the longitudinal wave.

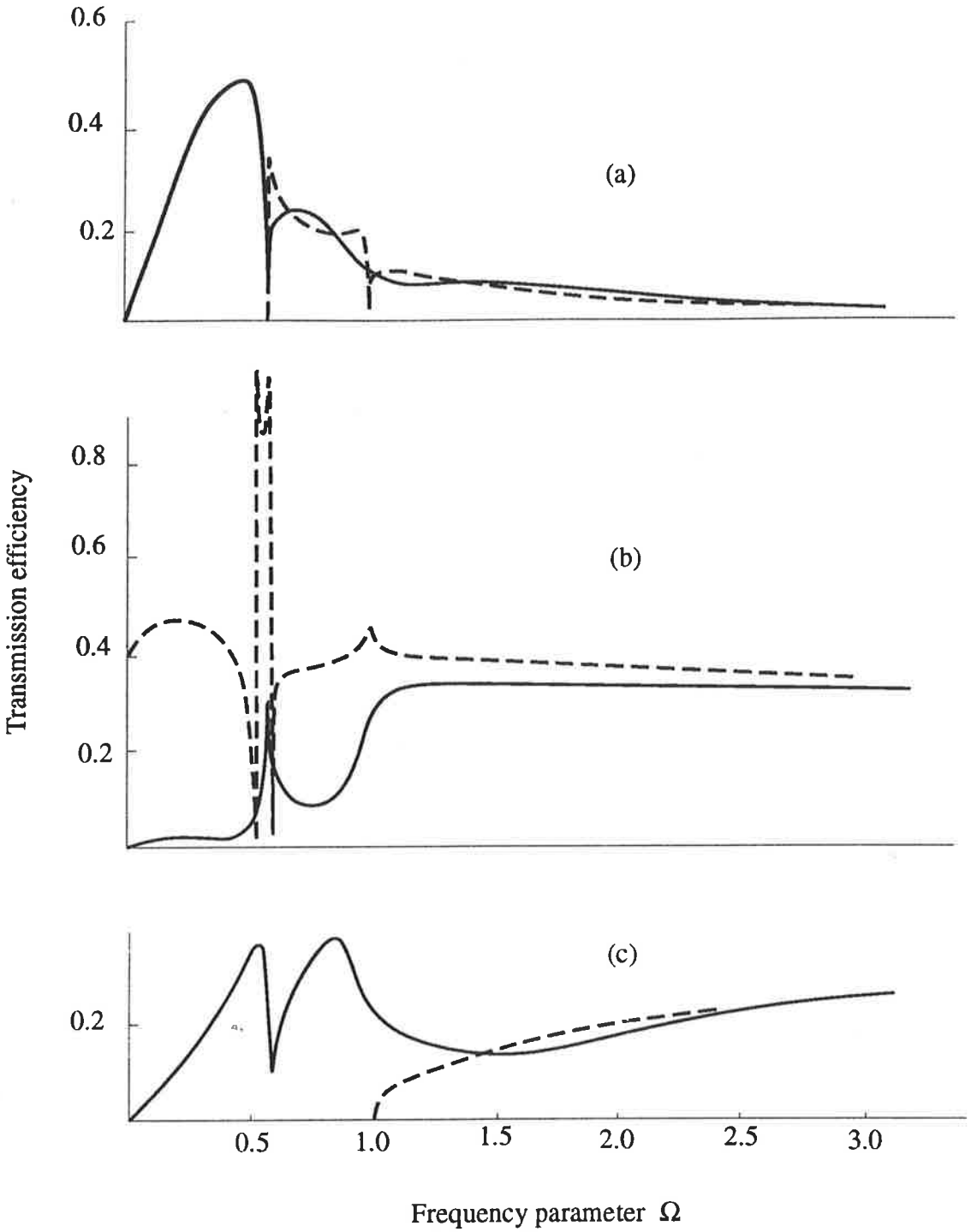

Figure 2.22 Transmission efficiency for (a) shear, (b) bending and (c) longitudinal wave motion in the plate subjected to a type I incident wave in the cylinder with a circumferential mode number $n = 1$.

———— , cylinder / infinite plate junction;

– – – – – – , equivalent plate / plate junction.

2.7 Summary

The analysis presented in this chapter dealt with the vibratory power flow through structural junctions that consisted of elements of semi-infinite extent. Detailed studies on three types of structural junctions were presented; they included :- plate elements coupled to a thin rectangular section beam, three-dimensional beam junctions and cylinder/plate junctions. The effects of mode conversion at a junction (for example, from bending wave to longitudinal and shear waves in a plate/beam junction), together with the coupling between different vibration modes in an element (for example, the bending and torsional mode coupling in a beam element) were fully accounted for. Particular attention was given to the effect of cross sectional deformation of stiffening elements in a junction due to vibration. Such an effect is significant in junctions that characterise naval ship structures as demonstrated in Section 2.6.1 of this chapter.

Although the preceding analysis provided an insight into the transmission of different wave types through structural junctions, the analysis is limited to elements of semi-infinite extent coupled at a single junction. Real structures differ from this idealised consideration in that they are finite in extent and are characterised by multiple junctions. The next two chapters consider respectively the wave propagation in periodic structures and the application of SEA to study vibration transmission in complex built-up structures. The work presented in this chapter is used as a basis for the analysis of periodic structures and the evaluation of coupling loss factors in SEA studies.

CHAPTER 3

COUPLED PERIODIC STRUCTURES

3.1 Introduction

Periodic structures are used extensively in engineering constructions. Examples of these may be found in many engineering applications such as ship structures (for example, decks, bulkheads and hull structures) where relatively lightweight uniform plates or shells are reinforced by the attachment of stiffeners at regular intervals. The study of wave transmission through periodic structures is an integral part in the overall investigation of noise and vibration transmission through complex built-up structures such as naval ships.

Brillouin (1946) studied the wave motion of a number of periodic systems such as atoms, crystals and transmission lines using the Bloch (or Floquet) theorem. This approach greatly simplifies the analysis by relating the wave solutions in adjacent bays of the system. For a periodically supported beam of infinite extent in bending motion, the Bloch theorem gives the spatial variation of transverse displacement through each bay of the structure as (Mead, 1971):

$$w(x + l) \exp(j\omega t) = \exp(\lambda)\, w(x) \exp(j\omega t), \tag{3.1}$$

where l is the length of an element in the periodic structure and λ is the propagation constant. If the propagation constant is purely imaginary, the bending wave will travel freely in the periodic structure. The frequency band in which wave propagation occurs is referred to as the pass band. On the other hand, if the propagation constant contains a real component, the bending wave will behave in an evanescent manner and the corresponding frequency band is referred to as the stop band.

The wave transmission properties of a large number of periodic structures (for example, beams, plates and shells) have been studied extensively (see, for example, Heckl, 1964; Mead, 1971; Mead and Bardell, 1986, 1987 and Langley, 1991). However, periodic structures are often coupled to other structural elements and the transmission of vibration through such coupled structures has received less attention. The present study is concerned with the transmission of vibratory power through coupled periodic structures and the application of SEA for response prediction of such structures.

In this chapter, the wave transmission properties of a plate with periodic stiffeners are analysed following the work of Mead (1971). The stiffened plate is then coupled to a uniform plate at right angles (both of semi-infinite extent) and the transmission efficiency of this coupled structure is investigated based on the method described in Chapter 2.

3.2 Wave Transmission Through a Plate with Periodic Stiffeners

To demonstrate the effects of pass and stop bands on the wave transmission properties of periodic structures, a simple structure which consists of stiffening beams attached symmetrically to both sides of the plate is chosen for the analysis (see Figure 3.1). This arrangement avoids the generation of in-plane waves in the plate/beam junction. The bending wave displacement of the plate may be obtained in a similar way as was done by Mead (1971) in his treatment of a periodically supported beam, except that in this case the bending wave number has components in both the x - and y - directions due to the nature of the oblique wave. A detailed analysis of the plate with periodic stiffeners is given in Appendix 5. This section outlines the procedures and results of the analysis.

For an arbitrary bay i ($i = 0, 1, 2, 3, \ldots \infty$), the plate displacement is given by:

$$w(x_i) = \exp(\lambda i) \{ \sum_{m=1}^{4} A_m \exp(k_{mx} x_i) \} \exp(k_y y + j\omega t), \qquad (3.2)$$

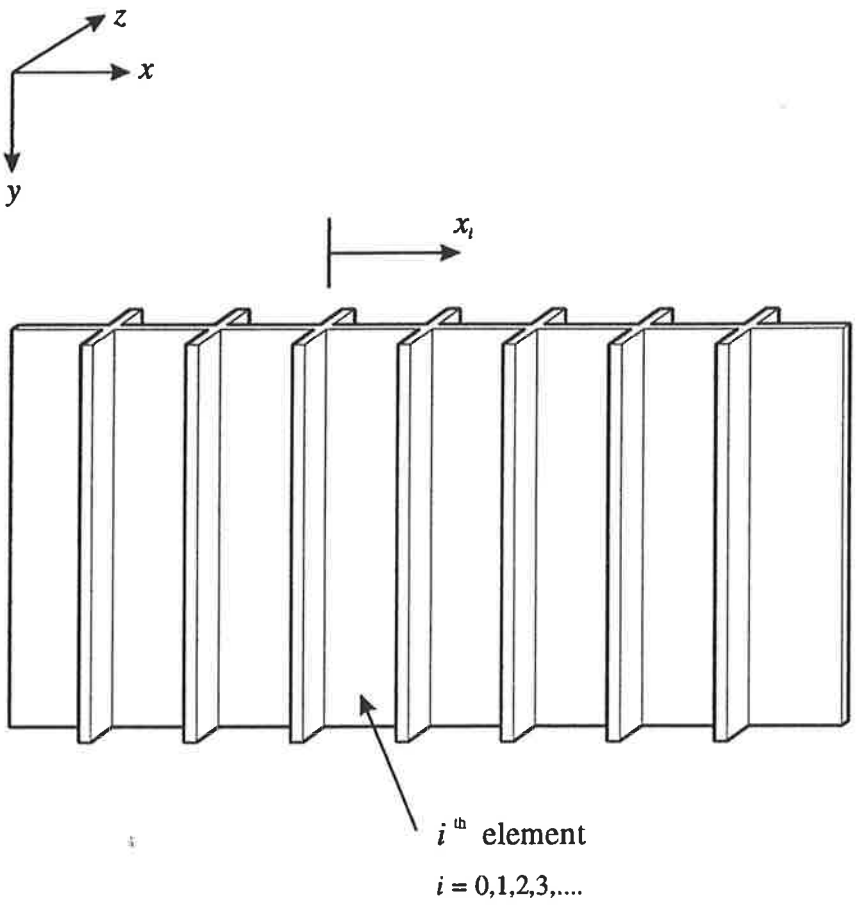

Figure 3.1 A plate with periodic beam stiffeners.

where l is the stiffener spacing, $x_i = x - i\,l$, k_{mx} is the root of the dispersion equation for plate bending and A_m is the associated wave amplitude. The last exponential factor on the right hand side of equation (3.2) represents the y - direction dependency and time dependency of the wave amplitude.

Applying the compatibility and equilibrium conditions to two adjacent bays of the structure, the following matrix equation can be obtained :

$$\Lambda\,[A_m] = \exp(\lambda)\,[A_m], \tag{3.3}$$

where $m = 1....4$, Λ is a 4×4 matrix defined by the system parameters and $[A_m]$ is a column vector representing the wave amplitudes.

Thus the analysis of wave propagation through a periodic structure may be reduced to a standard eigenvalue form. The four eigenvalues exist in two pairs, one of each pair being the reciprocal of the other, indicating the propagation of waves in both the positive and negative directions. The eigenvector which corresponds to each eigenvalue may be normalised to give $[1, A_2/A_1, A_3/A_1, A_4/A_1]^T$.

As an example, the wave transmission properties of the plate with periodic stiffeners shown in Figure 3.1 were evaluated in terms of the wave heading angle and frequency. The plate and beam materials are steel with a elastic modulus of 1.95×10^{11} N/m^2, density of 7700 kg/m^3 and Poisson's ratio of 0.3. The thickness of plate is 2 mm and the beams are 6 × 14 mm sections spaced at 100 mm apart. Figure 3.2 shows the propagation and attenuation zones of the structure. At normal incidence (zero wave heading angle), the first four stop bands lie within a frequency range of 359 - 483 Hz, 1535 - 1884 Hz, 3598 - 4048 Hz and 6591 - 6730 Hz.

The wave transmission through two-dimensional elements such as plates with periodic stiffeners differs from that through one-dimensional elements in that the former is dependent

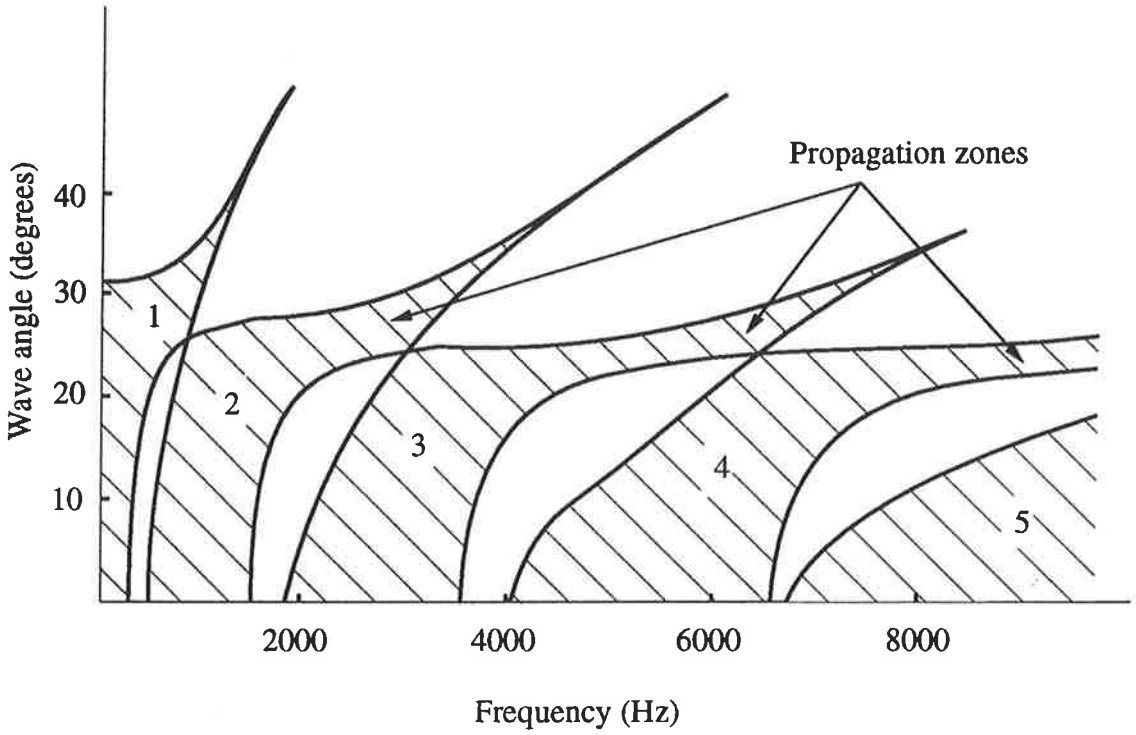

Figure 3.2 Propagation and attenuation zones of a plate with periodic stiffeners.

on the wave heading angle and frequency. Consider a beam stiffened plate subjected to a diffuse vibration wave field. The incident wave will find a range of angles that transmit the wave freely and therefore two-dimensional elements do not normally exhibit a single pass or stop band at a particular frequency as is the case for one-dimensional periodic structures. This may explain the good agreement between experimental results on coupled plate structures with periodic stiffeners and SEA predictions using uniform plate theory as reported by Ødegaard Jensen (1978). However, the complex nature of wave transmission through coupled periodic structures and its effect on SEA modelling warrants a more detailed investigation and this is outlined in the next section.

3.3 Coupled Periodic Structure

Figure 3.3 shows a coupled periodic structure which consists of a plate with periodic stiffeners coupled at right angles to a uniform plate. Both plate elements are assumed to be of semi-infinite extent to avoid the complication of wave reflection at the plate edge boundaries. This particular structural junction is chosen on the basis of simplicity as well as its resemblance to many practical engineering structures including naval ship structures. If the uniform plate is considered as the source plate which carries an oblique incident bending wave of wave angle α and unit amplitude, then the out-of-plane displacement for the source plate is given by (see Appendix I for solution to plate bending equation):

$$w_S = \{\exp(\mathrm{j}\, k_{sx} x_S \cos\alpha) + A_S \exp(-\mathrm{j}\, k_{sx} x_S \cos\gamma) + A'_S \exp[-k_{sx} x_S \sqrt{(1+\sin^2\gamma)}]\}$$

$$\times \exp(k_{sy} y + \mathrm{j}\omega t), \qquad (3.4)$$

where A_S and A'_S are the complex wave amplitudes of the travelling and decaying reflected waves respectively, subscript s represents the source plate, and γ is the reflected wave angle which is related to the incident wave angle α through Snell's law (see Appendix 1).

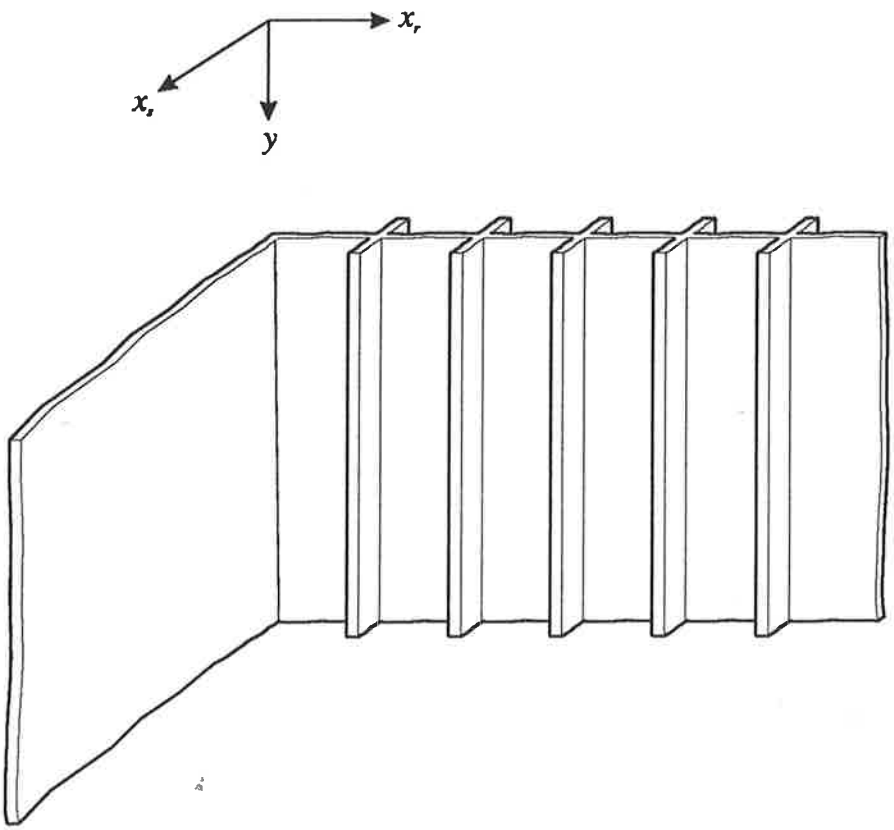

Figure 3.3 A coupled periodic structure.

For the plate with periodic stiffeners (the receiving plate), the out-of-plane displacement due to waves in the positive x- direction may be expressed in terms of two eigenvalues λ_1 and λ_2, together with their associated eigenvectors :

$$w_r = \exp(\lambda_1 i)\{[A_1 \sum_{m=1}^{4}(A_m/A_1)\exp(k_{mx} x_i)] + \exp(\lambda_2 i)[A'_1 \sum_{m=1}^{4}(A'_m/A'_1)\exp(k_{mx} x_i)]\}$$
$$\times \exp(k_y y + j\omega t), \qquad (3.5)$$

where subscript r represents the receiving plate.

The expressions for plate displacements of the coupled structure therefore consist of four unknown wave amplitudes (A_S, A'_S, A_1 and A'_1). If only the bending wave is considered in the analysis, then the boundary conditions can be expressed in terms of the displacements, rotations and moments as shown below:

- the plate displacements at the junction are equal to zero,

$$w_S = 0, \qquad (3.6)$$

$$w_r = 0, \qquad (3.7)$$

- the plate rotations at the junction must be compatible,

$$\partial w_S / \partial x_S = \partial w_r / \partial x_i , \qquad (3.8)$$

- the plate bending moments must be in equilibrium,

$$D_r [\partial^2 w_r / \partial x_i^2 + \mu_r \partial^2 w_r / \partial y^2] + D_S [\partial^2 w_S / \partial x_S^2 + \mu_S \partial^2 w_S / \partial y^2] = 0, \qquad (3.9)$$

where D_r, D_S are the flexural rigidity of the receiving and source plates respectively, and μ_r, μ_S are the Poisson's ratios of the receiving and source plates respectively. All the above

boundary conditions are evaluated at the junction (i.e., $x_S = 0$, $i = 0$ and $x_i = 0$). Solution of the boundary conditions leads to the four complex wave amplitudes and the wave powers and transmission efficiency can be evaluated according to the procedure as described in Section 2.5 of Chapter 2.

3.4 Numerical Example

Calculations of the transmission efficiency were performed on the coupled periodic structure as shown in Figure 3.3. The plate with periodic stiffeners has the same parameters as for the example presented in Section 3.2 of this chapter while the uniform steel plate has a thickness of 2 mm. Figure 3.4 shows the transmission efficiency as a function of the incident wave angle at a frequency of 1000 Hz. The incident angles that allow for free wave propagation are 0 - 26 degrees (propagation zone 2) and 30 - 36 degrees (propagation zone 1). The mean transmission efficiency of the coupled structure was also evaluated as a function of frequency and averaged in one-third octave bands as shown in Figure 3.5. It makes use of the expression presented in Section 2.5 of Chapter 2 with allowance for zero transmission in the attenuation zones. A drop in the transmission efficiency can be observed at band centre frequencies of 1600 Hz, 2000 Hz and 4000 Hz where the wave transmission properties are dominated by the attenuation zones. The application of mean transmission efficiency to evaluate the coupling loss factor for periodic structures is discussed in Section 4.2.2 of Chapter 4. It is interesting to note that for two uniform plates of equal thickness coupled at right angles, the mean transmission efficiency has a constant value (independent of frequency) of 0.333 (Cremer *et al.*, 1988).

3.5 Summary

The analysis of wave transmission in a plate with periodic stiffeners may be reduced to an eigenvalue problem where the eigenvalues represent the propagation constants and the eigenvectors give the complex wave amplitudes. Wave propagation can only exist if the

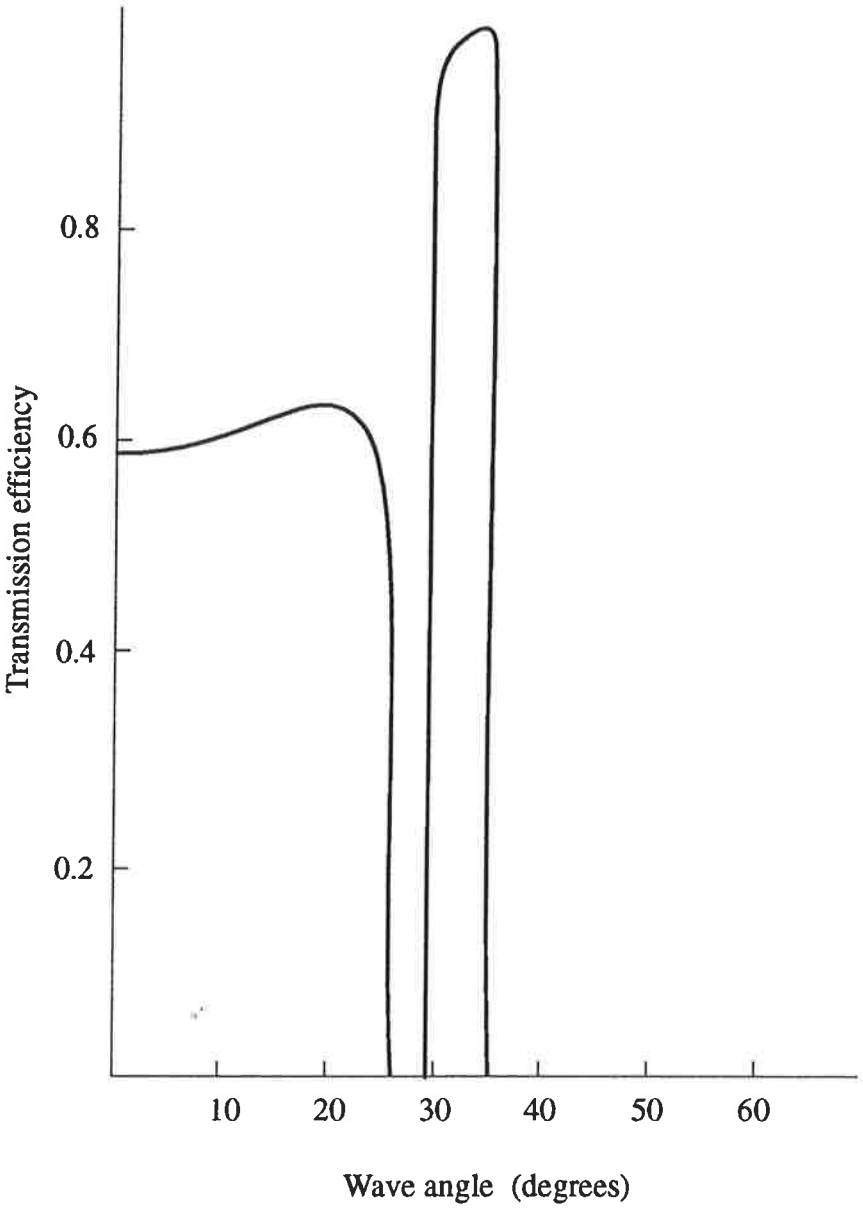

Figure 3.4 Transmission efficiency as a function of the incident wave angle for a uniform plate connected at right angles to a plate with periodic stiffeners.

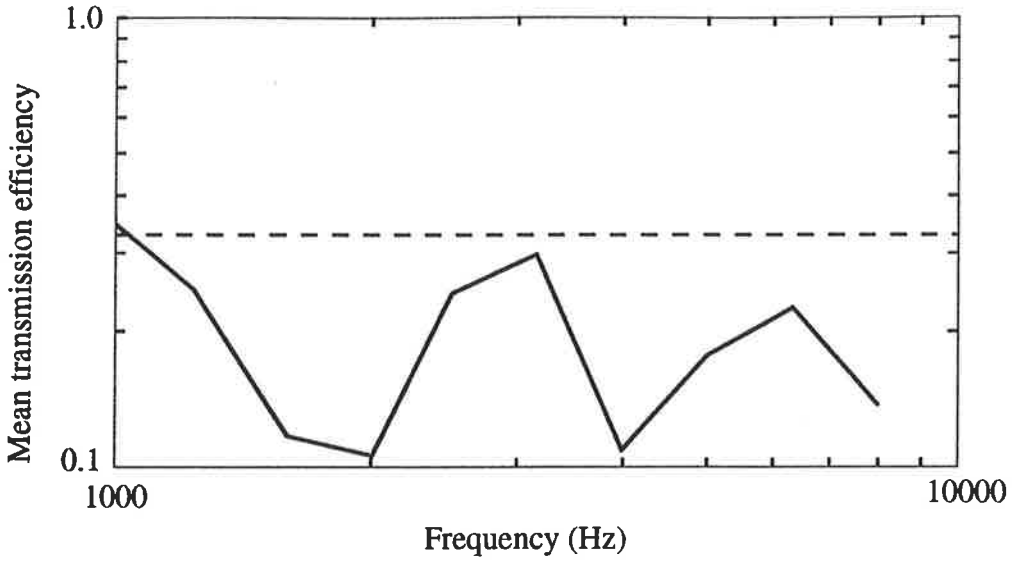

Figure 3.5 Mean transmission efficiency of a coupled periodic structure consisting of a uniform plate coupled to a plate with periodic stiffeners. The mean transmission efficiency of a plate / plate structure is also shown for comparison.

———— , coupled periodic structure;

– – – – – , plate / plate structure.

propagation constant is purely imaginary. The propagation constant of a two-dimensional periodic structure such as a plate with periodic stiffeners is governed by the wave heading angle and the frequency in addition to the physical properties of the structure. For a bending wave propagating in one direction, the wave motion may be expressed in terms of two unknown wave amplitudes, representing the travelling and decaying components in a similar manner as the wave motion in a uniform plate.

Junctions that consist of periodic structural elements may be analysed by using the expressions for wave motion of the individual elements and then applying the boundary conditions at the junction to obtain the wave powers and transmission efficiency. Results from an example structural junction show that the band pass nature of the periodic element has a significant effect on transmission efficiency. The frequency bands which are dominated by the attenuation zones of the periodic element correspond to regions of low transmission efficiency.

CHAPTER 4

COMPLEX BUILT-UP STRUCTURES - THE APPLICATION OF STATISTICAL ENERGY ANALYSIS

4.1 Introduction

4.1.1 General introduction

Chapters 2 and 3 have considered the wave transmission through junctions that consists of uniform or periodic structural elements of semi-infinite extent. The analysis of a real structure is more difficult since it consists of structural elements of finite extent coupled together at a number of junctions. A method known as Statistical Energy Analysis (SEA) has been developed for the analysis of complex built-up structures. SEA is a framework of study for analysing the average vibration levels of interacting elements based on energy flow relationships. This study has its origins in the aero-space industry and was developed by Lyon (1975) and others for the analysis of complex mechanical and acoustical systems, especially at high frequencies, where an exact analysis is difficult because of the large number of modes that have to be considered. With the availability of modern computer technology and numerical methods such as FEM, it would appear that the dynamic response of a large number of complex systems can be solved readily by numerical means. However, experience shows that FEM is very sensitive to system parameters at high frequencies and any uncertainties in system parameters may result in considerable discrepancy between the numerical prediction and actual system response.

In contrast, SEA deals with the average behaviour of complex systems based on the concept of a statistical ensemble of nominally identical systems and does not suffer from the drawback just mentioned (FEM could, in principle, determine the average response by repeating the calculations with a large number of system parameters randomly varied about their nominal

values and then averaging the results, but the computational effort would be prohibitively large for practical engineering structures). The average response is a more reliable indicator at high frequencies since it eliminates the effects of small variations in construction details on system response. In this method, a complex system is considered to be an ensemble average of a set of physically similar systems. The system is then sub-divided into a number of inter-connecting subsystems, usually at locations where the coupling between subsystems may be considered as 'weak' (for example, at structural discontinuities where incident waves are substantially reflected). The subsystems are then modelled as SEA elements, each consisting of a group of resonant modes of the same nature. For example, a uniform plate under bending and in-plane motions may be modelled as two SEA subsystems representing the resonant modes in these two types of motion respectively. The mean energy of the subsystems may be related to the input power by SEA parameters, known as internal loss factors and coupling loss factors, to form a set of linear, power balance equations. Solution of the power balance equations leads to the mean energy level of the individual elements. The fundamental equations of SEA, as well as the basic theory and assumptions concerning the interaction between multi-mode subsystems, are given by Lyon (1975). In addition, review papers on this subject have been presented by Hodges and Woodhouse (1986) and Fahy (1974, 1994).

The work described in this chapter is concerned with the modelling of ship structural elements as SEA subsystems and in particular, the coupling loss factor for cylinder/plate coupled structures and coupled periodic structures. Some of the findings in Chapters 2 and 3 serve as the basis for the development of these SEA parameters.

4.1.2 Power balance equation

Before considering the modelling of ship structural elements as SEA subsystems, it is perhaps useful to review briefly the power balance equation and the determination of SEA parameters. Based on the simplifying assumptions that are normally used for a practical

application of SEA (see, for example, Lyon, 1975), the mean energy of the SEA subsystems may be related to the input power via the following power balance equation:

$$\begin{bmatrix} \langle \Pi_1 \rangle \\ \langle \Pi_2 \rangle \\ \\ \\ \langle \Pi_K \rangle \end{bmatrix} = \omega \begin{bmatrix} (\eta_1 + \sum_{i \neq 1}^{K} \eta_{1i})\, n(\omega)_1, & -\eta_{12}\, n(\omega)_1, & \cdots\cdots & -\eta_{1K}\, n(\omega)_1, \\ -\eta_{21}\, n(\omega)_2, & (\eta_2 + \sum_{i \neq 2}^{K} \eta_{2i})\, n(\omega)_2, & \cdots\cdots & -\eta_{2K}\, n(\omega)_2, \\ \cdots\cdots & \cdots\cdots & \cdots\cdots & \cdots\cdots \\ \cdots\cdots & \cdots\cdots & \cdots\cdots & \cdots\cdots \\ -\eta_{K1}\, n(\omega)_K, & \cdots\cdots & (\eta_K + \sum_{i \neq K}^{K} \eta_{Ki})\, n(\omega)_K, & \end{bmatrix} \begin{bmatrix} \langle E_1 \rangle / n(\omega)_1 \\ \langle E_2 \rangle / n(\omega)_2 \\ \\ \\ \langle E_K \rangle / n(\omega)_K \end{bmatrix} \tag{4.1}$$

where $\langle \Pi_i \rangle$ and $\langle E_i \rangle$ are the time averaged input power and energy in element i respectively, η_i is the internal loss factor of element i, η_{ij} is coupling loss factor between elements i and j, K is total number of subsystems and $n(\omega)_i$ is the modal density of element i. Given the modal densities, internal loss factors, coupling loss factors and input powers, the energy level of individual elements of the system may be evaluated by solving the power balance equation.

4.1.3 Modal density

Since SEA is based on the energy flow between groups of resonant modes, the modal density is effectively a measure of the energy storage capability of a subsystem. For homogeneous elements (for example, uniform plates and beams), the modal density will converge to an asymptotic value regardless of the boundary conditions at high frequencies. The asymptotic modal density expressions for one and two-dimensional elements are given below:

for one-dimensional elements (for example, beams)

$$n(\omega) = l / (\pi c_g), \tag{4.2}$$

for two-dimensional elements (for example, plates)

$$n(\omega) = k A / (2\pi c_g), \tag{4.3}$$

where l and A are the length and area of the element respectively, k is the wave number and c_g is the group velocity.

Other theoretical or empirical expressions for modal density exist for uniform elements such as thin cylinders (see, for example, Szechenyi, 1971 and Hart and Shah, 1971). Langley (1994b) derived modal density expressions for one- and two-dimensional periodic systems based on the derivative of the phase constant (the imaginary part of the propagation constant) with respect to frequency. However, for the majority of structural elements that are not considered to be ideal or homogeneous, theoretical expressions are not normally available and experimental methods may be the only practical means to obtain modal density values. Modal density may be measured by the direct structural mode count technique, but for most SEA applications where the frequency is high, this method is prone to errors since resonant modes are very close to one another in frequency. A more suitable method based on drive point mobility is described by Cremer *et al* (1973) and has been successfully applied by Clarkson and Pope (1981) and Keswick and Norton (1987). The expression for modal density in terms of drive point mobility is given by:

$$n(\omega) = 1/(\omega_2 - \omega_1) \int_{\omega_1}^{\omega_2} 4 \rho_A A \, \mathrm{Re}\,(Y) \, d\omega, \tag{4.4}$$

where ρ_A is the mass per unit area of element and Re (Y) is the real part of point mobility.

4.1.4 Internal loss factor

Internal loss factors of structural elements consist of two components, the material damping and the acoustic radiation damping. Thus, the internal loss factor depends on the material properties as well as the geometry of an element. Unlike the modal density which sometimes may be estimated from theoretical considerations, internal loss factors are generally obtained experimentally by separately measuring the energy dissipation in each of the uncoupled elements. Structural elements are subjected to bending, longitudinal and shear waves. Thus, there are three loss factors which pertain to the three wave types for each element. In practice, it is the bending wave internal loss factor that is of main concern in SEA studies, not only because it is most important with respect to sound radiation, but also because bending waves can be excited easily for a practical measurement of the internal loss factor without causing other wave types to be generated simultaneously. The internal loss factors for longitudinal and shear waves are sometimes estimated as a certain percentage of the bending wave value depending on the geometry and material properties of the element.

A commonly used method for measuring the band-averaged internal loss factor involves exciting the element by a random force with a flat spectral density in the frequency band of interest. The force is then cut off and the decay of response is noted. The internal loss factor may be deduced from the decay record using the following expression:

$$\eta = 2.2 / (f\ T_{60}), \tag{4.5}$$

where T_{60} is the reverberation time (i.e., the time taken for the response to decay by 60 dB).

Ranky and Clarkson (1983) found that for elements with approximately equal modal internal loss factors in the frequency band, the reverberation time method provides a good estimation

of the band-averaged internal loss factor. However, when groups of modes in the frequency band do not have similar loss factors, the logarithmic decay record is not linear with respect to time and it is difficult to determine the appropriate average value. In this case, the steady state energy balance method gives a better estimation of the internal loss factor. This method requires an accurate measurement of the input power and vibrational energy. The input power may be determined from the force and velocity signals from an impedance head while the vibrational energy for uniform structural elements may be determined from the mass and the spatially-averaged mean square velocity. For non-uniform structures, Lalor (1989) introduced the concept of equivalent mass to evaluate the vibrational energy.

The internal loss factor may be expressed in terms of the input power and vibrational energy as :

$$\eta = \langle \Pi \rangle / (\omega \langle E \rangle). \tag{4.6}$$

For lightly damped elements, care must be taken to ensure that the contact damping introduced by the excitation system is not sufficient to affect the accuracy of measurement. This problem can be eliminated by disconnecting the excitation system from the structure during the vibration decay measurement.

4.1.5 Coupling loss factor

The coupling loss factor (CLF) defines the amount of energy flow from one element to the other and may be evaluated experimentally by measuring the input power as well as the distribution of vibrational energy (see, for example, Bies and Hamid, 1980; Clarkson and Ranky, 1984; and Lalor, 1990). Unfortunately, for most practical engineering structures, the energy in the subsystems is not sensitive to the CLF and as a result, significant errors can occur in the CLF values due to small experimental errors in measuring the energy and power. For this reason, CLFs are often determined theoretically, perhaps with some simplifications to

the structural junction so that a theoretical analysis can be carried out. The method of wave transmission analysis for semi-infinite elements as described in Chapter 2 may be used to determine the CLF provided that there is a sufficient modal overlap (Fahy and Mohammed, 1992; modal overlap is measured by the modal overlap factor which is defined as a product of the modal density, internal loss factor and circular frequency). In this section, the conventional derivation of CLF for two-dimensional subsystems (Lyon, 1975 and Cremer *et al.*, 1988) is briefly reviewed. Consider two coupled two-dimensional elements such as a plate/plate junction, the power transmitted one way from plate i to plate j may be expressed in standard SEA form as:

$$\langle \Pi_{ij} \rangle = \omega \, \eta_{ij} \langle E_i \rangle, \tag{4.7}$$

where η_{ij} is the CLF between plate i and j and $\langle E_i \rangle$ is the time averaged energy of plate i. From wave transmission analysis, the power transmitted to plate j due to an incident wave in plate i with a wave angle α may be expressed as a product of the transmission efficiency and incident power :

$$\langle \Pi_{ij}(\alpha) \rangle = \tau_{ij} \langle \Pi_{inc.}(\alpha) \rangle. \tag{4.8}$$

Under the assumption of a diffuse wave field, the total transmitted power may be written as:

$$\langle \Pi_{ij} \rangle = [\, c_{gi} \, l_c \langle E_i \rangle / (2\pi A_i) \,] \int_{-\pi/2}^{\pi/2} \tau_{ij} \cos\alpha \, d\alpha ,$$

$$= [\, c_{gi} \, l_c \langle E_i \rangle / (\pi A_i) \,] \int_{0}^{1} \tau_{ij} \, d \sin\alpha , \tag{4.9}$$

where l_c is the coupling line length, A_i is the area of plate i and c_{gi} is the group velocity of plate i. From equations (4.7) and (4.9), the CLF becomes:

$$\eta_{ij} = [\, c_{gi}\, l_c / (\pi\, \omega\, A_i)\,] \int_0^1 \tau_{ij}\ \mathrm{d}\sin\alpha\,. \tag{4.10}$$

SEA studies on plate/plate structures using this approach have been presented by Swift (1977) and Tratch (1985). Both studies reported good agreement between calculated and experimental results. Recently, Lyon and DeJong (1995) argued that the energy term $\langle E_i \rangle$ in equation (4.9) should be related to the sum of the incident and reflected powers rather than the incident power alone as stated in equations (4.8) and (4.9). They suggested that the CLF should be expressed in the form:

$$\eta_{ij} = [\, c_{gi}\, l_c / (\pi\, \omega\, A_i)\,] \int_{-\pi/2}^{\pi/2} [\tau_{ij} / (2 - \tau_{ij})] \cos\alpha\ \mathrm{d}\alpha\,. \tag{4.11}$$

However, for most practical structural junctions, the transmission efficiency τ_{ij} is typically an order of magnitude less than two and hence both formulations will give approximately the same value of CLF. The present study follows the conventional approach (equation (4.10)) in the derivation of CLF.

Based on the same reasoning as a plate/plate junction subjected to a diffuse wave field, the CLF for a beam/beam junction may be expressed as:

$$\eta_{ij} = c_{gi}\, \tau_{ij} / (2\, \omega\, l_i), \tag{4.12}$$

where l_i is the length of beam i. The application of travelling wave theory and SEA to study the vibration transmission through a two-dimensional beam network has been reported by Sablik *et al.* (1985) and Moore (1990 b). For general three-dimensional beam networks that consist of beam elements of arbitrary sections, the CLFs may be evaluated from the transmission efficiencies as described in Section 2.3 of Chapter 2.

4.2 SEA Modelling of Ship Structures

4.2.1 CLF for a cylinder/plate coupled structure

A number of researchers have studied plate/plate coupled structures using SEA (for example, Hwang and Pi, 1973; Swift, 1977 and Tratch, 1985) and derived the CLFs on the assumption that the wave field in each subsystem is diffuse. The concept of a diffuse wave field poses no difficulty for isotropic elements like uniform flat plates but is less clear from an SEA point of view for non-isotropic elements like curved plates and cylinders. Langley (1994a) pointed out that the assumption of a diffuse wave field is equivalent to the equipartition of energy amongst the resonant modes for an isotropic element. He then derived the CLFs for structural junctions between curved plates based on the modal concept of equipartition of energy. In this Section, the modal concept is extended to a cylindrical shell coupled to an end plate. The plate is assumed to have a hole cut out to accept the cylinder. This arrangement enables the results to be compared with those of an equivalent plate/plate structure.

Before proceeding to formulate the CLF, it is perhaps worthwhile to review briefly the wave propagation characteristics of a cylindrical shell. As mentioned in Section 2.4 of Chapter 2, a cylindrical shell is subjected to three types of waves, often classified as Type I, II and III, and the behaviour of these waves depends strongly on the frequency of vibration. Above the ring frequency, the response of the cylinder is similar to that of a flat plate and the three types of waves in the cylinder (i.e., Type I, II and III) are therefore similar to the bending, shear and longitudinal waves respectively in a flat plate. However, the response of a cylinder below the ring frequency is strongly influenced by the effect of curvature which couples the cylinder displacements in the radial, circumferential and longitudinal directions. A measure of the degree of coupling of cylinder displacements is given by the amplitude ratios U/W and V/W, where U, V and W are the displacement amplitudes in the longitudinal, circumferential and radial directions. The amplitude ratios are functions of the frequency and the circumferential mode number n. A detailed discussion of the displacement characteristics of propagating

waves in a cylindrical shell is given by Smith (1955) where he shows that the Type I wave cuts on at a progressively higher frequency as the circumferential mode number is increased, together with lower amplitude ratios *U/W* and *V/W*. Thus the Type I wave has a higher radial component as the circumferential mode number is increased. Since the response of a cylinder may be considered as a superposition of each of the allowable circumferential modes at a particular frequency, it is argued that for a cylindrical shell having a response dominated by high order circumferential modes, the total response due to a Type I wave is dominated by the out-of-plane motion. The response of a thin cylindrical shell will be further discussed in Section 5.2.2 of Chapter 5 where different methods for the measurement of loss factor are investigated.

When a cylindrical shell is coupled to an end plate, a Type I wave will generate bending and in-plane waves in the plate element. The significance of in-plane waves in the transmission of vibration has been investigated by Tratch (1985) where he studied a number of coupled plate structures with different levels of complexity (from two to twelve coupled plates). He found that the in-plane waves act as 'flanking paths' for the bending motion and increase the energy transmission for complex structures which consist of more than two structural elements. However, for a simple structure with only two structural elements, as is the case for the present study, the in-plane waves generated in the elements have little effect on the flexural energy level.

It follows from the preceding discussion that the transmission of vibration through a cylinder/plate coupled structure is dominated by the out-of-plane motion and as a result, only such motion is considered in the present study. By modelling the cylindrical shell as a number of wave components representing each of the circumferential modes, the power loss by the cylinder due to coupling to the plate may be expressed as (Cremer *et al.*, 1988):

$$\langle \Pi_{cp} \rangle = (l_c / A_c) \sum_{n=0}^{N} \langle E_{cn} \rangle c_{gcn} \tau_{cpn} , \qquad (4.13)$$

where l_c is the coupling line length, A_c is the surface area of cylinder, n is the circumferential mode number, N is the number of modes, $<E_{cn}>$ is the energy of the cylinder for the n^{th} mode, c_{gcn} is the group velocity of the cylinder for the n^{th} mode and τ_{cpn} is the transmission efficiency between the cylinder and plate for the n^{th} mode when the cylinder is subjected to a Type I incident wave. It should be noted that cylindrical waves of the form $\cos(n\theta)$ are generated in the plate due to an incident wave in the cylindrical shell.

The equipartition of subsystem energy amongst resonant modes implies that:

$$<E_{cn}> = <E_c> n(\omega)_{cn} / n(\omega)_c \,, \tag{4.14}$$

where $<E_c>$ is the total energy of the cylinder, $n(\omega)_c$ is the modal density of the cylinder and $n(\omega)_{cn}$ is the modal density of the cylinder for the n^{th} circumferential mode.

Substituting equations (4.14) into (4.13) gives:

$$<\Pi_{cp}> = [l_c <E_c> / A_c n(\omega)_c] \sum_{n=0}^{N} c_{gcn} n(\omega)_{cn} \tau_{cpn} \,. \tag{4.15}$$

The transmitted power $<\Pi_{cp}>$ may be expressed in standard SEA form as :

$$<\Pi_{cp}> = \omega \eta_{cp} <E_c> \,, \tag{4.16}$$

where η_{cp} is the CLF between the cylinder and plate. It follows from equations (4.15) and (4.16) that :

$$\eta_{cp} = [l_c / \omega A_c n(\omega)_c] \sum_{n=0}^{N} c_{gcn} n(\omega)_{cn} \tau_{cpn} \,. \tag{4.17}$$

For a given circumferential mode, the number of resonance frequencies for a cylinder of length l is given by (Hart and Shah, 1971):

$$N(\omega)_{cn} = l\, k_{cn} / \pi, \tag{4.18}$$

and hence the modal density

$$n(\omega)_{cn} = \partial N(\omega)_{cn} / \partial\omega = (l / \pi)\, \partial k_{cn} / \partial\omega = l / \pi\, c_{gcn}\,, \tag{4.19}$$

where k_{cn} is the axial wave number of the cylinder for the n^{th} mode. From equations (4.17) and (4.19), the CLF may now be expressed as:

$$\eta_{cp} = [1 / \omega \pi\ n(\omega)_c] \sum_{n=0}^{N} \tau_{cpn}\,. \tag{4.20}$$

The transmission efficiency for a range of cylinder/plate coupled junctions τ_{cpn} has been derived in Section 4 of Chapter 2 and expressions for modal density of a cylindrical shell $n(\omega)_c$ may be obtained from the published literature (see, for example, Hart and Shah, 1971).

The concept of equipartition of energy amongst resonant modes in a subsystem as presented in the preceding derivation of CLF may be shown to be equivalent to the assumption of a diffuse wave field in an isotropic system. Consider two plates i and j coupled at right angles and subjected to a diffuse vibration field. If plate i is simply supported along two parallel edges l_c apart (see Figure 4.1), the incident wave will consist of a component 'standing' in the y - direction (analogous to the circumferential mode) and a component 'propagating' in the x - direction (analogous to the axial mode of a cylinder). The incident wave angle α may be expressed in terms of the wave number as:

$$\sin\alpha = 2\,\pi\,n / l_c\,k_i. \tag{4.21}$$

It can be observed that the wave angle α can only accept discrete values which are governed by the 'standing' wave in the y - direction (i.e., for n = 1,2,3,...). As a result, the general expression for CLF of a two-dimensional system (equation (4.10)) must be modified by replacing the integration sign with a summation sign. Also, d $\sin\alpha$ from equation (4.10) must be discretised and by using equation (4.21), it can be expressed as 2π / $l_c\,k_i$. The CLF may now be written as:

$$\eta_{ij} = [c_{gi}\,l_c / \omega\,A_i\;\pi]\,[2\,\pi / l_c\,k_i] \sum_{n=0}^{N} \tau_{ijn}. \tag{4.22}$$

Upon noting that the modal density for a two-dimensional system is given by

$$n(\omega)_i = k_i\,A_i / 2\pi\,c_{gi}, \tag{4.23}$$

and substituting the modal density expression into equation (4.22),

$$\eta_{ij} = [1 / \omega\,\pi\,n(\omega)_i] \sum_{n=0}^{N} \tau_{ijn}. \tag{4.24}$$

It can be seen that equation (4.24) is identical to equation (4.20) for a cylinder/plate coupled structure derived under the assumption of equipartition of modal energy. A detailed discussion of this concept is presented by Lyon (1975).

One of the fundamental principles of SEA is that the CLFs must satisfy the requirement of reciprocity as stated below:

$$n(\omega)_p \, \eta_{pc} = n(\omega)_c \, \eta_{cp}, \tag{4.25}$$

and it is important to verify that the preceding analysis satisfies this requirement.

Consider a cylindrical shell coupled to an annular plate with the latter subjected to an out-of-plane incident wave of circumferential dependency of $\cos(n\theta)$ propagating towards the cylinder/plate interface. It can be shown from the asymptotic expansion of the Bessel functions (see, for example, McLachlan, 1955) that the wave amplitude is inversely proportional to the square root of the radius. Since the energy is proportional to the square of the wave amplitude, the energy density of the plate for a given circumferential mode number n may be expressed as:

$$\langle e_n \rangle \propto 1/r,$$

or

$$\langle e_n \rangle = K/r, \tag{4.26}$$

where K is a constant. The energy of the plate can be obtained by integrating the energy density over the entire plate area:

$$\begin{aligned} \langle E_{pn} \rangle &= \int_{r_1}^{r_2} (K/r)\, 2\pi r \, dr, \\ &= 2\pi K (r_2 - r_1), \end{aligned} \tag{4.27}$$

where r_2 and r_1 are the outer and inner radii of the plate respectively. From equations (4.26) and (4.27), the energy density of the plate at the plate/cylinder interface is given by:

$$\langle e_n \rangle = \langle E_{pn} \rangle / [2\pi r_1 (r_2 - r_1)]. \tag{4.28}$$

The wave number of this out-of-plane wave propagating in the radial direction at a circumferential mode number n may be obtained from the asymptotic expansion of the Bessel functions (McLachlan, 1955):

$$k_{pn} = k_p - n\pi/2r - \pi/4r, \tag{4.29}$$

for $k_p r >> 1$ and $k_p r >> n^2$; where k_p is the wave number of the plate. It follows from equation (4.29) that the group velocity of this wave may be expressed as:

$$c_{gpn} = 1/[\partial k_{pn}/\partial\omega]. \tag{4.30}$$

The power transmitted from the plate to the cylinder may now be expressed in terms of the energy density of the plate as:

$$\langle \Pi_{pc} \rangle = l_c \sum_{n=0}^{N} \langle e_n \rangle \tau_{pcn} c_{gpn}. \tag{4.31}$$

From equations (4.28) and (4.31):

$$\langle \Pi_{pc} \rangle = [1/(r_2 - r_1)] \sum_{n=0}^{N} \langle E_{pn} \rangle \tau_{pcn} c_{gpn}, \tag{4.32}$$

By using the assumption of equipartition of energy and the standard SEA expression for CLF (see equations (4.14) and (4.16)), the CLF between the plate and cylinder is given by:

$$\eta_{pc} = [1 / \omega\, n(\omega)_p (r_2 - r_1)] \sum_{n=0}^{N} c_{gpn}\, n(\omega)_{pn}\, \tau_{pcn}. \tag{4.33}$$

For a given order of nodal diameter n, the modal density of the plate may be written as (Hart and Shah, 1971):

$$n(\omega)_{pn} = \partial N(\omega)_{pn} / \partial\omega = [(r_2 - r_1)/\pi]\, \partial k_{pn} / \partial\omega = (r_2 - r_1)/\pi\, c_{gpn}\,, \tag{4.34}$$

Substituting equation (4.34) into (4.33) leads to the following expression for CLF :

$$\eta_{pc} = [1/\omega\pi\, n(\omega)_p] \sum_{n=0}^{N} \tau_{pcn}\,. \tag{4.35}$$

By comparing equation (4.20) with equation (4.35) and noting that the transmission efficiency is symmetric ($\tau_{cpn} = \tau_{pcn}$), it can be seen that the reciprocity requirement is satisfied.

4.2.2 CLF for a coupled periodic structure

The SEA modelling of one-dimensional periodic systems has been considered by Keane and Price (1989) by using a statistical description of the problem where a given deterministic system is regarded as one realisation taken from an infinite set of similar, but not identical systems. A piece-wise constant Probability Density Function (PDF) has been adopted by these authors to model the non-uniform distribution of natural frequencies of a periodic system where the boundaries of high and low probabilities represent the pass and stop bands respectively. This means that the modal density of the periodic system takes on a high level in the pass band and a low level in the stop band. The non-uniform natural frequency PDF has been incorporated into an enhanced SEA model and calculations of the system response in terms of the ensemble average showed a significant improvement over the normal SEA model.

In the present study, the emphasis is focused on the application of wave transmission analysis to evaluate the CLF of a coupled periodic structure which consists of two-dimensional elements (such as plates with periodic stiffeners) rather than the investigation of ensemble average statistics associated with the response of simple, one-dimensional, periodic systems. To this end, an SEA model may be regarded as an ensemble average of an infinite set of

similar systems so that the SEA parameters may be defined in a deterministic manner. To make use of the information gained from the analysis of periodic structures, and at the same time provide a practical solution to the noise and vibration problems of coupled periodic structures, the standard travelling wave analysis procedure is used to evaluate the CLF, with the proviso that wave transmission is not permitted in the attenuation zones in calculating the mean transmission efficiency. This approach allows the salient characteristic of a periodic system (i.e., the existence of propagation and attenuation zones) to be incorporated into the standard CLF formulation. Consider an example structure which consists of a uniform plate coupled to a plate with periodic stiffeners as shown in Figure 3.3 of Chapter 3. The CLF can be obtained from the standard expression for two-dimensional systems (equation (4.10)) together with the appropriate mean transmission efficiency as presented in Chapter 3. It can be shown that the present formulation of CLF satisfies the reciprocity requirement by representing both plate elements as an assembly of one-dimensional components corresponding to each of their standing waves in the y-direction (see Sections 2.6.4 and 4.2.1 where the response of a cylindrical shell is modelled as a plate element subjected to a combination of standing and travelling waves). The derivation procedure for reciprocity is similar to that of a cylinder/plate structure as outlined in Section 4.2.1. Considering the transmission of vibratory power from the plate with periodic stiffeners (subsystem i) to the uniform plate (subsystem j), by using the assumption of equipartition of subsystem energy amongst all resonant modes, the CLF can be expressed as (see the derivation of equation (4.17) in Section 4.2.1):

$$\eta_{ij} = [l_c / \omega A_i n(\omega)_i] \sum_{n=0}^{N} c_{gin} n(\omega)_{in} \tau_{ijn} . \tag{4.36}$$

For a given standing wave, the modal density of the one-dimensional component of the plate with periodic stiffeners is given by (Langley, 1994b) :

$$n(\omega)_{in} = lK_p / (\pi c_{gin}), \tag{4.37}$$

where l is the length of each element of the periodic plate structure in the x-direction, K_p is the number of elements and c_{gin} is the group velocity of the one-dimensional component.

From equations (4.36) and (4.37), the CLF between subsystems i and j can be expressed as:

$$\eta_{ij} = [1 / \omega \pi n(\omega)_i] \sum_{n=0}^{N} \tau_{ijn}. \tag{4.38}$$

Similarly, the CLF between subsystems j and i is given by:

$$\eta_{ji} = [1 / \omega \pi n(\omega)_j] \sum_{n=0}^{N} \tau_{jin}. \tag{4.39}$$

It is evident from equations (4.38) and (4.39) that the reciprocity condition is satisfied.

4.3 Numerical Examples

4.3.1 Cylinder/plate coupled structure

Calculations were performed on the CLFs of three steel cylinders each coupled to a 2 mm thick steel end plate. The shell thicknesses of the three cylinders are 0.5, 1.0 and 2.0 mm respectively. The length and mean diameter of all cylinders are chosen as 0.8 m and 0.45 m respectively to coincide with an example structure for an experimental investigation which is described in Chapter 5. Figure 4.1 shows the CLFs of the three cylinder/plate structures. The CLFs of their corresponding equivalent plate/plate structure based on a diffuse bending wave field are also plotted in the figure for comparison. The source plates are assumed to have the same surface area and thickness as those of their corresponding cylindrical shells.

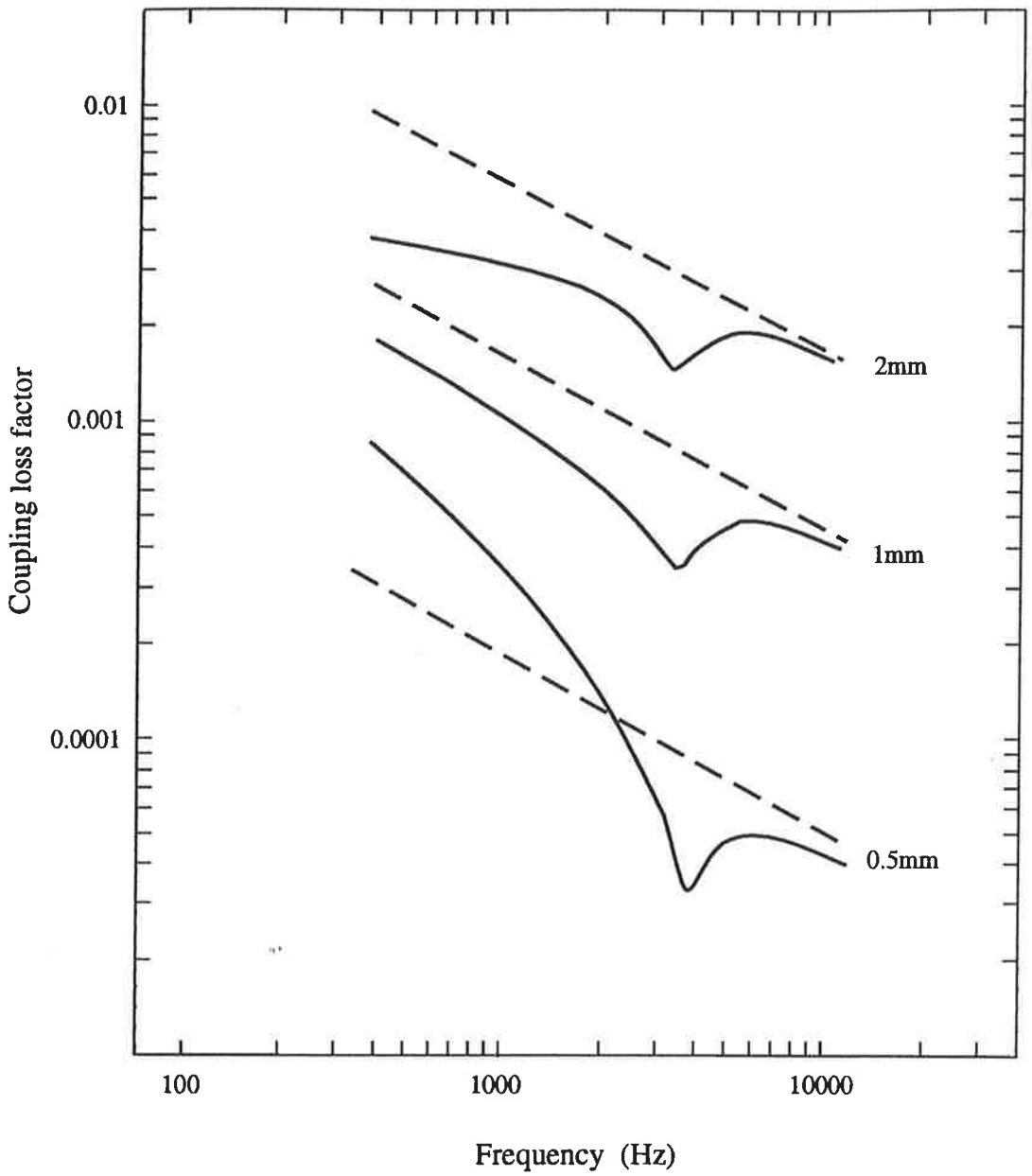

Figure 4.1 Coupling loss factors of three cylinder / plate structures with different shell thicknesses . The coupling loss factors of their equivalent plate / plate structure are also shown for comparison.

——— , cylinder / plate structure;
– – – , equivalent plate / plate structure.

It can be seen from Figure 4.1 that all of the cylinder/plate structures show a dip in the CLF at around the ring frequency of 3730 Hz, presumably caused by the increase in modal density of the cylinder around the ring frequency region. Thereafter the CLFs asymptote to the values of their equivalent plate/plate structures as the frequency increases. This finding is consistent with the well established fact that the response of a cylinder may be approximated by a flat plate at high frequencies. Below the ring frequency, the response of a cylinder is dominated by the membrane effects and as a result, the CLFs of the cylinder/plate structures differ considerably from their equivalent plate/plate structures.

4.3.2 Coupled periodic structure

An example structure which consists of a plate with periodic stiffeners coupled at right angles to a uniform plate as shown in Figure 3.3 is considered in this section. The coupling line length of the structure is 0.7m. Both plates are rectangular in shape with overall dimensions of 0.7 m × 1 m and 0.7 m × 1.2 m for the uniform plate and the plate with periodic stiffeners respectively. All other plate parameters are the same as for the examples discussed in Sections 3.2 and 3.4 of Chapter 3.

Figure 4.2 shows the CLF between the uniform plate and the plate with periodic stiffeners. As predicted from the calculation of mean transmission efficiency (see Figure 3.5), the CLF shows a drop in value in the 1600 Hz, 2000 Hz and 4000 Hz frequency bands where the wave transmission properties are dominated by the attenuation zones of the plate with periodic stiffeners. Calculations were also performed on the CLF of the coupled structure by removing the stiffening beams from the structure (effectively a structural junction with two uniform plates coupled together) and the results are also plotted in Figure 4.2 for comparison. As expected, the removal of stiffening beams eliminates the band pass characteristics of the system and increases the CLF.

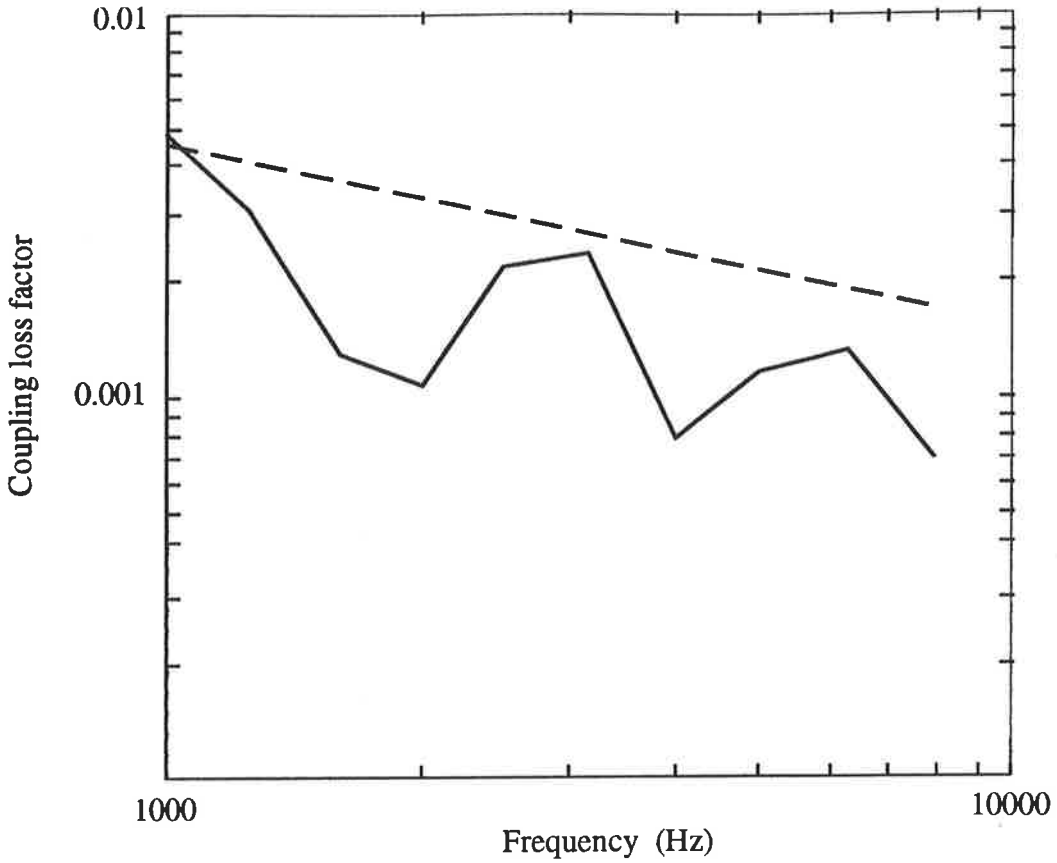

Figure 4.2 Coupling loss factor between a uniform plate and a plate with periodic stiffeners. The coupling loss factor of a plate / plate structure is also shown for comparison.

———— , coupled periodic structure ;

— — — — , plate / plate structure.

4.4 Summary

In this chapter, methods for evaluating SEA parameters for simple structural elements such as beams and plates were reviewed. The modal density may be estimated theoretically using asymptotic modal density expressions. Alternatively, an experimental method based on drive point mobility may be used for complex systems. The internal loss factor of an element depends on the material properties and geometry and is normally determined experimentally using either the steady state power balance method or the reverberation time method. CLFs may be derived from the travelling wave analysis based on semi-infinite elements.

For cylinder/plate coupled structures, the CLF may be derived from travelling wave analysis and the assumption that the vibrational energy is distributed equally amongst circumferential modes. It was demonstrated that the condition of reciprocity is satisfied in the present formulation of CLF by using a cylinder/annular plate coupled structure. Numerical results for three examples of cylinder/plate structures were presented and compared with those of their equivalent plate/plate structures. The results show that the CLF values of the cylinder/plate structures asymptote to those of their equivalent plate/plate structures above the ring frequency.

Complex built-up structures often consist of elements of a periodic nature. This chapter presented the analysis of an example structure which consisted of a plate with periodic stiffeners coupled at right angles to a uniform plate. To formulate the CLF for this type of coupled periodic structures, it was proposed that the standard travelling wave analysis procedure, with due allowance for zero transmission in the attenuation zones, be used.

CHAPTER 5

EXPERIMENTAL INVESTIGATION

5.1 Introduction

The derivation of CLFs as presented in Chapter 4 has involved a number of assumptions. For the cylinder/plate coupled structure, it is argued that the assumption of a diffuse wave field which is normally used for the derivation of CLF for coupled uniform plates, is equivalent to an equipartition of energy amongst the circumferential modes of a cylinder. The latter assumption is subsequently applied to the cylinder/plate structure in Chapter 4. While the former assumption has been supported by a number of experimental studies in plate/plate coupled structures (see, for example, Swift, 1977 and Tratch, 1985), the latter assumption has yet to be verified. As for the coupled periodic structure, it is proposed that the standard travelling wave analysis may be used for deriving the CLF, provided that the band pass nature is accounted for in the evaluation of mean transmission efficiency. Again, this is an assumption that requires experimental verification.

This chapter describes an experimental program to verify the CLF for a cylinder/plate structure and a coupled periodic structure. The program involves a measurement of the internal loss factor of the individual elements, after which the elements are welded together to form a rigid connection and further measurements taken to determine the input power and distribution of vibrational energy due to a random input excitation. The application of welding to form a rigid connection between the structural elements is consistent with previous experimental studies on the transmission of vibration in coupled structures (see, for example, Tratch, 1985 and Pollard, 1992). To control the dissipation of heat during the welding process, it was decided to run a small section of weld at a time and alternate the process at different parts of the joint in order to maintain an even distribution of heat across the structural elements. These measures minimise the distortion of the elements and the effect

of heat on the damping material. The effect of welding on the response and damping of the structural elements is investigated in Sections 5.2.2 and 5.3.2 where the internal loss factors of the individual elements are compared with *in-situ* measurements.

The measured internal loss factors, together with the input power and spatially averaged vibrational energy of the coupled elements, are used in a numerical procedure to estimate the CLF and compare with the theoretical values.

5.2 Cylinder/plate Structure

5.2.1 Experimental arrangements

The objective of the experiment was to measure the CLF of a cylinder/plate structure. The test structure consisted of a thin cylinder and an end plate as shown in Figure 5.1. Steady state power balance measurements (Bies and Hamid, 1980) and reverberation time measurements were conducted on the individual cylinder and plate elements to determine their internal loss factors. Further tests were conducted on the coupled structure to determine the input power and distribution of vibrational energy due to a random input excitation.

The frequency range of the experiment was selected to be 500 - 8000 Hz, corresponding to a ring frequency ratio Ω of 0.11 - 2.14. This enabled the effects of cylinder curvature on vibratory power transmission to be investigated at low frequencies ($\Omega << 1$). Also, at the higher end of the frequency spectrum ($\Omega > 2$), the cylinder is expected to behave approximately as a flat plate and well established results on plate/plate structures may be used to check against the present theory. In line with previous research work on the transmission of vibration through coupled cylindrical structures (for example, Hwang and Pi, 1973; Blakemore *et al.*, 1992 and Pollard, 1992) and the discussion presented in Section 4.2.1 of Chapter 4, the present experimental investigation is limited to the out-of-plane motion (in the radial direction) of the cylindrical shell. To check that the in-plane motion has no significant effect on the flexural energy level, the modal density of the plate element subjected to an in-

plane motion was calculated and compared with the out-of-plane modal density. The in-plane modal density was found to be 4.02×10^{-5} and 6.43×10^{-4} s/rad at a frequency of 500 and 8000 Hz respectively, compared with an out-of-plane modal density of 1.52×10^{-2} s/rad (independent of frequency). Thus the plate energy is dominated by the out-of-plane motion. Both the cylinder and plate have more than 10 resonant modes (out-of-plane) in the lowest third octave band. Calculations performed on the dispersion equation of the cylindrical shell show that 10 circumferential modes exist at a frequency of 500 Hz.

Consideration was given to the damping requirement for the cylinder and plate. If the cylinder/plate structure has a CLF very much greater than the internal loss factor of the individual structural elements, then the modal energy of the elements would be approximately equal and insensitive to any variations in the CLF. To determine the CLF from energy and power measurements, it is therefore desirable to have the internal loss factors at least the same order of magnitude as that of the CLF. For the present study, this was achieved by adding self-adhesive damping strips to the cylinder and plate (see Figure 5.1). The added damping also increased the modal overlap of the structural elements to a level that enabled the travelling wave analysis procedure to be used for the determination of CLF (Fahy and Mohammed, 1992).

Figure 5.2 shows the set up of the experiment for steady state power balance measurements. The structure was suspended by strings and driven by an electromagnetic shaker through an impedance head. Care was taken to align the shaker axis normal to the test structure and a thin stinger was used to connect the shaker to the impedance head to minimise the input of bending moment and in-plane force. Band limited random signals were used as the excitation source.

Another point of consideration for the present experimental study was the excitation source. Fahy (1970) has suggested that the injection of power into a structure with point excitation will result in modes which are not statistically independent (i.e., coherent modes) and violate

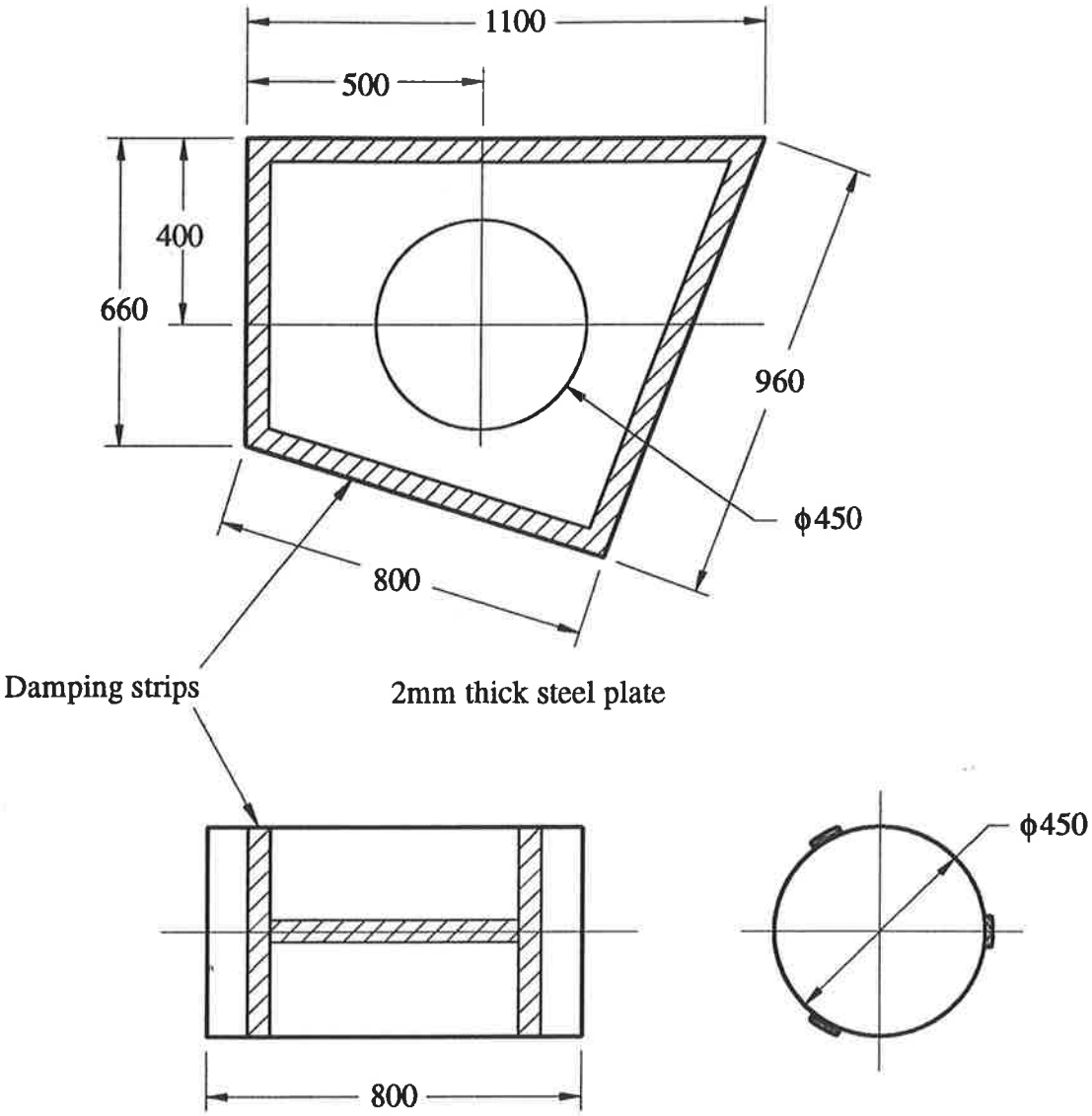

Figure 5.1 Cylinder and plate elements.

All dimensions in mm.

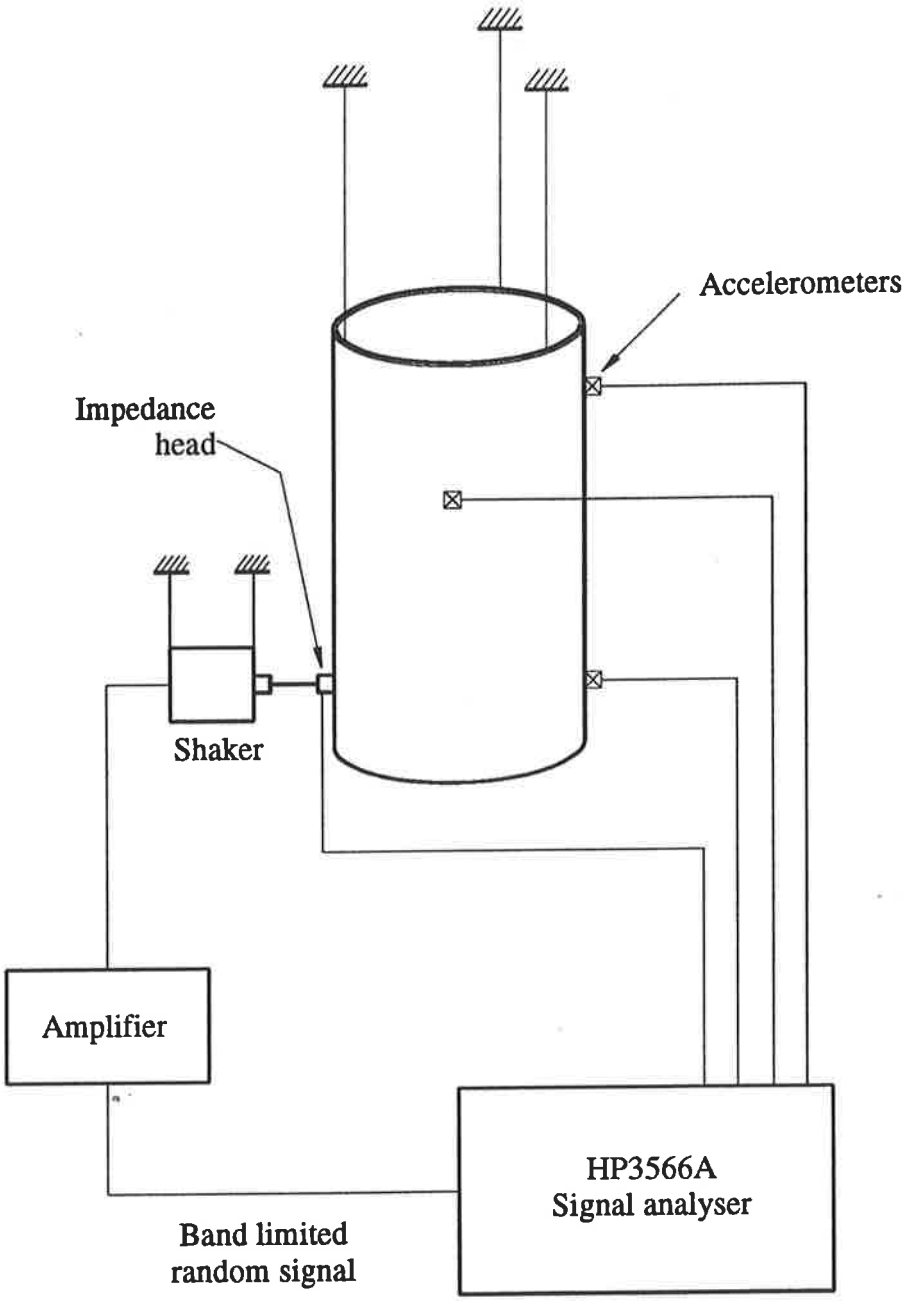

Figure 5.2 Experimental setup for damping measurement.

a basic assumption used in SEA modelling. Bies and Hamid (1980) have studied this problem and showed that modal incoherence can be achieved by averaging the results over three randomly chosen excitation points. The present study followed this approach in the measurement of internal loss factor using the steady state power balance method and the distribution of vibrational energy for the coupled structure. In the latter measurement, the cylinder was first excited and measurements taken to determine the input power and vibrational energy of the cylinder and plate. The experiment was then repeated by injecting power into the plate element to check for reciprocity. To determine the power injected into the structural element, the force and acceleration signals from the impedance head were processed using the following expression:

$$\Pi = 1/2\ \mathrm{Re}\{F_h \times (A_h/j\omega)^*\}, \tag{5.1}$$

where F_h and A_h are respectively the complex amplitudes of the force and acceleration measured by the impedance head, and * denotes the complex conjugate. To ensure that the acceleration signal is in phase with the force signal, the impedance head was arranged in such a way that the acceleration of the structure was measured directly from an accelerometer attached to the opposite side of the force transducer as shown in Figure 5.3 (a factor of -1 was introduced to reverse the direction of the acceleration signal). It should be noted that the seismic mass of the force transducer has no effect on the measurement of input power since it only results in an imaginary term as can be shown readily from equation (5.1).

The vibrational energy was determined from the spatial average of the acceleration signals from a number of randomly chosen points on each element. To determine the number of measurement points necessary for an accurate estimation of the spatially averaged response, preliminary tests were conducted on each element by using six and eight accelerometers in turn for spatial averaging. It was found that both test configurations resulted in approximately the same value of spatially averaged acceleration and henceforth six accelerometers were used to evaluate the vibrational energy of each of the elements. Before calculating the

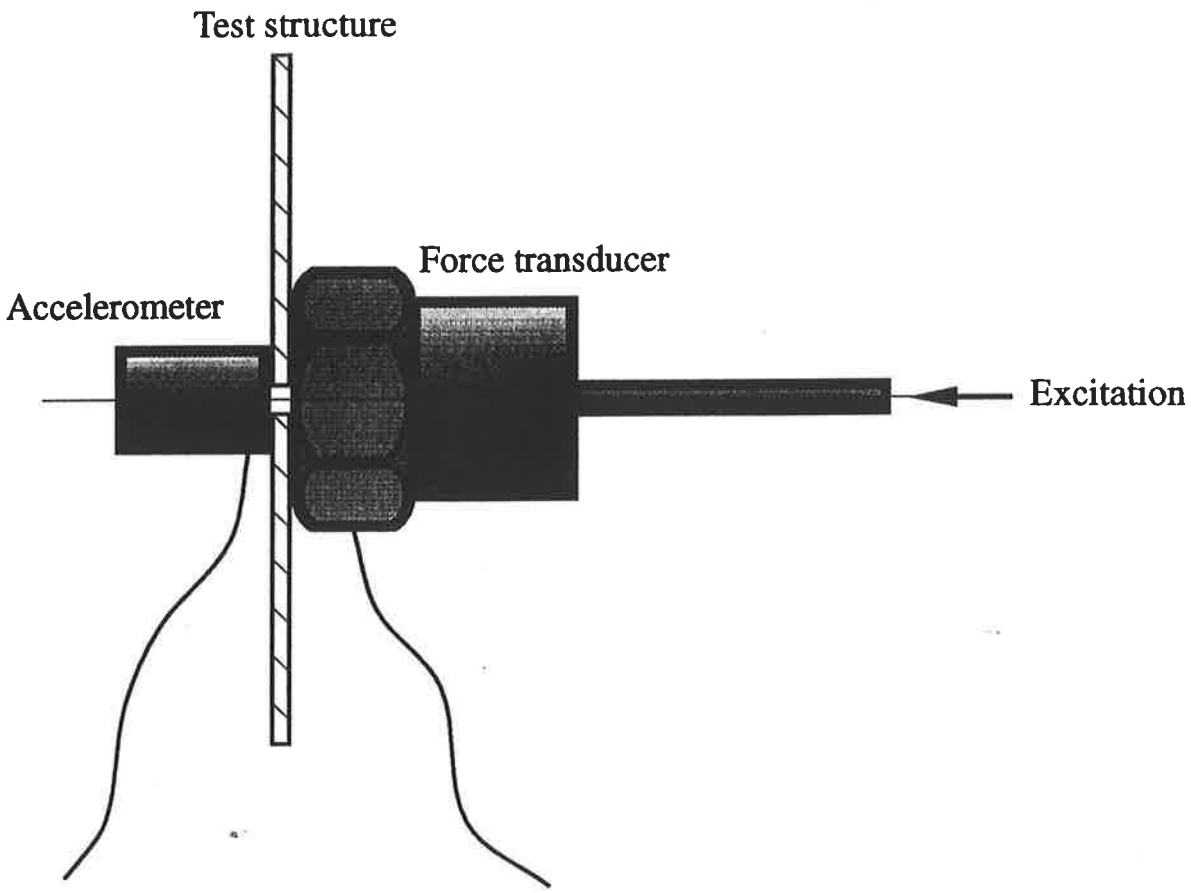

Figure 5.3 Impedance head for the measurement of force and acceleration.

vibrational energy, the accelerometer signals were corrected to allow for the effect of mass loading due to the accelerometers using the following expression (Beranek, 1971):

$$|A_u/A_a|^2 = 1 + |\omega m_a/Z|^2, \tag{5.2}$$

where A_u is the complex amplitude of the acceleration of the unloaded structure, A_a is the complex amplitude of the acceleration as measured by the accelerometer and m_a is the accelerometer mass. The impedance of the test structure, Z, was obtained from Table 11.5 of the book by Beranek (1971). The vibrational energy was then determined from the following expression :

$$\langle E \rangle = 1/2\, m_S\, \overline{|A_u/j\omega|^2}, \tag{5.3}$$

where m_S is the mass of the structural element and $\overline{\ }$ denotes the spatial average.

5.2.2 Results

Experiments were carried out to determine the internal loss factors of the cylinder and plate using the steady state power balance method and the reverberation time method as described in Section 4.1.4 of Chapter 4. In the steady state power balance method, the results were averaged over three randomly chosen excitation points. For the reverberation time method, a hammer impact was used as the initial excitation. The time history of the acceleration signal was recorded after passing through a one-third octave filter and subsequently processed to obtain a complex signal with the real and imaginary parts given by the measured acceleration and its Hilbert Transform respectively (see, for example, Thrane, 1984). The magnitude of this complex signal representing the envelope function was then calculated and plotted on a logarithmic scale for the estimation of reverberation time. This measurement feature is available in a number of signal analysers for the measurement of system response and the advantages of this method of measurement over the traditional method where only the real

valued function is used has been discussed by Herlufsen (1984). Five averages of the time history were taken for each measurement point and the internal loss factor was averaged over three randomly chosen measurement points. A typical envelope of the acceleration time history is shown in Figure 5.4.

Figures 5.5 and 5.6 show the internal loss factor of the cylinder and plate respectively. It can be seen that the results given by the reverberation time method and the steady state power balance method are in reasonable agreement. However, due to the coupling of in-plane and out-of plane motions in the cylinder, the results for the cylinder internal loss factor have to be interpreted carefully. In the first method of measurement (i.e., the reverberation time method), the internal loss factor of the cylinder is related to the decay of the out-of-plane motion. This is not the case for the steady state power balance method since the total energy dissipated includes both in-plane and out-of-plane motions. Coupling of these two types of motion will result in in-plane motion which is not measured by the accelerometer at the power injection point. However, there is no in-plane external power input into the cylinder provided that the external excitation transmits no in-plane force or moment into the cylinder. This condition was met in the present experimental study by mounting the axis of the shaker normal to the cylinder and using a thin stinger (1mm in diameter by 40 mm in length) to attach the shaker to the impedance head which in turn was bonded directly to the cylinder. On the other hand, the energy in the cylinder is distributed into components associated with both in-plane and out-of-plane motions. The latter motion was damped in the present experiment by self-adhesive damping strips which were arranged to give an effective damping for both the circumferential and axial modes. Referring back to Figure 5.5 which shows the internal loss factor of the cylinder using the steady state power balance method and the reverberation time method, an agreement between these two methods of measurement suggests that the input power to the cylinder is predominantly dissipated by the out-of-plane motion and justifies the present experimental investigation where only such motion is considered. This is expected from the theoretical considerations in Section 4.2.1 of Chapter 4 since the cylindrical shell has a high order of circumferential modes.

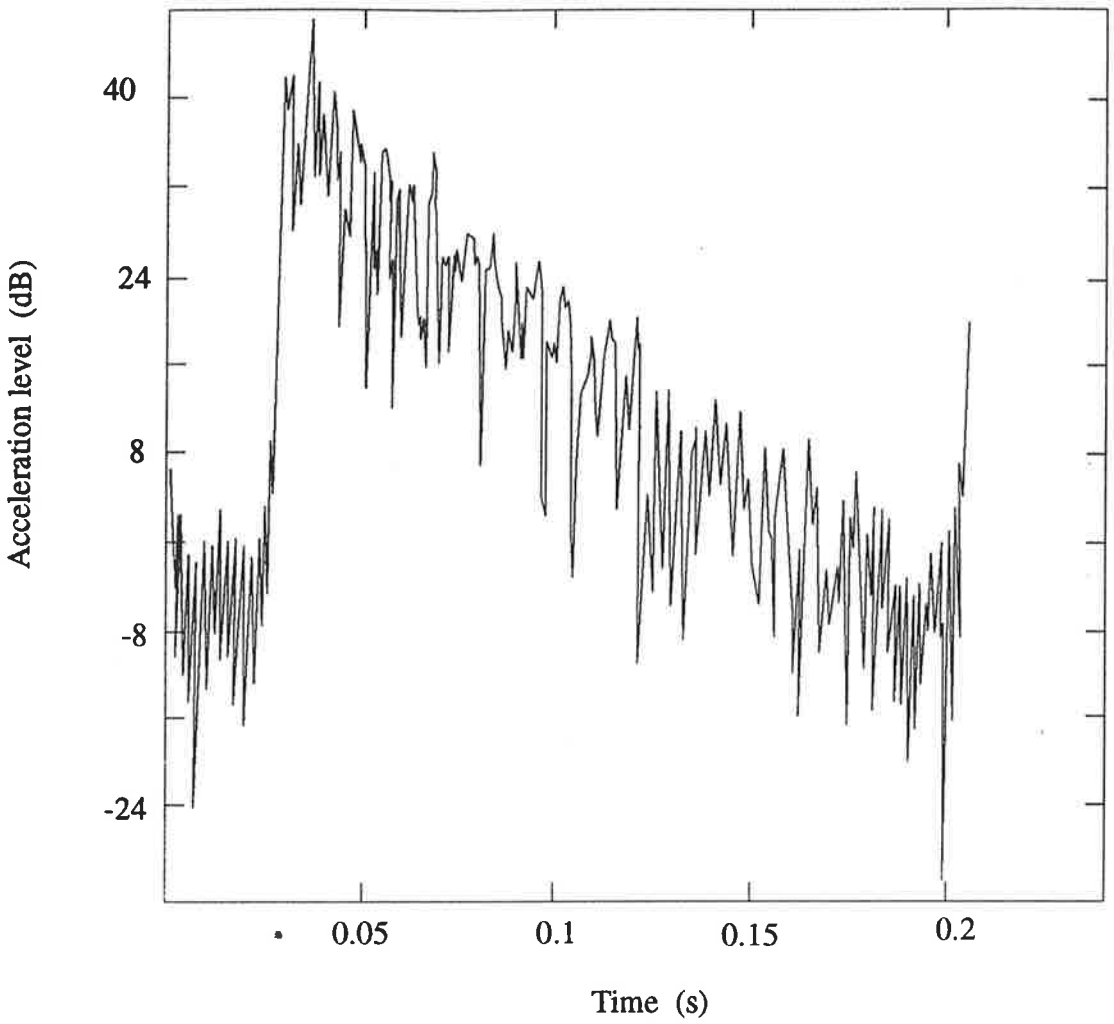

Figure 5.4 Typical decay record for cylindrical shell.

Third octave band at a centre frequency of 1.25 kHz.

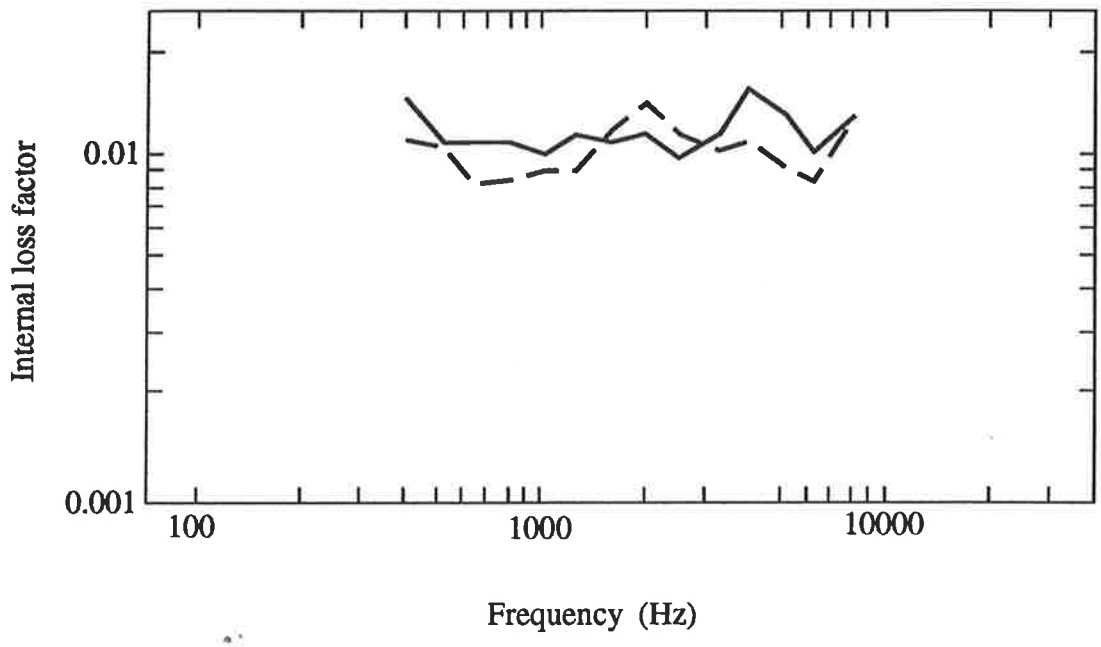

Figure 5.5 Internal loss factor of cylinder.

———— , steady state power balance method;

– – – – – , reverberation time method.

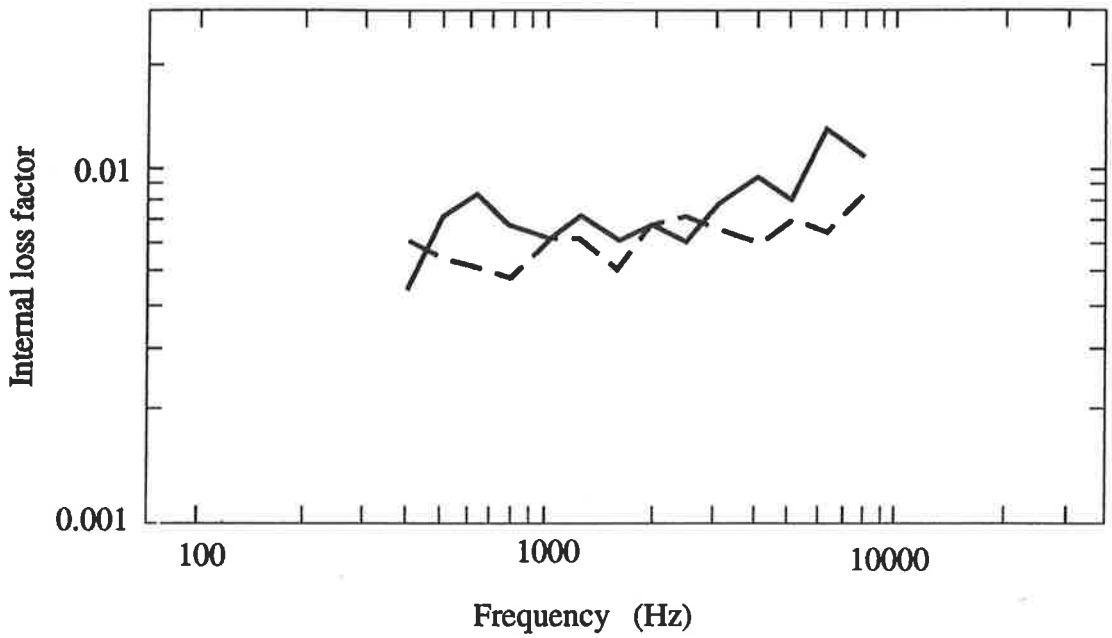

Figure 5.6 Internal loss factor of plate.

———— , steady state power balance method;

— — — , reverberation time method.

Subsequent to the joining of the cylinder to the end plate, measurements were carried out to determine the input power and the vibrational energy distribution by first exciting the cylinder and then repeating the experiment by exciting the plate. Before determining the CLF from the power and energy measurements of the coupled structure, the results were first checked for reciprocity. Clarkson and Ranky (1984) have shown that the reciprocity requirement is satisfied when

$$[\langle E_{ij}\rangle/\langle \Pi_j\rangle\, n(\omega)_i] \,/\, [\langle E_{ji}\rangle/\langle \Pi_i\rangle\, n(\omega)_j] = 1, \tag{5.4}$$

where $\langle E_{ij}\rangle$ is the energy of element i due to an input excitation at element j. The left hand side of equation (5.4) representing the energy ratio was determined from the measured subsystem power and energy, together with the modal densities obtained from theoretical and empirical expressions (see Section 4.1.3 of Chapter 4) for the uniform plate and cylinder respectively. It can be seen from Figure 5.7 that the energy ratio is reasonably close to unity, thus the results satisfy the requirement for reciprocity. A matrix inversion routine based on the minimisation of the sum of the squared errors (Bies and Hamid, 1980) was used to determine the internal loss factors of the cylinder and plate, as well as the CLF of the structure. This method involved a re-arrangement of the energy balance equations in the following form :

$$\Delta_1 = \eta_1 \langle E_{11}\rangle + \eta_{12} \langle E_{11}\rangle - \eta_{21} \langle E_{21}\rangle - \langle \Pi_1\rangle/\omega, \tag{5.5}$$

where Δ_1 denotes the experimental errors in determining the power and vibrational energy associated with subsystem 1. Similar equations may be formulated for other subsystems and for the present experimental set up, a total of four equations were formulated (two subsystems for each configuration of input excitation). The sum of the squared errors may then be expressed as :

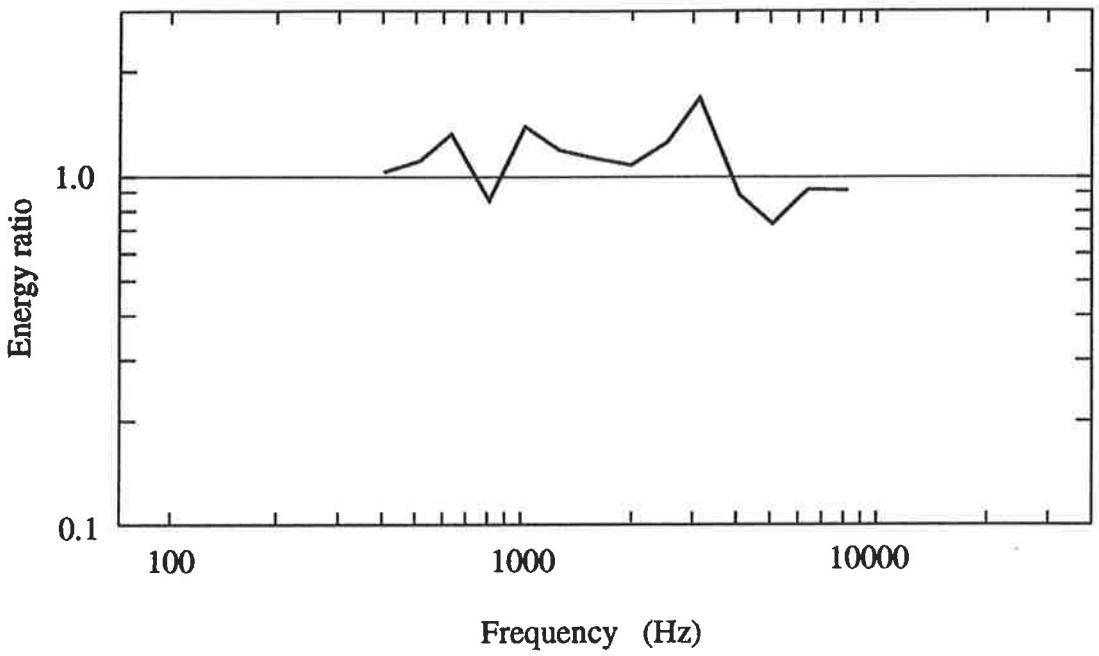

Figure 5.7 Energy ratio of the coupled cylinder / plate structure as a measure of reciprocity.

$$\Gamma = \sum_{i=1}^{4} \Delta_i^2 . \tag{5.6}$$

Following the least square procedure, the sum of the squared errors was minimised with respect to the internal loss factors and CLFs. It is convenient to generalise the internal loss factors and CLFs at this stage by denoting them as η_m. By using this notation, the expression for minimised error is given by:

$$\partial\Gamma/\partial\eta_m = 0. \tag{5.7}$$

The reciprocity condition (i.e., $n(\omega)_p\, \eta_{pc} = n(\omega)_c\, \eta_{cp}$) was incorporated into equation (5.7) and resulting in three linear algebraic equations (for m = 1, 2 and 3). The internal loss factors and CLF were then determined by standard matrix inversion of these equations.

Figures 5.8 and 5.9 show the internal loss factor of the cylinder and plate respectively. The results given by the *in-situ* method (inversion of matrix) are in close agreement with the steady state power balance method. This finding is consistent with earlier work reported by Bies and Hamid (1980) for the case of flat plates and supports the present experimental approach in determining the CLF. It also suggests that the coupled modal energies of the elements are approximately equal to the uncoupled modal energies. Furthermore, the welding process has little effect on the damping of the structural elements. Figure 5.10 shows the CLFs of the cylinder/plate structure obtained by equation (4.20) and measurement. The experimental results are fairly well predicted by the theory presented in Section 4.2.1 of Chapter 4 although the theoretical values are slightly higher than the measured values in the frequency range of 800 - 2500 Hz. The dip in CLF which is predicted in the theoretical analysis can be observed in the experimental data. It occurs at a frequency of around 2500 Hz compared with a predicted value of 3730 Hz which corresponds to the ring frequency of the cylinder. The experimental data also shows some discrepancy with the predicted CLF above a frequency of 6300 Hz. An attempt to conduct further tests (above 8000 Hz) to confirm the

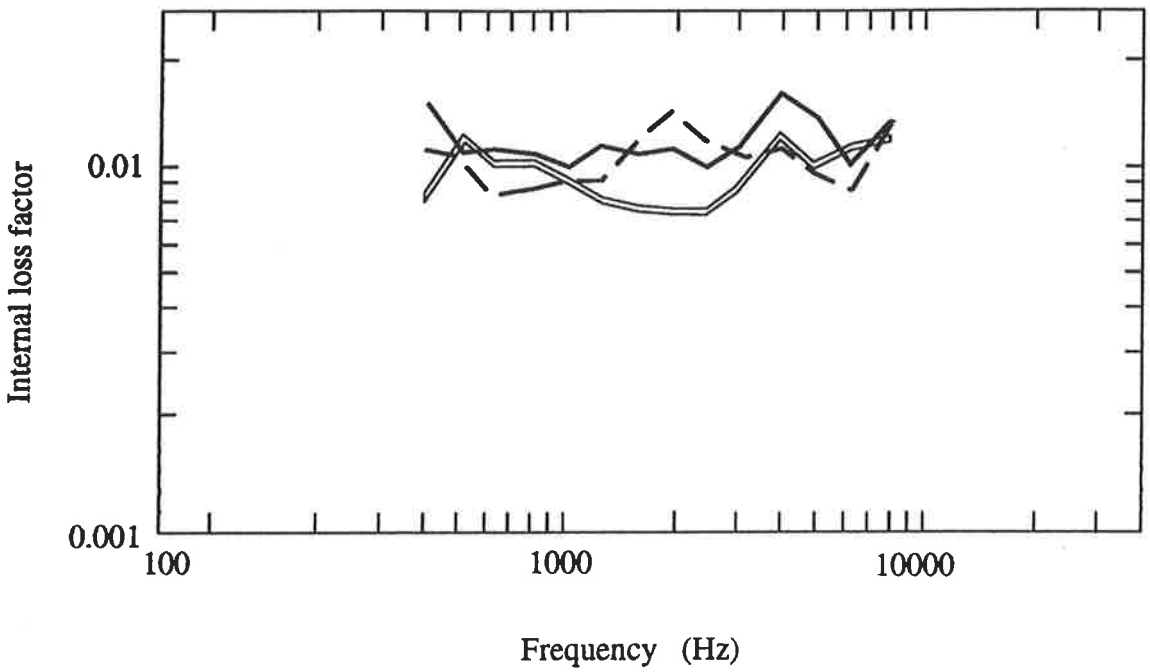

Figure 5.8 Internal loss factor of cylinder.

——— , steady state power balance method;
— — — , reverbration time method;
═══ , *in-situ* method.

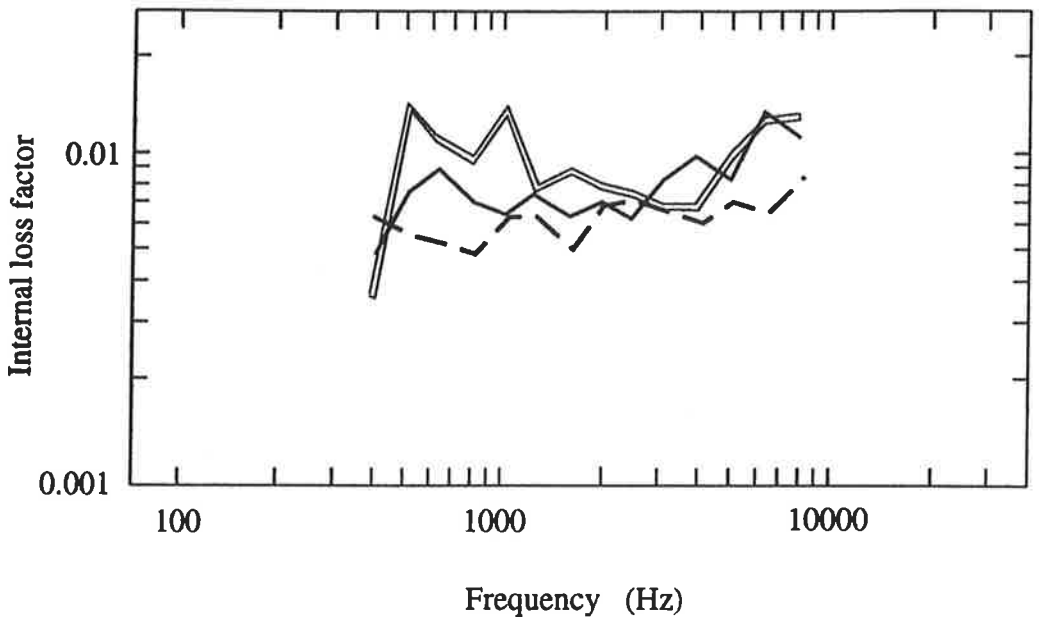

Figure 5.9 Internal loss factor of plate.

——— , steady state power balance method;
— — — , reverbration time method;
═══ , *in-situ* method.

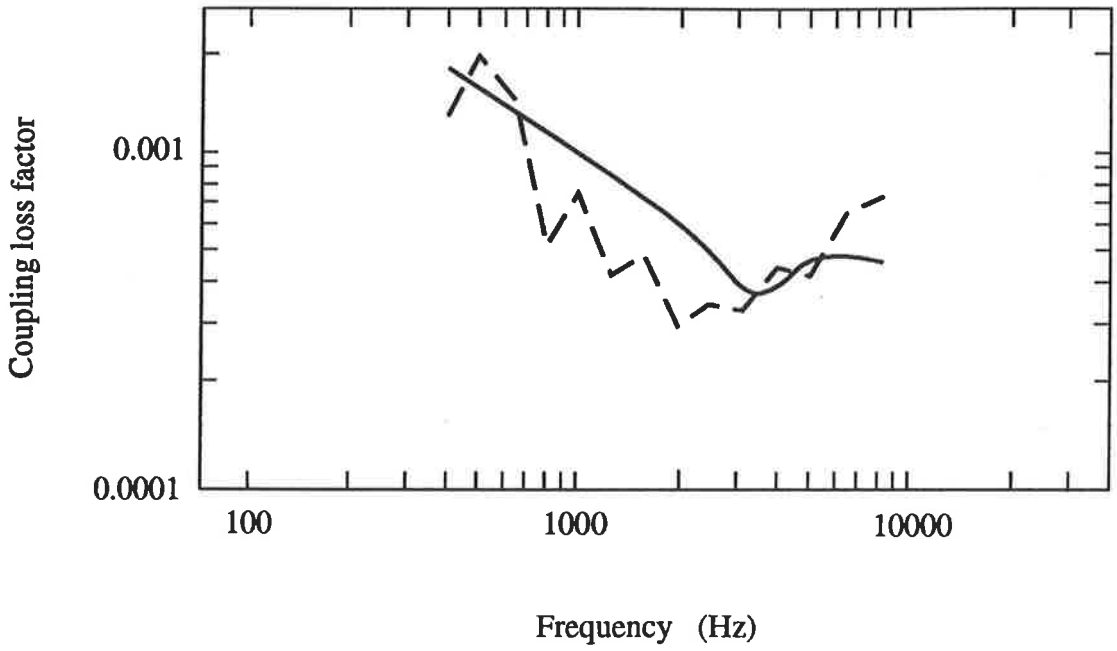

Figure 5.10 Coupling loss factor of cylinder / plate structure.

——— , theory;
– – – , experiment.

convergence of the experimental results to the theoretical CLF of a plate/plate structure was hampered by the limitation in sampling rate of the data acquisition system. However, further examination of the results reveals that the discrepancy is consistent with pervious work on the experimental investigation of CLF (see, for example, Bies and Hamid, 1980 and Clarkson and Ranky, 1984) and may be partially attributed to the random nature of the experiment as well as the assumptions involved in the derivation of CLF (for example, the equipartition of energy amongst circumferential modes). Overall, the calculated CLF is considered to be satisfactory as an SEA parameter for the estimation of response levels in a cylinder/plate structure.

5.3 Coupled Periodic Structure

5.3.1 Experimental arrangements

The test structure was made up of a uniform plate and a plate with periodic stiffeners as for the example discussed in Section 4.3.2 of Chapter 4. To determine the modal density of the plate with periodic stiffeners, it was decided to measure the drive point mobility of the structure and then obtain the modal density from equation (4.4) of Chapter 4. The modal density of the uniform plate was also measured by this method so that the validity of the experimental procedure could be checked by comparing the experimental results of the uniform plate with the asymptotic modal density expression (equation (4.3)). In line with the test procedure for the cylinder/plate structure, self adhesive damping strips were added to the structural elements. After the measurement of modal density and internal loss factor, the elements were welded at right angles to each other and further tests conducted to determine the internal loss factors *in-situ* and the CLF. Figure 5.11 shows the test structure used for the measurement of input power and vibrational energy. The experimental procedure for the measurement of internal loss factors and CLF was similar to that of the cylinder/plate structure which has been described in detail in Sections 5.2.1 and 5.2.2.

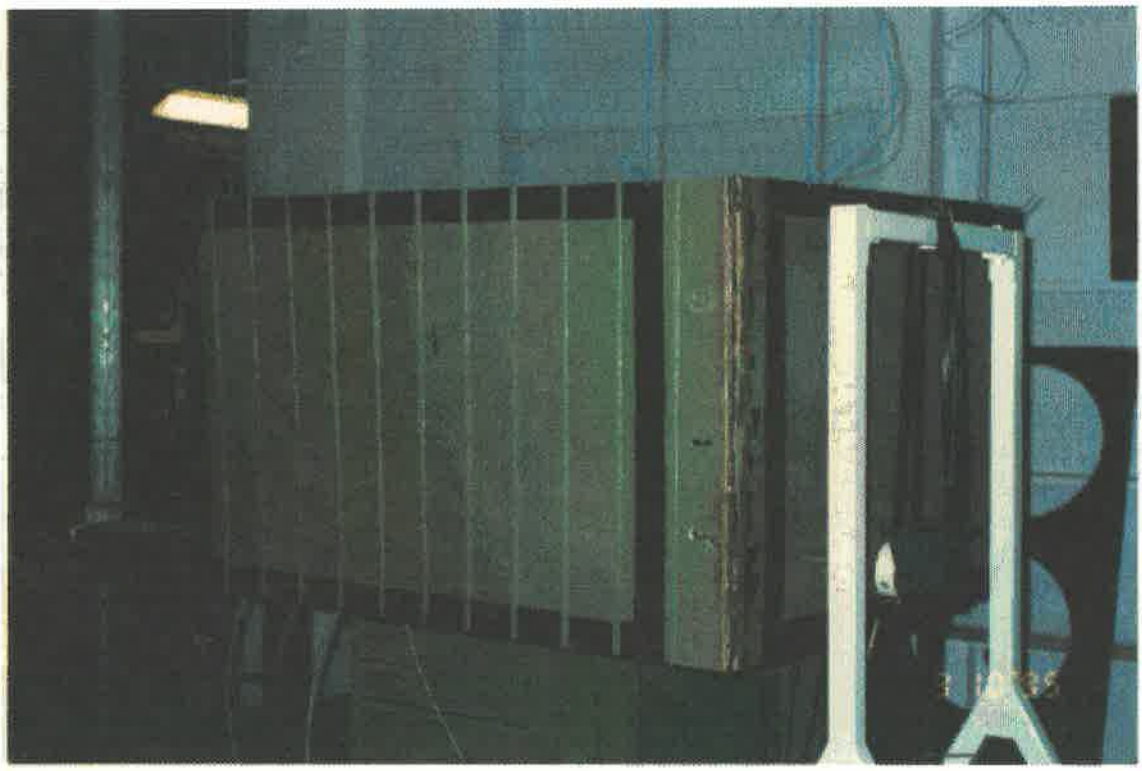

Figure 5.11 Coupled periodic structure set up for the measurement of input power and vibrational energy.

To determine the mobility of the structure, the following expression which allows for a correction of the effect of seismic mass was used:

$$Y = (A_h/j\omega)/(F_h - A_h m_S), \tag{5.8}$$

where Y is the drive point mobility, A_h and F_h are respectively the complex amplitudes of the acceleration and force measured by the impedance head, m_S is the seismic mass which includes the mass between the sensing element and the surface of the structure plus the associated mounting accessories.

5.3.2 Results

The experimental procedure for the measurement of modal density was checked by comparing the experimental results of the uniform plate with equation (4.4). Figure 5.12 shows the modal density of the uniform plate. It can be seen that the measured modal density is somewhat lower that the theoretical value, especially at high frequencies. The large contact area between the impedance head and the structure (13 mm diameter) was thought to be the main reason for such discrepancy. To improve the accuracy of modal density measurement, a spacer of 5 mm diameter was inserted between the impedance head and the structure to reduce the force contact area so that the results measured by the impedance head could be regarded as the drive point mobility. For the present experiment, the structural wavelength at the highest one-third octave band (8000 Hz band centre frequency) was approximately ten times the diameter of the contact area, thus the attachment of the impedance head to the structure could be regarded as a point contact. Figure 5.13 shows the modal density of the uniform plate measured by this experimental arrangement. The measured modal density is in excellent agreement with the theoretical prediction, thus confirming the validity of the experimental procedure. Figure 5.14 shows the modal density of the plate with periodic stiffeners. The experimental results are somewhat higher than the sum of the modal densities for the plates and beams, possibly due to the addition of coupled modes in the system.

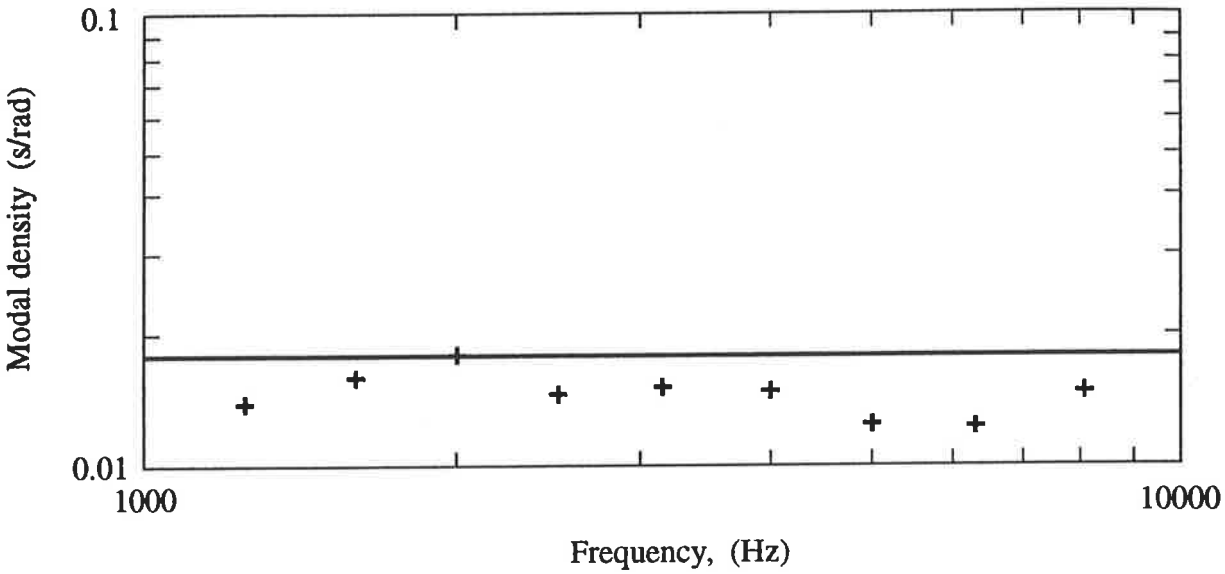

Figure 5.12 Modal density of uniform plate.

———— , theory;

\+ , experiment (measured with the impedance head mounted directly on the test stucture).

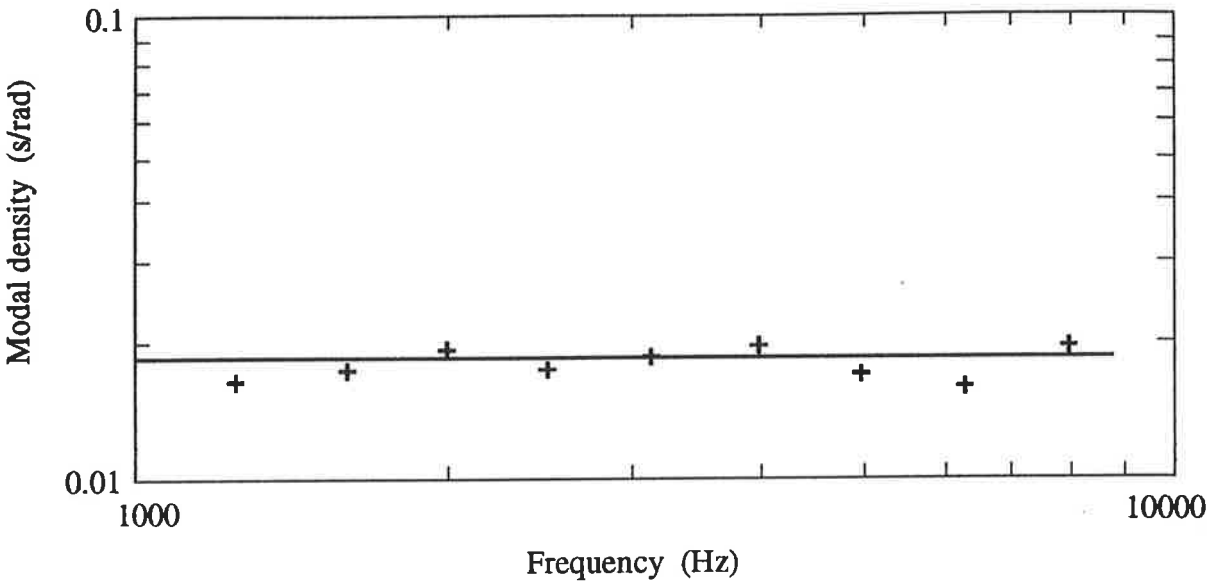

Figure 5.13 Modal density of uniform plate.

———— , theory;

\+ , experiment (measured with a 5mm diameter spacer between the impedance head and the test structure).

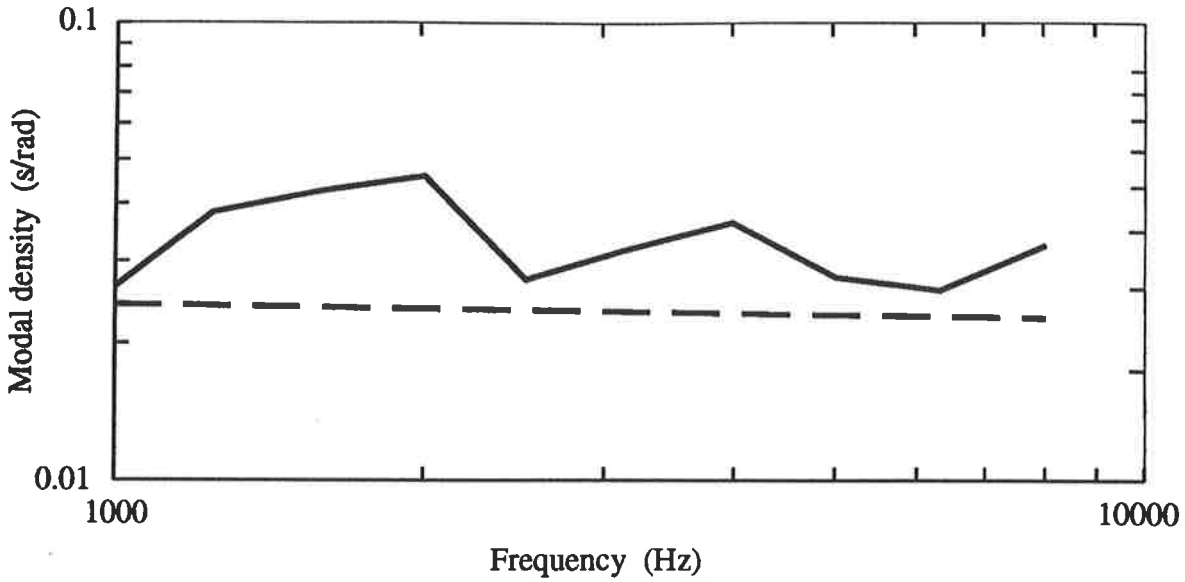

Figure 5.14 Modal density of a plate with periodic stiffeners.

——— , measured;
— — — , sum of plate and beam modes.

After the structural elements were welded together, further tests were conducted on the coupled periodic structure using a procedure similar to that used for the cylinder/plate structure. The reciprocity requirement was again checked by evaluating the energy ratio in equation (5.4) from the measured input power, energy and modal density. It can be seen from Figure 5.15 that the energy ratio is close to unity across the entire frequency range; thus the results satisfy the requirement for reciprocity.

The numerical procedure described in Section 5.2.2 was used to determine the internal loss factors *in-situ* and the CLF. Figures 5.16 and 5.17 show the internal loss factors of the uniform plate and the plate with periodic stiffeners respectively. Results from both the *in-situ* method and the steady state power balance method are shown in the figures. In line with the finding for the cylinder/plate structure, results from both methods of measurement are in close agreement and hence the validity of the *in-situ* method is again verified.

Figure 5.18 shows the CLFs of the coupled periodic structure obtained by the travelling wave analysis (equation(4.10)) and measurement. The results are in very good agreement in the lower frequency bands. At higher frequencies, the theoretical results appear to have shifted by one-third of an octave compared with the experimental data. The apparent shift in frequency may have been caused by the assumptions and simplifications involved in the theoretical analysis. For example, it is assumed in Section 3.2 of Chapter 3 that the boundary conditions of the plate with periodic stiffeners can be applied on the plate/beam centreline. However, the plate/beam attachment point is in fact offset from the beam centreline by an amount equal to half the beam width and this has an effect on the accuracy of the theoretical model, especially at high frequencies where the cross sectional dimensions of the junction are not negligible compared with the bending wavelength. Also, the offset of the attachment point from the beam centreline means that the bending wave will travel in the plate elements by a distance (in the x-direction) equal to the beam spacing minus the beam width rather than the beam spacing as used in the theoretical model. In an attempt to investigate the effect of plate offset from the beam centreline, the beam spacing was decreased by 3 mm and the corresponding

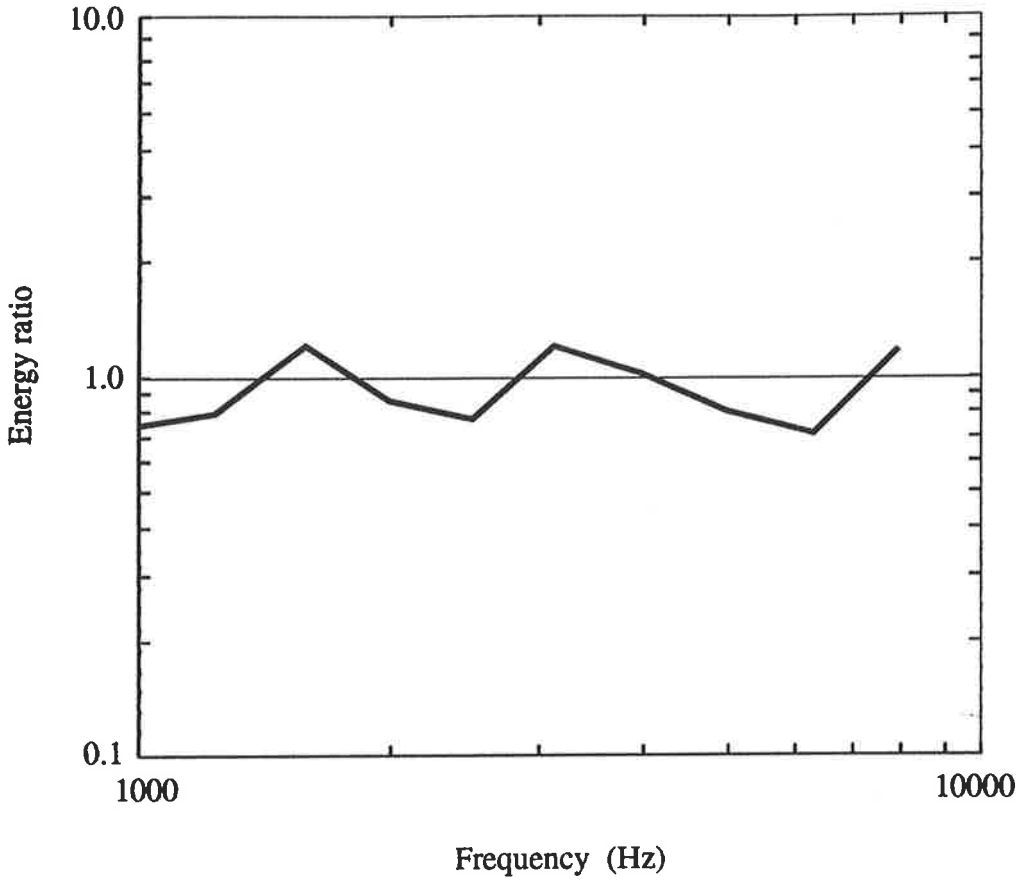

Figure 5.15 Energy ratio of the coupled periodic structure as a measure of reciprocity.

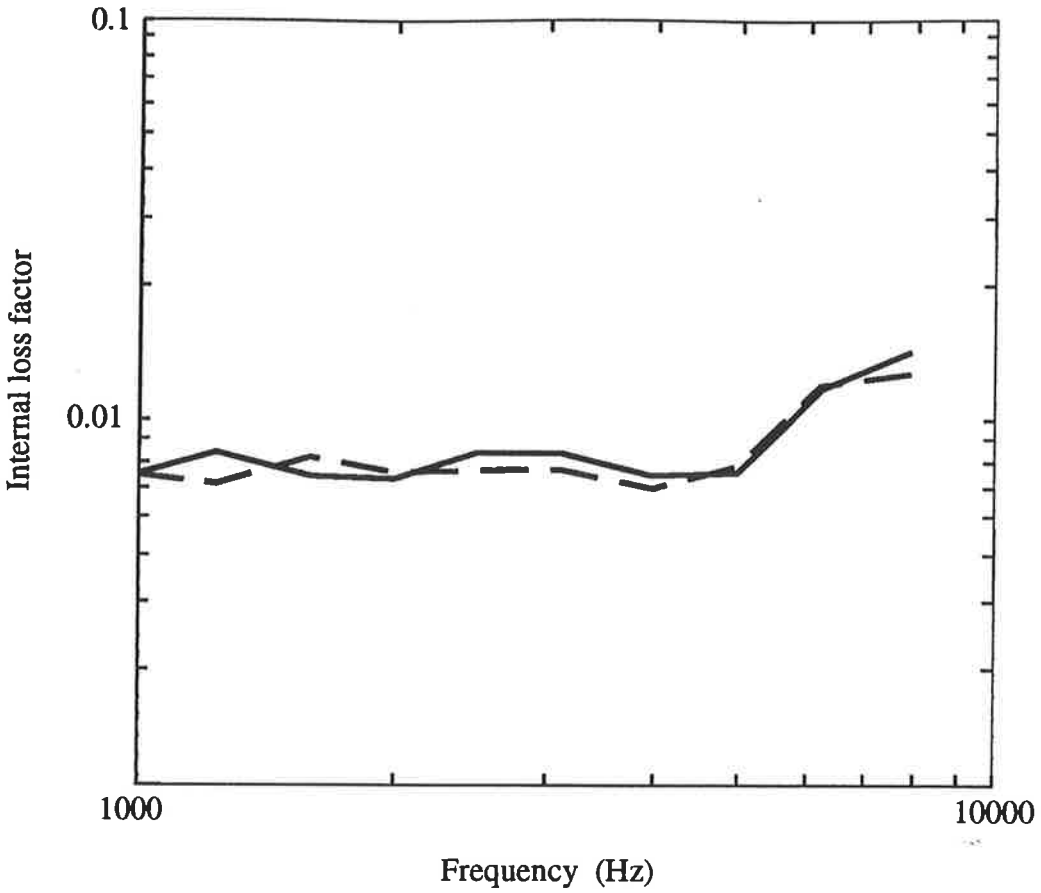

Figure 5.16 Internal loss factor of uniform plate.

———— , steady state power balance method;
— — — , *in-situ.*

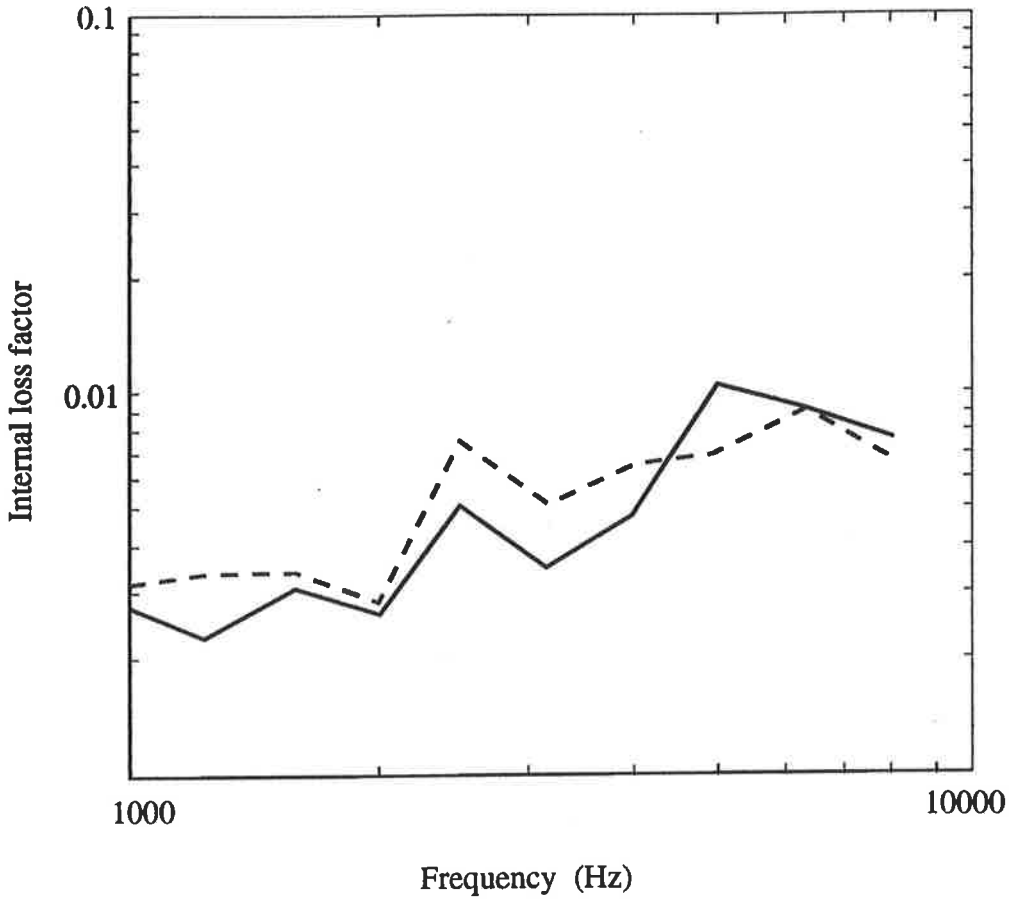

Figure 5.17 Internal loss factor of a plate with periodic stiffeners.

——— , steady state power balance method;

– – – – , *in-situ.*

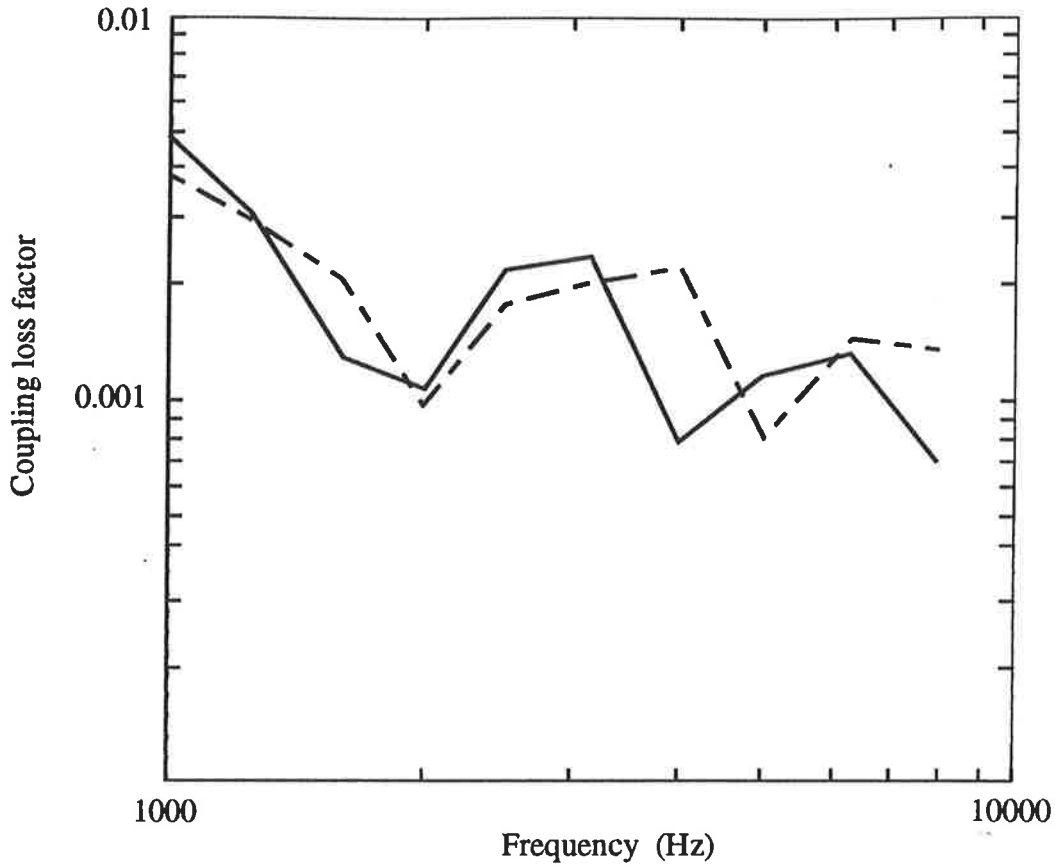

Figure 5.18 Coupling loss factor between a uniform plate and a plate with periodic stiffeners.

———— , theory ;

– – – – , experiment .

shift in propagation and attenuation zones of the plate with periodic stiffeners was calculated and shown in Figure 5.19. It can be seen that the shift in propagation zones is more significant in high frequencies. This is due to the reduction in bending wavelength as the frequency is increased so that the beam spacing plays a more significant role in bending wave propagation. Another factor that may have contributed to the discrepancy between the experimental and theoretical results is the welding process in the construction of the periodic structure that has resulted in a fillet of metal at the plate/beam interface. As a first approximation to account for the addition of metal at the welded junctions, the beam width was increased by 2 mm and Figure 5.20 shows the corresponding change in propagation and attenuation zones. In general, an increase in beam width results in a widening of attenuation zones. From Figures 5.19 and 5.20, it can be seen that the combined effect of reducing the beam spacing and increasing the beam width is to shift the attenuation zones upward in the frequency scale. The effects of a shift in attenuation zones on the CLF can be seen in Figure 5.21. Despite the discrepancy at 4000 Hz, the results confirm that the drop in CLF at 2000 Hz and 5000 Hz corresponds to the frequency regions which are dominated by the attenuation zones. Overall, the experimental results are reasonably well predicted by the present theory.

5.4 Summary

An experimental program has been conducted to verify the CLF of a cylinder/plate coupled structure over a frequency range of 500 - 8000 Hz. This corresponds to a ring frequency ratio Ω of 0.11 - 2.14.

The internal loss factors of the cylinder and plate were measured individually by the steady state power balance method and the reverberation time method. Results from these two methods of measurement were used as the benchmark to check against the *in-situ* measurement method where the internal loss factors and CLF of the coupled structure were evaluated. All three methods of internal loss factor measurement give results that are in close

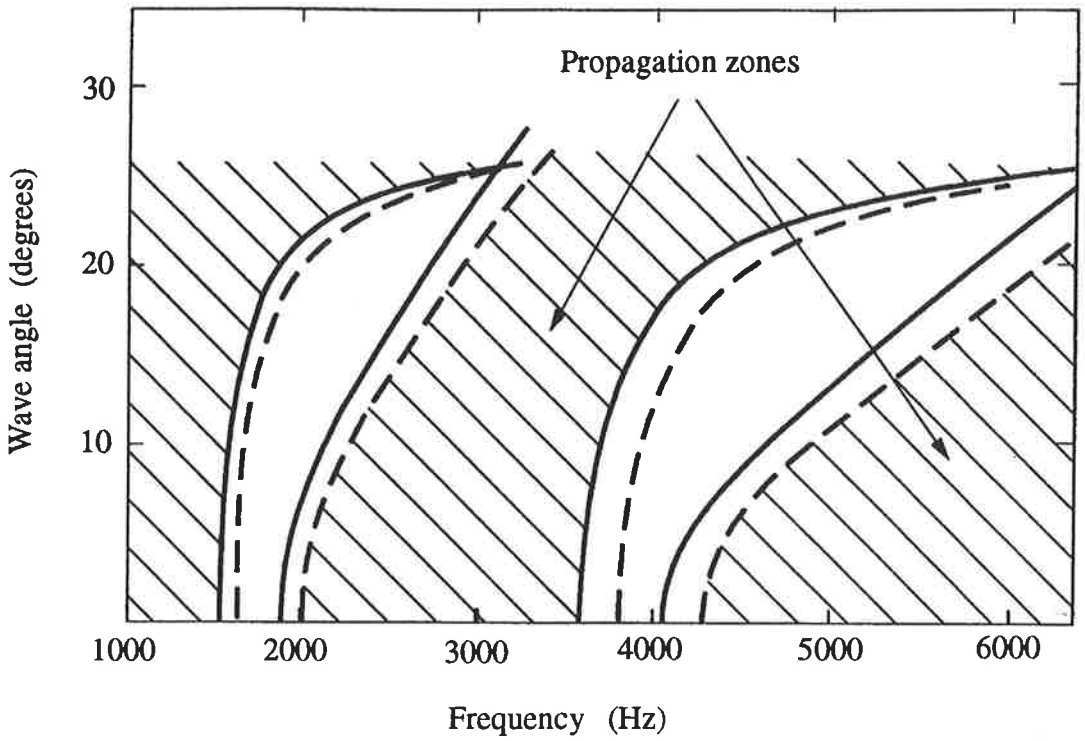

Figure 5.19 Shift in propagation and attenuation zones with beam spacing.

——— , nominal beam spacing of 100mm;

— — — , beam spacing decreased by 3mm.

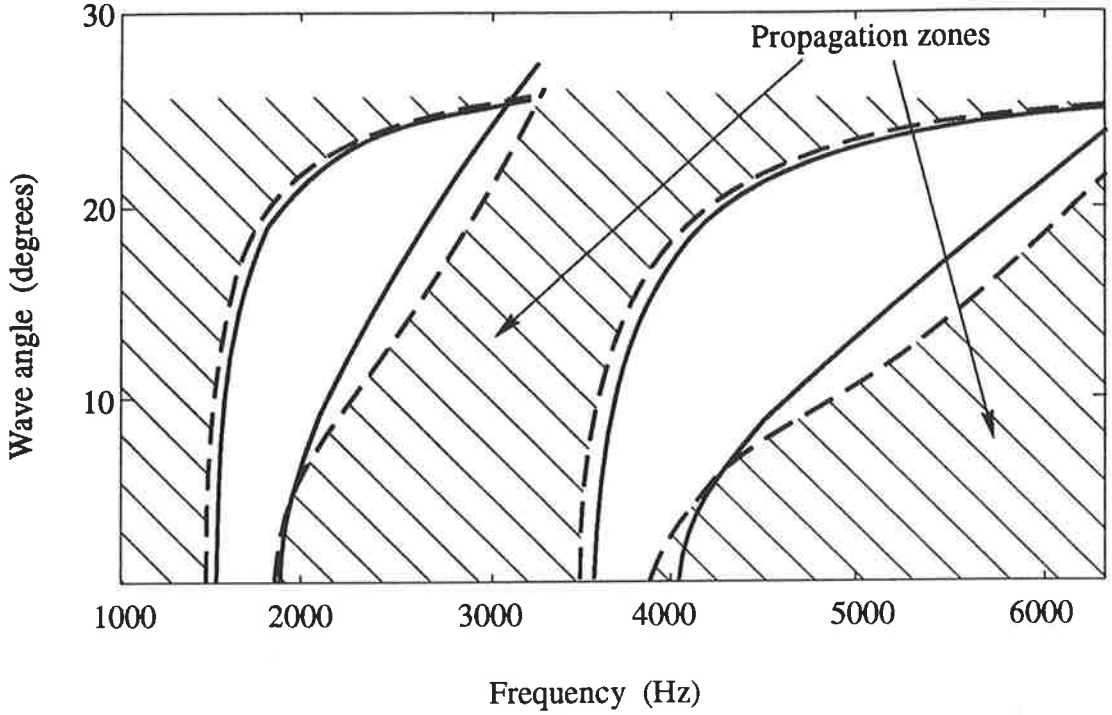

Figure 5.20 Shift in propagation and attenuation zones with beam width.

———— , nominal beam with of 6mm;
— — — , beam width increased by 2mm.

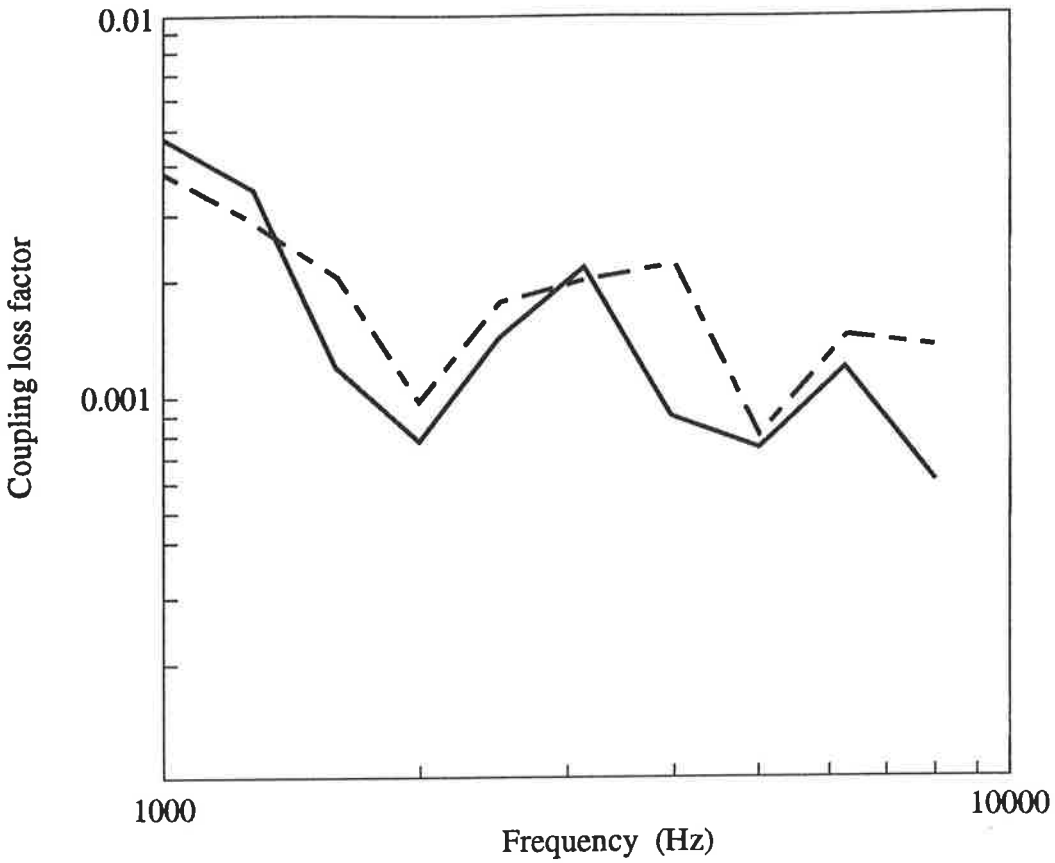

Figure 5.21 Coupling loss factor between a uniform plate and a plate with periodic stiffeners.

———— , theory (with beam spacing decreased by 3mm and beam width increased by 2mm);

– – – – – , experiment .

agreement and therefore the validity of the *in-situ* measurement procedure is confirmed. The experimental results for the CLF are fairly well predicted by the theory presented in Section 4.2 of Chapter 4.

Modal density measurements were conducted on the uniform plate and the plate with periodic stiffeners using the frequency-averaged drive point mobility. The measurement procedure was verified by comparing the experimental results of the uniform plate with the asymptotic modal density expression.

The internal loss factors and CLF of the coupled periodic structure were evaluated by an experimental procedure similar to that used in the cylinder/plate structure. Despite the slight discrepancy at high frequencies which may have been caused by the assumptions and simplifications involved in the analysis, the measured CLF and the theoretical prediction are in good agreement.

CHAPTER 6

CONCLUSIONS AND RECOMMENDATIONS FOR FURTHER WORK

6.1 Conclusions

A naval ship structure may be considered as an assembly of plate, beam and shell elements coupled together at a number of structural junctions. As a first step towards understanding the transmission of vibration in such structure, the present study first examined the wave transmission properties of a number of structural junctions including plate/beam junctions, three-dimensional beam junctions and cylinder/plate junctions.

The plate/beam junctions considered in the present study consist of thin stiffening beams which are commonly used in naval ship structures. These beams were modelled as finite plates subjected to bending and in-plane vibrations. The effect of beam vibrations on wave propagation through a plate/beam junction was demonstrated by examples and found to be significant in the evaluation of vibratory power transmission.

For general beam elements in a three-dimensional beam junction, the attachment point and the beam centroid may not coincide with the shear centre and as a result, a bending-torsional coupling exists in the beam. The effect of such mode coupling, together with shear deformation and rotary inertia of a beam element in vibratory power transmission of beam junctions was investigated. Results from an example beam junction show that mode coupling increases the transmission of bending waves.

The method of analysis for wave transmission through a coupled cylinder/plate structure was applied to a junction which consists of two semi-infinite cylinders coupled to an annular plate. The total transmission efficiency of the junction was found to be in good agreement with that obtain by Harari (1977) who treated the annular plate as a ring stiffener. However, the present method of analysis is more general in that it can be applied to junctions where the

stiffening plate has a large width to thickness ratio, and in the extreme case where the stiffener becomes a circular plate (for example, hull/bulkhead coupling of a submarine structure). It can also be applied to cylinder/infinite plate junctions.

Another area of concern in this thesis is the transmission of vibration through periodic structures such as uniform plates reinforced with periodic beam stiffeners. The wave transmission properties of a plate with periodic stiffeners were investigated using the Bloch theorem and found to be dependent on the wave angle and frequency. This implies that for a plate with periodic stiffeners subjected to a diffuse wave field, the incident wave will find a range of angles that allows a free transmission of waves. By identifying the transmission angles of the periodic structure at a particular frequency, a method based on travelling wave analysis has been developed to evaluate the transmission efficiency of a uniform plate coupled to a plate with periodic stiffeners. Calculations performed on an example structure reveal that the mean transmission efficiency reflects regions of low transmissibility due to the dominance of attenuation zones.

Following the analyses of structural junctions and coupled periodic structures, the present study then reviewed briefly the application of SEA for predicting the transmission of vibration in built-up structures and the methods for evaluating SEA parameters. In line with previous SEA studies on coupled plate and beam structures, the method of wave transmission analysis as presented in earlier parts of this thesis was used to derive the CLF for a cylinder/plate coupled structure and a coupled periodic structure. For the cylinder/plate structure, it is assumed that the vibrational energy is distributed equally amongst the circumferential modes. This is equivalent to the assumption of a diffuse wave field which has been used successfully for the derivation of CLF for isotropic elements. Numerical examples for a number of cylinder/plate structures were presented and the results confirm that the response of a cylinder may be approximated by a flat plate when the excitation frequency to ring frequency ratio is higher than one. To derive the CLF for the coupled periodic structure, it is necessary to incorporate the band pass characteristics of a periodic structure into the analysis. The

present study suggested that this can be achieved by using the standard travelling wave analysis procedure with the appropriate mean transmission efficiency that accounts for no wave being transmitted in the attenuation zones.

An experimental program has been conducted to verify the formulation of CLFs for the cylinder/plate coupled structure and the coupled periodic structure. The internal loss factors and CLF of the test structures were determined *in-situ* by a numerical procedure which involves the inversion of power balance equations similar to that described by Bies and Hamid (1980). The validity of this procedure has been confirmed by comparing the internal loss factors measured *in-situ* against the benchmark results from measurements of the individual structural elements. Experimental results of the CLF for both structures show good agreement with theoretical predictions and it is therefore suggested that the present formulation of CLF may be used for SEA studies.

6.2 Further Work

This study has taken a step towards characterising the wave transmission properties of structural junctions typical of naval ship constructions and the development and refinement of SEA parameters for the analysis of vibration transmission in built-up structures. However, mention must be made of a number of areas that warrant further study. First, the present study has only selected three types of structural junction for analysis, on the grounds that they are representative of naval ship constructions. Real structures of course consist of many more different combinations of elements in a junction, each of which has to be studied in order to determine the wave transmission properties. The method of analysis presented here may be of use for guiding the direction of further studies in this area.

In the analysis of coupled periodic structures, the present work has only considered bending waves to simplify the analysis. In reality, the stiffeners of ship structures are often offset to one side of the plate and thus generate in-plane waves which may have a significant effect on

vibration transmission. A more detailed study of coupled periodic structures which includes in-plane waves would be worthwhile. Also, the coupling between other types of periodic structure typical of naval ship constructions such as ring stiffened cylindrical shells requires further investigation.

Finally, it should be mentioned that the long term goal of the present study is to develop methods for predicting vibration levels of naval ships at high frequencies. To this end, attempts should be made to investigate some example naval ships, using SEA, and to conduct full-scale experimental measurements to verify the theoretical predictions.

APPENDIX 1

Evaluation of Wave Amplitudes for a Plate/thin beam Junction

A1.1 Expressions for plate displacements

Figure A1.1 shows the displacements and junction forces of an arbitrary semi-infinite plate in a plate/thin beam junction due to the transmitted/reflected waves. The wave equations for bending and in-plane motions of the plate are given by (see, for example, Love, 1927):

$$\nabla^4 w + [12\rho(1-\mu^2)/Eh^2]\partial^2 w/\partial t^2 = 0, \tag{A1.1}$$

$$\partial^2 u/\partial x^2 + [(1-\mu)/2]\partial^2 u/\partial y^2 + [(1+\mu)/2]\partial^2 v/\partial x\partial y - [\rho(1-\mu^2)/E]\partial^2 v/\partial t^2 = 0, \tag{A1.2}$$

$$\partial^2 v/\partial y^2 + [(1-\mu)/2]\partial^2 v/\partial x^2 + [(1+\mu)/2]\partial^2 u/\partial x\partial y - [\rho(1-\mu^2)/E]\partial^2 u/\partial t^2 = 0, \tag{A1.3}$$

where u, v and w are the plate displacements in the x, y and z directions respectively; E, ρ, μ and h are the elastic modulus, density, Poisson's ratio and thickness of plate respectively and $\nabla^4 = \{\partial^2/\partial x^2 + \partial^2/\partial y^2\}^2$. The in-plane wave equations (equations (A1.2) and (A1.3)) are functions of the plate displacements u and v. To obtain a solution to these equations, one may make use of the following substitutions:

$$u = -\partial\varphi/\partial x - \partial\varpi/\partial y, \tag{A1.4}$$

$$v = -\partial\varphi/\partial y + \partial\varpi/\partial x. \tag{A1.5}$$

Using equations (A1.4) and (A1.5), each of the in-plane wave equations may be reduced to a function of one independent variable (φ or ϖ) only:

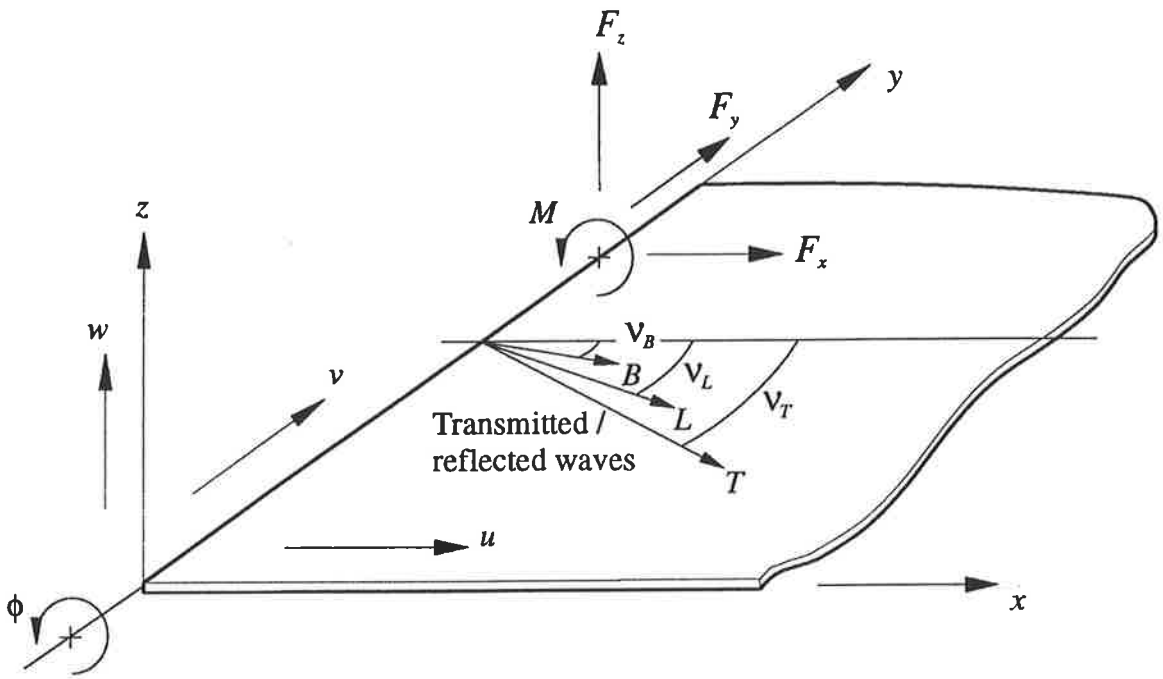

Figure A1.1 Co-ordinate system of an arbitrary plate showing transmitted / reflected waves, plate displacements and junction forces and moment.

$$\nabla^2\varphi - [\rho(1-\mu^2)/E]\partial^2\varphi/\partial t^2 = 0, \tag{A1.6}$$

$$\nabla^2\varpi - [2\rho(1+\mu)/E]\partial^2\varpi/\partial t^2 = 0. \tag{A1.7}$$

The parameter φ is associated with longitudinal waves while ϖ with shear waves. The general solutions to equations (A1.1), A(1.6) and A(1.7) may be expressed as:

$$w = W \exp(k_{Bx}x + k_{By}y + j\omega t), \tag{A1.8}$$

$$\varphi = \vartheta \exp(k_{Lx}x + k_{Ly}y + j\omega t), \tag{A1.9}$$

$$\varpi = \varsigma \exp(k_{Tx}x + k_{Ty}y + j\omega t), \tag{A1.10}$$

where W, ϑ and ς are the wave amplitudes. For the solutions to be valid, the following conditions must be satisfied (these conditions may be obtained by substituting the solutions back to equations (A1.1), (A1.6) and (A1.7)):

$$-(k_{Bx}^2 + k_{By}^2) = \pm[12\rho\omega^2(1-\mu^2)/Eh^2]^{1/2} = \pm k_B^2, \tag{A1.11}$$

$$-(k_{Lx}^2 + k_{Ly}^2) = [\rho\omega^2(1-\mu^2)/E] = k_L^2, \tag{A1.12}$$

$$-(k_{Tx}^2 + k_{Ty}^2) = [2\rho\omega^2(1+\mu)/E] = k_T^2, \tag{A1.13}$$

where k_B, k_L and k_T are the bending, longitudinal and shear wave numbers respectively. These wave numbers may be expressed by their components in the x and y directions as shown in equations (A1.11 - 1.13). Snell's law states that the trace velocity of all wave types at the junction must be the same. This implies that the y components of the wave numbers

(i.e., k_{By} ,k_{Ly} and k_{Ty}) for the transmitted and reflected waves must be the same as that of the incident wave. The x component of wave numbers may be determined from equations (A1.11 - A1.13). For bending waves, equation (A1.11) yields four roots, the negative imaginary root and the negative real root must be chosen for the reflected and transmitted waves since they represent travelling and decaying waves respectively in the positive x direction (i.e., away from the junction). Similarly, the solutions for longitudinal and shear waves must be negative imaginary. Equations (A1.4), (A1.5) and (A1.8) - (A1.10) give the plate displacements u, v and w. By expressing the x and y components of wave numbers in terms of the wave angles γ_B, γ_L and γ_T, the plate displacements may now be written as:

$$u = [B_1 \cos\gamma_L \exp(-j\, k_L x \cos\gamma_L) - B_2 \sin\gamma_T \exp(-j\, k_T x \cos\gamma_T)] \exp(k_y y + j\omega t), \quad \text{(A1.14)}$$

$$v = [-B_1 \sin\gamma_L \exp(-j\, k_L x \cos\gamma_L) - B_2 \cos\gamma_T \exp(-j\, k_T x \cos\gamma_T)] \exp(k_y y + j\omega t), \quad \text{(A1.15)}$$

$$w = \{A_1 \exp(-j\, k_B x \cos\gamma_B) + A_2 \exp[-k_B x \sqrt{(1 + \sin^2\gamma_B)}]\} \exp(k_y y + j\omega t), \quad \text{(A1.16)}$$

where k_y is the y component of the incident wave number and A_1, A_2, B_1, B_2 are the complex wave amplitudes. The last exponential factor on the right hand side of the above equations represents the y direction dependency and time dependency of the displacements. The source plate of the junction is subjected to an oblique incident wave with the wave heading angle α related to the reflection/transmission angles through Snell's law:

$$k_B \sin\gamma_B = k_L \sin\gamma_{BL} = k_T \sin\gamma_T = k \sin\alpha, \quad \text{(A1.17)}$$

where k is the incident wave number. Given the incident wave angle α, the bending and in-plane displacements of the plate depend only on four unknowns representing the complex wave amplitudes; namely, the amplitudes for longitudinal and shear waves, as well as the travelling and decaying bending waves.

Some engineering structures (for example, ships, aircraft) often make use of thin, rectangular section beams to reinforce plate elements. A thin beam in the context of this thesis implies that the beam thickness is of the same order as that of the plate and is therefore subjected to bending and in-plane vibrations. Figure A1.2 shows a schematic diagram of the structure which consists of two semi-infinite plates coupled to a thin beam. The analysis of this type of structure may be conducted by assuming that the thin rectangular beam behaves as a finite plate with waves travelling in both the positive and negative x directions. Referring back to equations (A1.11) - (A1.13), the solutions to wave motion must include the positive and negative roots. Following the derivation procedures as presented for the semi-infinite plate leads to the beam displacements in terms of eight unknown complex wave amplitudes.

Before the plate and beam displacement equations may be assembled through the boundary conditions and solved for the wave amplitudes, one must also consider the incident wave that is carried by the source plate. The incident wave may be either bending, longitudinal or shear and the plate displacements due to the incident wave may be obtained in a similar manner as that of the reflected/transmitted waves. The only difference being that the positive imaginary solution of the wave numbers must be used since the incident wave propagates towards the junction. For the purpose of evaluating the transmission efficiency, the incident wave may be regarded as having a unit amplitude.

A1.2 Boundary conditions

To consider the boundary conditions, it is convenient to introduce the subscript i to denote the plate number (i = 1, 2, 3, ... K; the thin beam is regarded as a finite plate). The first set of boundary conditions deals with the compatibility of plate motion and requires that the displacements of all plates along a set of reference co-ordinates (for example, x_1, y and z_1) at the junction must be the same. In addition, the rotation about the y axis of all plates must be equal. The plate rotation is given by:

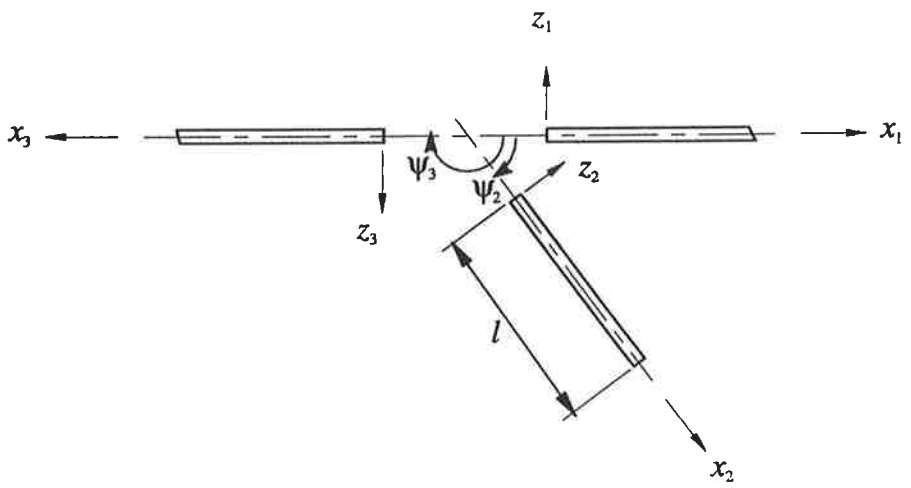

Figure A1.2 Schematic diagram of a plate / thin beam junction.

$$\phi_i = \partial w_i/\partial x_i. \tag{A1.18}$$

Resolving the displacements of plate 1 along co-ordinates x_i, y and z_i leads to the following compatibility equation:

$$\begin{bmatrix} u_i \\ v_i \\ w_i \\ \phi_i \end{bmatrix}_{i=2}^{K} = \begin{bmatrix} \cos\psi_i, & 0, & -\sin\psi_i, & 0 \\ 0\ , & 1, & 0\ , & 0 \\ \sin\psi_i, & 0, & \cos\psi_i, & 0 \\ 0\ , & 0, & 0\ , & 1 \end{bmatrix} \begin{bmatrix} u_1 \\ v_1 \\ w_1 \\ \phi_1 \end{bmatrix}, \tag{A1.19}$$

where ψ_i is the angle between plate 1 and plate i. The second set of boundary conditions deals with the equilibrium of forces and moments. For thin isotropic plates, the junction forces and moment per unit length (along the y - direction) may be expressed as:

$$F_{xi} = -[E_i h_i/(1-\mu^2)][\partial u_i/\partial x_i + \mu_i\, \partial v_i/\partial y], \tag{A1.20}$$

$$F_{yi} = -[E_i h_i/2(1+\mu)][\partial u_i/\partial y + \partial v_i/\partial x_i], \tag{A1.21}$$

$$F_{zi} = [E_i h_i^3/12(1-\mu^2)][\partial^3 w_i/\partial x_i^3 + (2-\mu_i)\, \partial^3 w_i/\partial x_i \partial y^2], \tag{A1.22}$$

$$M_i = -[E_i h_i^3/12(1-\mu^2)][\partial^2 w_i/\partial x_i^2 + \mu_i\, \partial^2 w_i/\partial y^2]. \tag{A1.23}$$

Note that equation (A1.22) represents the effective edge force which consists of the shear force plus the effect of twisting moment. Equilibrium requirements for the balance of forces and moments at the junction lead to the following equation :

$$F_{x1} + \sum_{i=2}^{K} F_{xi} \cos \psi_i + \sum_{i=2}^{K} F_{zi} \sin \psi_i = 0, \tag{A1.24}$$

$$\sum_{i=2}^{K} F_{yi} = 0, \tag{A1.25}$$

$$F_{z1} - \sum_{i=2}^{K} F_{xi} \sin \psi_i + \sum_{i=2}^{K} F_{zi} \cos \psi_i = 0, \tag{A1.26}$$

$$\sum_{i=2}^{K} M_i = 0. \tag{A1.27}$$

Equations (A1.19) and (A1.24) - (A1.27) give the boundary conditions at the junction. These equations are evaluated at the origin of the co-ordinate system (i.e., x_1, x_2,...x_K = 0). In addition to these boundary conditions, the forces and moment at the free end of the finite plate must vanish. Together these conditions are sufficient to permit solution for the wave amplitudes of interest.

APPENDIX 2

Evaluation of Wave Amplitudes for a Three-dimensional Beam Junction

A2.1 Expressions for beam displacements

The equations of motion for a beam vibrating in coupled bending and torsional modes, taking into account of the shear deformation and rotary inertia, are given by (see Figure A2.1 for beam co-ordinates):

$$GAK_z(\partial\theta_y/\partial x_p + \partial^2 w/\partial x_p^2) = \rho A(g\,\partial^2\theta_x/\partial t^2 + \partial^2 w/\partial t^2), \tag{A2.1}$$

$$EI_y\,\partial^2\theta_y/\partial x_p^2 - GAK_z(\theta_y + \partial w/\partial x_p) = I_y\rho\,\partial^2\theta_y/\partial t^2, \tag{A2.2}$$

$$GAK_y(\partial^2 v/\partial x_p^2 - \partial\theta_z/\partial x_p) = \rho A(\partial^2 v/\partial t^2 - b\,\partial^2\theta_x/\partial t^2), \tag{A2.3}$$

$$EI_z\,\partial^2\theta_z/\partial x_p^2 - GAK_y(\partial v/\partial x_p - \theta_z) = I_z\rho\,\partial^2\theta_z/\partial t^2, \tag{A2.4}$$

$$GJ\,\partial\theta_x/\partial x_p = I_S\,\partial^2\theta_x/\partial t^2 - \rho Ab\,\partial^2 v/\partial t^2 + \rho Ag\,\partial^2 w/\partial t^2. \tag{A2.5}$$

where I_y, I_z are the second moment of area of beam about the y_p and z_p axes respectively; K_y, K_z are the shear factors in the y_p and z_p directions respectively, J is the torsional constant of beam, I_S is the second moment of inertia per unit length of beam about the shear centre, A is the cross-sectional area of beam, G is the shear modulus and b, g represent the offset between the shear centre and beam centroid as shown in Figure A2.4. These equations are satisfied by solutions of the exponential form:

$$v = V\exp(-\mathrm{j}\,k\,x_p + \mathrm{j}\,\omega\,t), \tag{A2.6}$$

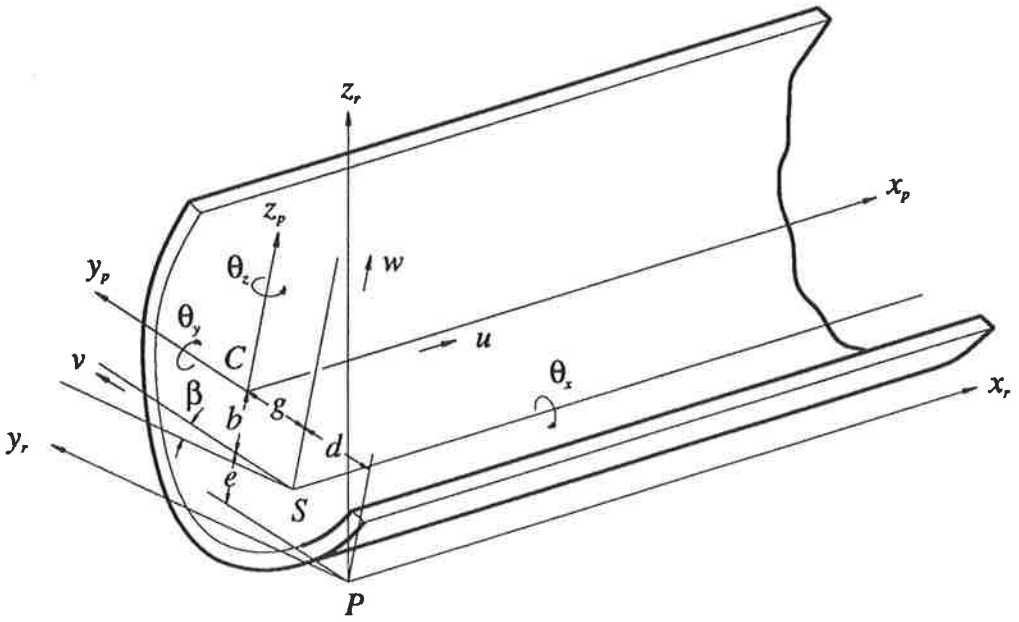

Figure A2.1 An arbitrary beam element.

$$w = W \exp (-j k x_p + j \omega t), \tag{A2.7}$$

$$\theta_x = \Theta_x \exp (-j k x_p + j \omega t), \tag{A2.8}$$

$$\theta_y = \Theta_y \exp (-j k x_p + j \omega t), \tag{A2.9}$$

$$\theta_z = \Theta_z \exp (-j k x_p + j \omega t). \tag{A2.10}$$

By substituting the solutions into equations (A2.1) - (A2.5), one obtains five linear equations in terms of the wave amplitudes V, W, Θ_x ,Θ_y and Θ_z :

$$\mathbf{B} \begin{bmatrix} V \\ W \\ \Theta_x \\ \Theta_y \\ \Theta_z \end{bmatrix} = 0. \tag{A2.11}$$

For a non-trivial solution, the determinant of matrix **B** must be zero. The expanded determinant leads to a fifth order dispersion equation in k^2 and results in five wave numbers for one direction of wave propagation. These wave numbers represent five types of waves including travelling and decaying waves of predominantly bending in nature in the direction of the two principal axes y_p and z_p, and a predominant torsional wave. It should be noted that the magnitude of the propagating and decaying wave numbers for such predominant bending modes are not equal, as opposed to the case for simple bending where they are equal. The positive real roots and the negative imaginary roots represent propagating and decaying waves respectively in the positive x_p direction.

The general solutions for waves travelling in the positive x_p direction become :

$$v = \sum_{m=1}^{5} V_m \exp(-j k_m x_p + j\omega t), \tag{A2.12}$$

$$w = \sum_{m=1}^{5} W_m \exp(-j k_m x_p + j\omega t), \tag{A2.13}$$

$$\theta_x = \sum_{m=1}^{5} \Theta_{xm} \exp(-j k_m x_p + j\omega t), \tag{A2.14}$$

$$\theta_y = \sum_{m=1}^{5} \Theta_{ym} \exp(-j k_m x_p + j\omega t), \tag{A2.15}$$

$$\theta_z = \sum_{m=1}^{5} \Theta_{zm} \exp(-j k_m x_p + j\omega t). \tag{A2.16}$$

By substituting each of the roots back into equations (A2.1) - (A2.5), the amplitude ratios V/Θ_x, W/Θ_x, Θ_y/Θ_x and Θ_z/Θ_x can be obtained. Hence the equations for coupled bending and torsional beam displacements may be expressed in terms of five unknowns $\Theta_{x1}.....\Theta_{x5}$.

The longitudinal vibration mode is not coupled to the bending-torsional mode and may be expressed in terms of the longitudinal wave amplitude U and wave number k_L as :

$$u = U \exp(-j k_L x_p + j\omega t). \tag{A2.17}$$

Equations (A2.12) - (A2.17) show that there are six unknown wave amplitudes for a beam element. These equations fully describe the transmitted or reflected waves in a beam element of a junction. The source beam carries the incident and reflected waves while the receiving

beams carry the transmitted waves. To calculate the transmission efficiency, the incident component may be regarded as a wave of unit amplitude in either longitudinal or a predominantly bending or torsional mode. The unknown reflected and transmitted wave amplitudes may be solved by the boundary conditions of the junction.

A2.2 Boundary conditions

The subscript i is used to denote the beam number. Figure A2.2 shows the orientation of an arbitrary receiving beam (beam i) with respect to the source beam (beam 1). Two position angles ξ_i (measured on the x_{r1} - y_{r1} plane) and ψ_i (measured on the x_{ri} - z_{r1} plane) are used to define the orientation of the beams with respect to their reference co-ordinates. The beams are assumed to be rigidly connected at a common attachment point P. The displacements shown in Figure A2.1 (u, v, w, θ_x, θ_y, and θ_z) are referred to as the local beam displacements while Figure A2.3 shows the reference beam displacements about the attachment point.

From Figure A2.1, the local displacements for each beam may be resolved about the respective reference beam axes x_{ri}, y_{ri}, z_{ri} and expressed as a component of the reference values as follows :

$$\mathbf{d'}_i = \mathbf{C}_i\,\mathbf{d}_i + \mathbf{E}_i\,\mathbf{r}_i, \quad \mathbf{r'}_i = \mathbf{C}_i\,\mathbf{r}_i\,, \tag{A2.18, A2.19}$$

where $\mathbf{d}_i = (u_i, v_i, w_i)^T$, $\mathbf{r}_i = (\theta_{xi}, \theta_{yi}, \theta_{zi})^T$; $\mathbf{d'}_i$, $\mathbf{r'}_i$ are the respective reference values and

$$\mathbf{C}_i = \begin{bmatrix} 1, & 0, & 0 \\ 0, & \cos\beta_i, & -\sin\beta_i \\ 0, & \sin\beta_i, & \cos\beta_i \end{bmatrix}, \qquad \mathbf{E}_i = \begin{bmatrix} 0, & -(b_i+e_i), & (g_i+d_i) \\ e_i\cos\beta_i + d_i\sin\beta_i\,, & 0, & 0 \\ -d_i\cos\beta_i + e_i\sin\beta_i\,, & 0, & 0 \end{bmatrix}.$$

The symbol β_i denotes the angle between the reference axes and principal axes of beam i; b_i, g_i are the offset between the centroid and the shear centre measured along the z_p and y_p axes

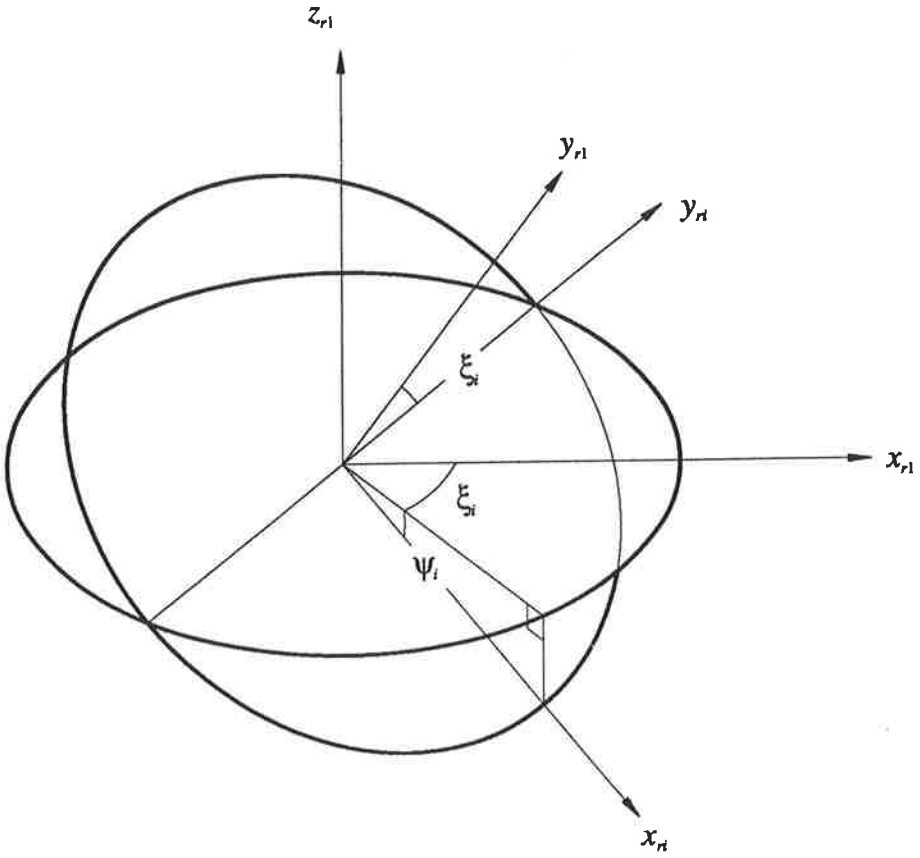

Figure A2.2 Co-ordinate system showing beam orientations.

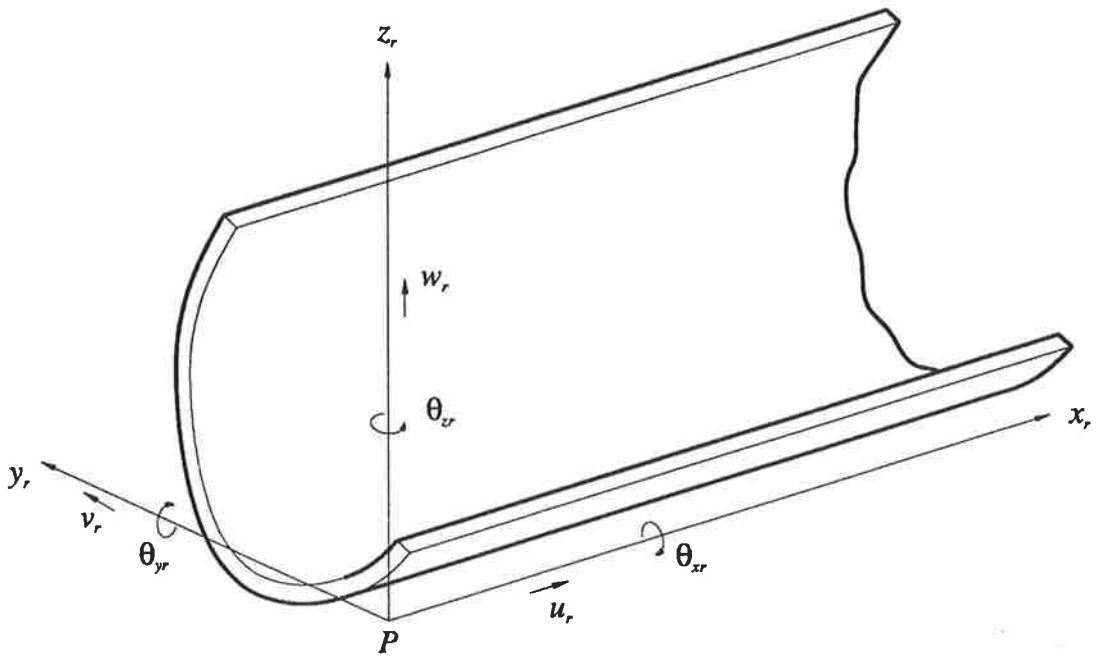

Figure A2.3 Reference displacements of beam.

of beam i respectively and e_i, d_i are the offset between the shear centre and the attachment point measured along the z_p and y_p axes of beam i respectively.

By considering the beam co-ordinates and displacements as shown in Figures A2.2 and A2.3, the compatibility requirements in terms of the reference displacements between beam i and beam 1 may be obtained :

$$\mathbf{d'}_1 = \mathbf{G}_i \mathbf{d'}_i, \quad \mathbf{r'}_1 = \mathbf{G}_i \mathbf{r'}_i, \tag{A2.20, A2.21}$$

$$\text{where } \mathbf{G}_i = \begin{bmatrix} \cos\psi_i \cos\xi_i, & \sin\xi_i, & \sin\psi_i \cos\xi_i \\ -\cos\psi_i \sin\xi_i, & \cos\xi_i, & -\sin\psi_i \sin\xi_i \\ -\sin\psi_i, & 0, & \cos\psi_i \end{bmatrix}.$$

Substituting equations (A2.18) into (A2.20) and (A2.19) into (A2.21) gives :

$$\mathbf{C}_1 \mathbf{d}_1 + \mathbf{E}_1 \mathbf{r}_1 = \mathbf{G}_i \{\mathbf{C}_i \mathbf{d}_i + \mathbf{E}_i \mathbf{r}_i\}, \qquad \mathbf{C}_1 \mathbf{r}_1 = \mathbf{G}_i \mathbf{C}_i \mathbf{r}_i. \tag{A2.22, A2.23}$$

Equations (A2.22, A22.23) represent the compatibility requirements for a general three-dimensional beam junction. The next step is to consider the equilibrium requirements. Figure A2.4 shows the junction forces and moments of a beam. It can be shown that these forces and moments are related to the local beam displacements by the following expressions:

$$F_{xi} = -E_i A_i \partial u_i/\partial x_p, \quad F_{yi} = -G A K_y (\partial v/\partial x_p - \theta_z), \quad F_{zi} = -G A K_z (\partial w/\partial x_p + \theta_y),$$

$$M_{xi} = -G_i J_i \partial\theta_{xi}/\partial x_p, \quad M_{yi} = -E_i I_{yi} \partial\theta_y,/\partial x_p, \quad M_{zi} = -E_i I_{zi} \partial\theta_z./\partial x_p. \tag{A2.24 - A2.29}$$

By summing the forces and moments at a junction with respect to the reference co-ordinates of beam 1, one obtains the equilibrium equations :

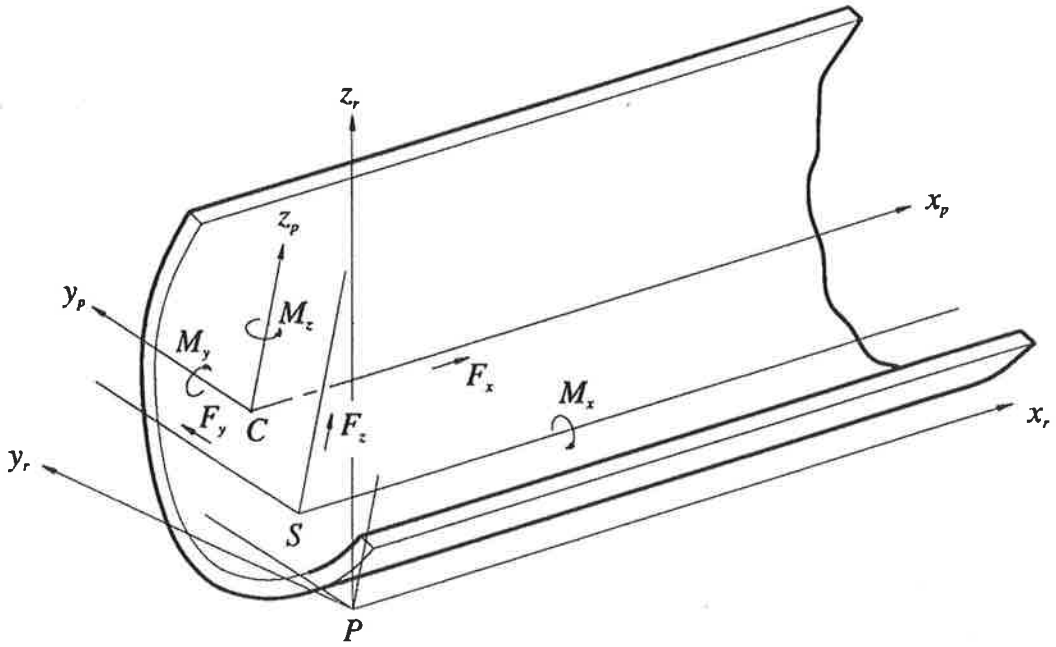

Figure A2.4 Junction forces and moments of a beam element.

$$-\mathbf{C}_1\,\mathbf{P}_1 + \sum_{i=2}^{K} \mathbf{G}_i\,\mathbf{C}_i\,\mathbf{P}_i = 0, \quad -\mathbf{C}_1\,\mathbf{Q}_1 - \mathbf{D}_1\,\mathbf{P}_1 + \sum_{i=2}^{K} \mathbf{G}_i\,\{\mathbf{C}_i\,\mathbf{Q}_i + \mathbf{D}_i\,\mathbf{P}_i\} = 0, \qquad \text{(A2.30, A2.31)}$$

where $\mathbf{P}_i = (\,F_{xi},\, F_{yi},\, F_{zi}\,)^{\mathrm{T}}$, $\mathbf{Q}_i = (M_{xi},\, M_{yi},\, M_{zi}\,)^{\mathrm{T}}$, K is the number of beams in a junction and

$$\mathbf{D}_i = \begin{bmatrix} 0, & -e_i, & d_i \\ (b_i + e_i)\cos\beta_i + (g_i + d_i)\sin\beta_i\,, & 0, & 0 \\ -(g_i + d_i)\cos\beta_i + (b_i + e_i)\sin\beta_i\,, & 0, & 0 \end{bmatrix}.$$

Equations (A2.22), (A2.23), (A2.30) and (A2.31) represent the boundary conditions for a three-dimensional beam junction. Solution of these equations will lead to the complex wave amplitudes of the beam elements, ie., U and Θ_{x1}.... Θ_{x5}.

APPENDIX 3

Evaluation of Wave Amplitudes for Cylinder/plate Junctions

A3.1 Expressions for shell displacements

The motion of a thin cylindrical shell u, v and w in the axial, circumferential and radial directions respectively (see Figure 2.5 for cylinder co-ordinates) may be described by the Donnell-Mushtari equation:

$$\mathbf{L} \begin{bmatrix} u \\ v \\ w \end{bmatrix} = 0, \qquad \text{(A3.1)}$$

where **L** is a matrix differential operator with matrix elements given by:

$$L_{11} = \partial^2/\partial x^2 + [(1-\mu)/2a^2]\partial^2/\partial\theta^2 - [\rho(1-\mu^2)/E]\partial^2/\partial t^2, \qquad L_{12} = [(1+\mu)/2a]\partial^2/\partial x\partial\theta,$$

$$L_{13} = (\mu/a)\partial/\partial x, \quad L_{21} = [(1+\mu)/2a]\partial^2/\partial x\partial\theta,$$

$$L_{22} = [(1-\mu)/2]\partial^2/\partial x^2 + (1/a^2)\partial^2/\partial\theta^2 - [\rho(1-\mu^2)/E]\partial^2/\partial t^2, \quad L_{23} = (1/a^2)\partial/\partial\theta,$$

$$L_{31} = (\mu/a)\partial/\partial x, \quad L_{32} = (1/a^2)\partial/\partial\theta,$$

$$L_{33} = 1/a^2 + (h^2/12a^4)[a^2\partial^2/\partial x^2 + \partial^2/\partial\theta^2]^2 + [\rho(1-\mu^2)/E]\partial^2/\partial t^2 .$$

The symbols h, a, E, ρ and μ denote the thickness, mean radius, elastic modulus, density and Poisson's ratio of the cylindrical shell respectively.

Equation (A3.1) is satisfied by solutions of the form:

$$u = U \cos(n\theta) \exp(-j k x + j \omega t), \tag{A3.2}$$

$$v = V \sin(n\theta) \exp(-j k x + j \omega t), \tag{A3.3}$$

$$w = W \cos(n\theta) \exp(-j k x + j \omega t). \tag{A3.4}$$

By substituting the solutions into equation (A3.1), one obtains three linear equations in terms of the displacement amplitudes U, V and W. For a non-trivial solution, the determinant of the coefficient matrix must be zero. The expanded determinant leads to a fourth order dispersion equation in k_n^2 for a particular circumferential mode number n. Solution of the dispersion equation results in eight roots, of which four represent the axial wave numbers for one direction of wave propagation. These roots may be expressed in terms of their real and imaginary parts and the conditions for waves travelling in the positive x direction are:

$$k_{mn} = \chi_{mn} + j \zeta_{mn} \quad \begin{cases} \zeta_{mn} = 0, \quad \chi_{mn} > 0, \\ \zeta_{mn} < 0, \end{cases} \tag{A3.5}$$

where m = 1, 2, 3, 4 and n = 0, 1, 2...∞. The general solutions for one direction of wave propagation may then be expressed as:

$$u = \sum_{m=1}^{4} \sum_{n=0}^{\infty} U_{mn} \cos(n\theta) \exp(-j k_{mn} x + j \omega t), \tag{A3.6}$$

$$v = \sum_{m=1}^{4} \sum_{n=0}^{\infty} V_{mn} \sin(n\theta) \exp(-j k_{mn} x + j \omega t), \tag{A3.7}$$

$$w = \sum_{m=1}^{4} \sum_{n=0}^{\infty} W_{mn} \cos(n\theta) \exp(-j k_{mn} x + j \omega t). \tag{A3.8}$$

By substituting each of the roots back into equation (A3.1), one can obtain the amplitude ratios U_{mn}/W_{mn} and V_{mn}/W_{mn} and the general solutions for wave motion in a cylindrical shell may be expressed in term of four unknown wave amplitudes W_{1n} ..... W_{4n}.

A3.2 Expressions for plate displacements in polar co-ordinates

The displacements of a plate in polar co-ordinates u_p, v_p and w_p are shown in Figure A3.1. Since the bending and in-plane motions of a plate are uncoupled, the equations that govern these two types of motion can be treated separately. Neglecting the effects of shear deformation and rotary inertia, the bending equation of motion for a thin plate in polar co-ordinates is given by :

$$\nabla^4 w_p - (\rho_p \omega^2 h_p / D_p) w_p = 0, \tag{A3.9}$$

where w_p is the out-of-plane plate displacement, $\nabla^4 = \{\partial^2/\partial r^2 + (1/r)\,\partial/\partial r + (1/r^2)\partial^2/\partial\theta^2\}^2$, $D_p = E_p h_p^3 / 12(1-\mu_p^2)$ and the subscript p denotes a plate element.

The general solution of the bending equation for an annular plate in terms of unknown constants A_{1n}, A_{2n}, A_{3n}, A_{4n} is :

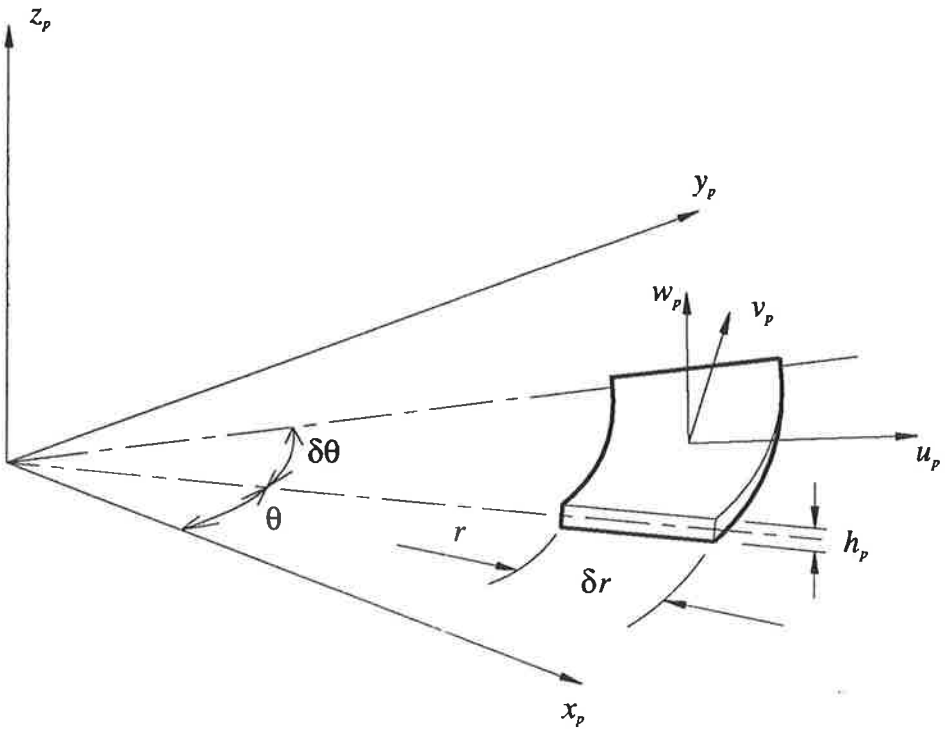

Figure A3.1 Polar co-ordinate system of a plate element.

$$w_p = \sum_{n=0}^{\infty} \{A_{1n} J_n(k_{pB} r) + A_{2n} Y_n(k_{pB} r) + A_{3n} I_n(k_{pB} r) + A_{4n} K_n(k_{pB} r)\} \cos(n\theta) \exp(j\omega t), \quad \text{(A3.10)}$$

where the plate bending wave number $k_{pB} = (\rho_p \omega^2 h_p / D_p)^{1/4}$. J_n, Y_n are Bessel functions of the first and second kind respectively and I_n, K_n are the modified Bessel functions of the first and second kind respectively. The subscript n indicates that the Bessel functions are of order n, and for a circular plate, $A_{2n} = A_{4n} = 0$. The circumferential mode number of the plate must be the same as that of the cylinder in a cylinder/plate junction since their trace velocities along the junction must be the same.

The equations of motion for in-plane waves in a plate are given by :

$$\partial/\partial r \{\partial u_p/\partial r + u_p/r + (1/r)\, \partial v_p/\partial\theta\} - \{(1-\mu_p)/2r\}\, \partial/\partial\theta \{\partial v_p/\partial r + v_p/r - (1/r)\, \partial u_p/\partial\theta\}$$

$$= \{\rho_p(1-\mu_p^2)/E_p\}\, \partial^2 u_p/\partial t^2 , \quad \text{(A3.11)}$$

$$(1/r)\partial/\partial\theta \{\partial u_p/\partial r + u_p/r + (1/r)\, \partial v_p/\partial\theta\} + \{(1-\mu_p)/2\}\, \partial/\partial r \{\partial v_p/\partial r + v_p/r - (1/r)\, \partial u_p/\partial\theta\}$$

$$= \{\rho_p(1-\mu_p^2)/E_p\}\, \partial^2 v_p/\partial t^2 . \quad \text{(A3.12)}$$

where u_p and v_p are the plate displacements in the r and θ directions respectively. The in-plane wave equations may be reduced to functions of one independent variable in a similar manner as that of the wave equations in cartesian co-ordinates (see Appendix 3.1) by using the following substitutions:

$$\varphi = \partial u_p/\partial r + u_p/r + (1/r)\, \partial v_p/\partial\theta, \quad \text{(A3.13)}$$

$$2\varpi = \partial v_p/\partial r + v_p/r - (1/r)\,\partial u_p/\partial\theta\,. \tag{A3.14}$$

With these substitutions, the equations of motion then become :

$$\nabla^2\varphi = \{\rho_p(1-\mu_p^2)/E_p\}\,\partial^2\varphi/\partial t^2\,, \tag{A3.15}$$

$$\nabla^2\varpi = \{2\rho_p(1+\mu_p)/E_p\}\,\partial^2\varpi/\partial t^2\,. \tag{A3.16}$$

For an annular plate, the solutions for equations (A3.15) and (A3.16) have the form :

$$\varphi = \{B'_{1n}\,J_n(k_{pL}r) + B'_{2n}\,Y_n(k_{pL}r)\}\cos(n\theta)\exp(j\omega t)\,, \tag{A3.17}$$

$$\varpi = \{B'_{3n}\,J_n(k_{pT}r) + B'_{4n}\,Y_n(k_{pT}r)\}\sin(n\theta)\exp(j\omega t)\,, \tag{A3.18}$$

where $k_{pL} = \omega\sqrt{\{\rho_p(1-\mu_p^2)/E_p\}}$, $k_{pT} = \omega\sqrt{\{2\rho_p(1+\mu_p)/E_p\}}$, and B'_{1n}, B'_{2n}, B'_{3n}, B'_{4n} are unknown constants.

It can easily be verified (by using equations (A3.13), (A3.14), (A3.17) and (A3.18)) that the general solutions for in-plane motion of an annular plate are :

$$u_p = \sum_{n=0}^{\infty}\{B_{1n}\,dJ_n(k_{pL}r)/dr + n\,B_{2n}\,J_n(k_{pT}r)/r + B_{3n}\,dY_n(k_{pL}r)/dr + n\,B_{4n}\,Y_n(k_{pT}r)/r\}\times \cos(n\theta)\exp(j\omega t)\,, \tag{A3.19}$$

$$v_p = \sum_{n=0}^{\infty} -\{n\,B_{1n}\,J_n(k_{pL}r)/r + B_{2n}\,dJ_n(k_{pT}r)/dr + n\,B_{3n}\,Y_n(k_{pL}r)/r + B_{4n}\,dY_n(k_{pT}r)/dr\}\times \sin(n\theta)\exp(j\omega t)\,, \tag{A3.20}$$

where $B'_{1n} = -B_{1n} k_{pL}^2$, $B'_{2n} = B_{2n} k_{pT}^2$, $B'_{3n} = -B_{3n} k_{pL}^2$ and $B'_{4n} = B_{4n} k_{pT}^2$.

For a circular plate, $B_{3n} = B_{4n} = 0$. The solutions for bending and in-plane motions of an infinite plate with a circular hole of radius a may be obtained more conveniently by using the Hankel functions. Upon noting that the waves must propagate outward from the junction, the following solution for the out-of-plane displacement may be obtained :

$$w_p = \sum_{n=0}^{\infty} \{A_{5n} H_n^{(2)}(k_{pB} r) + A_{6n} H_n^{(2)}(-j\, k_{pB} r)\} \cos(n\theta) \exp(j\omega t) \quad \text{for} \quad r \geq a. \qquad \text{(A3.21)}$$

Here $H_n^{(2)}$ is the Hankel function of the second kind of order n.

The solution for in-plane motion of an infinite plate may be obtained by replacing the Bessel functions J_n in equations (A3.19) and (A3.20) with the Hankel functions and putting $B_{3n} = B_{4n} = 0$:

$$u_p = \sum_{n=0}^{\infty} \{B_{5n} dH_n^{(2)}(k_{pL} r)/dr + n B_{6n} H_n^{(2)}(k_{pT} r)/r\} \cos(n\theta) \exp(j\omega t) \quad \text{for} \quad r \geq a, \qquad \text{(A3.22)}$$

$$v_p = \sum_{n=0}^{\infty} -\{n B_{5n} H_n^{(2)}(k_{pL} r)/r + B_{6n} dH_n^{(2)}(k_{pT} r)/dr\} \sin(n\theta) \exp(j\omega t) \quad \text{for} \quad r \geq a. \qquad \text{(A3.23)}$$

The preceding analysis expresses the wave motion of a cylinder as well as annular and infinite plates in terms of wave amplitudes (W_{1n}....W_{4n} for a semi-infinite cylinder, A_{1n}....A_{4n} and B_{1n}....B_{4n} for a finite annular plate and A_{5n}, A_{6n}, B_{5n}, B_{6n} for an infinite plate). Depending on the types of cylinder/plate coupled structure, the wave amplitude expressions for a finite annular plate and/or an infinite plate may be used in conjunction with a semi-infinite cylinder

to study the wave propagation characteristics of the junction. For example, consider an annular plate coupled to the inside of two semi-infinite cylinders as shown in Figure A3.2. The wave motion is described by equations (A3.6) - (A3.8) for the cylinders and equations (A3.10), (A3.19) and (A3.20) for the plate, giving a total of sixteen unknown wave amplitudes (four for each cylinder and eight for the annular plate). The wave amplitudes may be determined by consideration of the appropriate boundary conditions at the junction.

A3.3 Boundary conditions

The types of junction to be studied consist of semi-infinite cylinders rigidly coupled to various types of plate element. As an example, consider a semi-infinite cylinder with the outside edge coupled perpendicularly to the inside edge of an infinite annular plate. Compatibility of cylinder and plate displacements at the junction requires:

$$u = -w_p\,,\quad v = v_p\,,\quad w = u_p\,,\quad \phi = \phi_p\,, \qquad \text{(A3.24) - (A3.27)}$$

where the cylinder and plate displacements are given by equations (A3.6) - (A3.8) and (A3.21) - (A3.23) respectively and $\phi = \partial w/\partial x$, $\phi_p = \partial w_p/\partial r$.

Consider now the equilibrium of forces and moments at the junction. The direction of the junction forces and moments are shown in Figure A3.3. For a cylindrical shell, the junction forces and moment per unit length of circumference are given by:

$$F_x = \{-E\,h\,/(1-\mu^2)\}\{\partial u/\partial x + (\mu/a)\,(\partial v/\partial\theta + w)\}, \qquad \text{(A3.28)}$$

$$F_y = \{-E\,h\,/2(1+\mu)\}\{\partial u/a\partial\theta + \partial v/\partial x - (h^2/6a^2)\,\partial^2 w/\partial x\partial\theta\}, \qquad \text{(A3.29)}$$

$$F_z = \{E\,h^3/12(1-\mu^2)\}\{\partial^3 w/\partial x^3 + [(2-\mu)/a^2]\,\partial^3 w/\partial x\partial\theta^2\}, \qquad \text{(A3.30)}$$

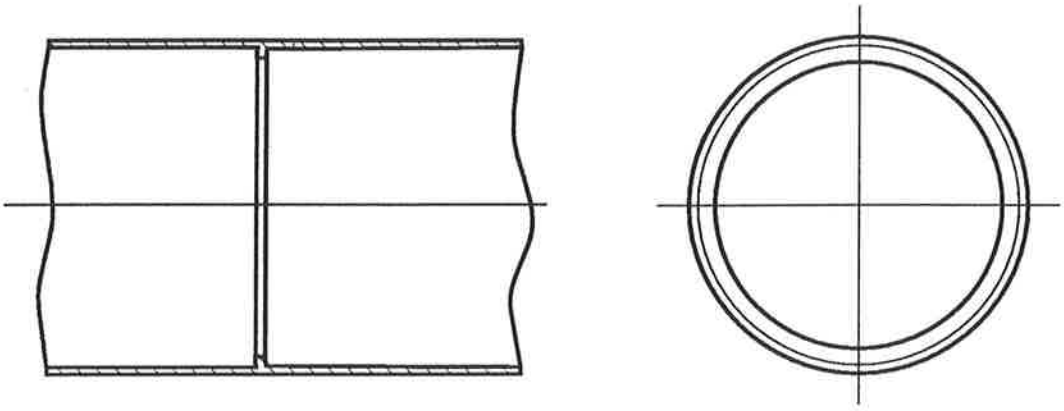

Figure A3.2 Cylinder / annular plate junction.

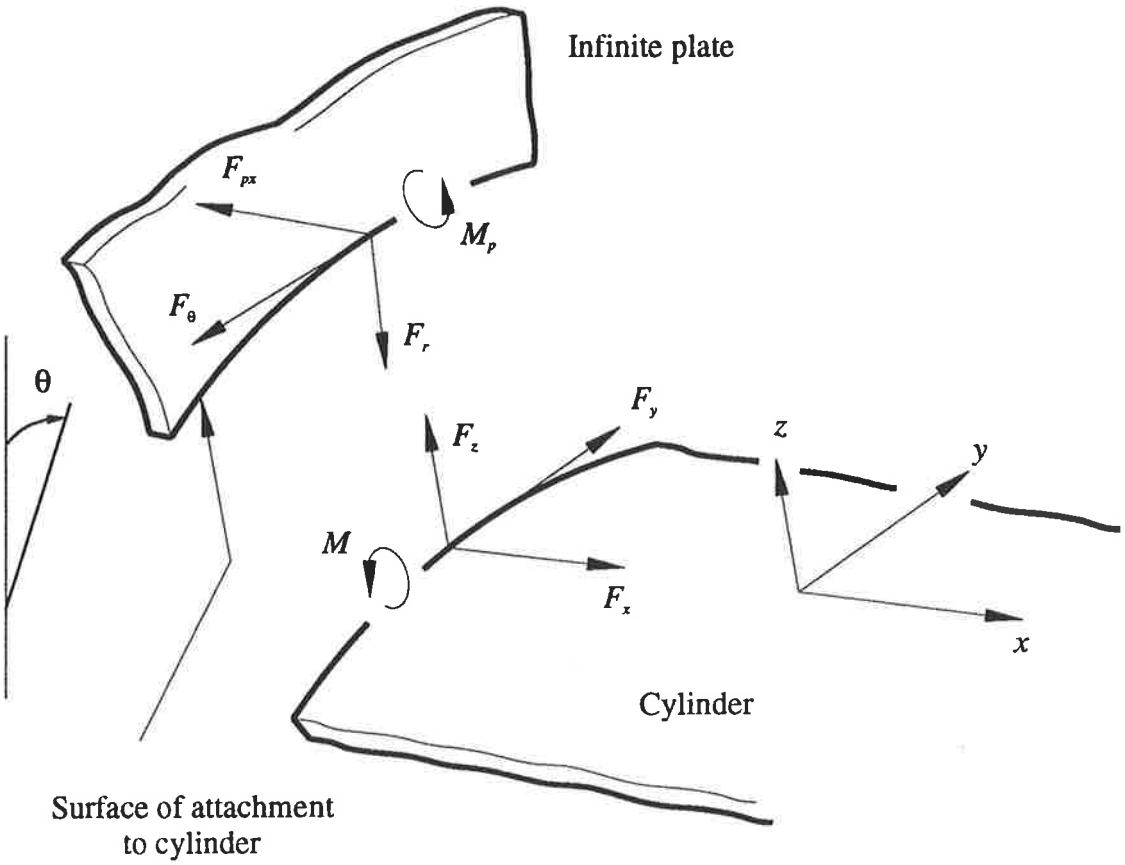

Figure A3.3 Junction forces and moments of a cylinder coupled to an infinite plate.

$$M = \{-E\,h^3/12(1-\mu^2)\}\{\partial^2 w/\partial x^2 + (\mu/a^2)\,\partial^2 w/\partial\theta^2\}, \tag{A3.31}$$

and for a plate element in polar co-ordinates:

$$F_{px} = D_p\,\{\partial^3 w_p/\partial r^3 + (1/a)\,\partial^2 w_p/\partial r^2 + [(2-\mu_p)/a^2]\,\partial^3 w_p/\partial r\partial\theta^2 - (1/a^2)\,\partial w_p/\partial r - [(3-\mu_p)/a^3]\partial^2 w_p/\partial\theta^2\}, \tag{A3.32}$$

$$F_r = \{E_p\,h_p / (1-\mu_p^2)\}\{\partial u_p/\partial r + (\mu_p/a)\,(u_p + \partial v_p/\partial\theta)\}, \tag{A3.33}$$

$$F_\theta = \{E_p\,h_p /2\,a(1+\mu_p)\}\{\partial u_p/\partial\theta + a\,\partial v_p/\partial r - v_p\}, \tag{A3.34}$$

$$M_p = -D_p\,\{\partial^2 w_p/\partial r^2 + (\mu_p/a^2)(a\partial w_p/\partial r + \partial^2 w_p/\partial\theta^2)\}. \tag{A3.35}$$

The equilibrium requirements lead to:

$$F_x = F_{px},\ F_y = F_\theta,\ F_z = F_r,\ M = -M_p, \tag{A3.36) - (A3.39}$$

These boundary conditions enable a solution to be obtained for the wave amplitudes $W_{1n}....W_{4n}$ and A_{5n}, A_{6n}, B_{5n}, B_{6n} for a given circumferential mode number and incident propagating wave in the cylinder.

APPENDIX 4

Evaluation of Wave Powers in Cylinder/plate Junctions

The cylinder wave power consists of components due to bending, longitudinal and torsional motions. Each of these components may be expressed in the following form :

$$\Pi_B = \tfrac{1}{2} \int_0^{2\pi} \mathrm{Re}\,\{M\dot{\phi}^* + F_z \dot{w}^*\} a \, d\theta \,, \tag{A4.1}$$

$$\Pi_L = \tfrac{1}{2} \int_0^{2\pi} \mathrm{Re}\,\{F_x \dot{u}^*\} a \, d\theta \,, \tag{A4.2}$$

$$\Pi_T = \tfrac{1}{2} \int_0^{2\pi} \mathrm{Re}\,\{F_y \dot{v}^*\} a \, d\theta \,, \tag{A4.3}$$

where $\dot{}$ denotes the time derivative, * denotes the complex conjugate, a is the mean cylinder radius, θ is the polar co-ordinate of the cylinder and $\phi = \partial w/\partial x$. The cylinder forces and moment F_x, F_y, F_z, M, and the cylinder displacements u, v and w, are shown in Figures (2.5) and (A3.3) respectively. Note that the second term on the right hand side of equation (A4.1) consists of the wave power due to shearing and twisting of the cylinder since F_z is made up of components due to the transverse shear force and twisting moment in the cylinder. Substituting the expressions for cylinder forces and moment (equations (A3.28) - (A3.31)) together with the expressions for cylinder displacements (equations (A3.6) - (A3.8)) into equations (A4.1) - (A4.3) leads to:

$$\Pi_B = \{\pi E h^3 \omega/[12a^2(1 - \mu^2)]\}\{(k_{mn}\, a)^3 \,|\, W_{mn} \,|^2 + n^2 k_{mn}\, a \,|\, W_{mn} \,|^2\} \quad \text{for } n \neq 0,$$

$$= \{\pi E h^3 \omega/[6a^2(1 - \mu^2)]\}(k_{mo}\, a)^3 \,|\, W_{mo} \,|^2 \quad \text{for } n = 0, \tag{A4.4}$$

$$\Pi_L = \{\pi E h\omega/[2(1-\mu^2)]\}\{k_{mn}\, a\,|U_{mn}|^2 + n\mu\,|U_{mn}|\,|V_{mn}| + \mu\,|W_{mn}|\,|U_{mn}|\} \quad \text{for } n \neq 0,$$

$$= \{\pi E h\omega/(1-\mu^2)\}\{k_{mo}\, a\,|U_{mo}|^2 + \mu\,|W_{mo}|\,|U_{mo}|\} \quad \text{for } n = 0, \qquad \text{(A4.5)}$$

$$\Pi_T = \{\pi E h\omega/[4(1+\mu)]\}\{k_{mn}\, a\,|V_{mn}|^2 + n\,|U_{mn}|\,|V_{mn}| + (n\, k_{mn}\, h^2/6a)\,|W_{mn}|\,|V_{mn}|\}$$

$$\text{for } n \neq 0,$$

$$= 0 \quad \text{for } n = 0, \qquad \text{(A4.6)}$$

where m denotes the travelling wave in the cylinder, n is the circumferential mode number, k_{mn} is the axial wave number of the cylinder; E, ρ, μ and h are the elastic modulus, density, Poisson's ratio and thickness of the cylinder respectively and U_{mn}, V_{mn} and W_{mn} are the complex wave amplitudes. Depending on the frequency of interest and the cut-on frequency of the Type I, II and III waves (see Section 2.4 of Chapter 2 for a discussion of the types of waves in a cylinder), there may be up to three waves propagating simultaneously in the cylinder. The total wave power is the sum of each of the propagating waves.

For an infinite plate, the bending, extensional and shear wave powers that propagate outward from the cylinder may be obtained by integrating the expressions for power per unit length over an arbitrary circle of radius r ($r > a$). The derivation for wave power can be considerably simplified by using the asymptotic approximation of the Hankel function:

$$H_n^{(2)}(k\,r) \approx \sqrt{[2/\pi k\, r]}\, \exp(-j\, k\, r + j\, \pi/4 + j\, n\pi/2), \qquad \text{(A4.7)}$$

$$\text{for } k\,r >> 1 \text{ and } k\,r >> n^2,$$

Following a derivation procedure similar to that of a cylinder, the wave powers of an infinite plate are given by:

$$\Pi_{pB} = \{E_p h_p^3 \omega/6(1-\mu_p^2)\}\{k_{pB}|A_{5n}|\}^2 \quad \text{for } n \neq 0,$$

$$= \{E_p h_p^3 \omega/3(1-\mu_p^2)\}\{k_{pB}|A_{50}|\}^2 \quad \text{for } n = 0, \tag{A4.8}$$

$$\Pi_{pL} = \{E_p h_p \omega/(1-\mu_p^2)\}\{k_{pL}|B_{5n}|\}^2 \quad \text{for } n \neq 0,$$

$$= 2\{E_p h_p \omega/(1-\mu_p^2)\}\{k_{pL}|B_{50}|\}^2 \quad \text{for } n = 0, \tag{A4.9}$$

$$\Pi_{pT} = \{E_p h_p \omega/2(1+\mu_p)\}\{k_{pT}|B_{6n}|\}^2 \quad \text{for } n \neq 0,$$

$$= 0 \quad \text{for } n = 0, \tag{A4.10}$$

where A_{5n}, B_{5n} and B_{6n} represent the complex wave amplitudes and the subscript p denotes a plate element.

APPENDIX 5

Wave Transmission Analysis of a Plate with Periodic Stiffeners

For a plate with periodic stiffeners of infinite extent as shown in Figure 3.1, the out-of-plane displacement of the plate at an arbitrary bay i is given by:

$$w(x_i) = \exp(\lambda i) \{ \sum_{m=1}^{4} A_m \exp(k_{mx} x_i) \} \exp(k_y y + j\omega t), \qquad \text{(A5.1)}$$

where l is the stiffener spacing, i is the element or bay number ($i = 0, 1, 2, \ldots \infty$), $x_i = x - il$, λ is the propagating constant, k_{mx} is the root of the dispersion equation for plate bending and A_m is the wave amplitude. If the plate is subjected to an oblique bending wave of wave number k_B and wave angle γ, then k_{mx} and k_y may be expressed as (see Appendix 1 for a more detailed discussion of the wave numbers for an oblique wave):

$$k_{1x} = j\, k_B \cos\gamma, \quad k_{2x} = -j\, k_B \cos\gamma, \quad k_{3x} = k_B \sqrt{[1 + \sin^2\gamma]}, \quad k_{4x} = -k_B \sqrt{[1 + \sin^2\gamma]};$$

and $k_y = \pm j\, k_B \sin\gamma$.

Consider an arbitrary junction of the periodic structure as shown in Figure A5.1, the forces and displacements at the left hand side of element i are related to the corresponding forces and displacements of element $i + 1$ by the Bloch theorem as:

$$\exp(\lambda)\, w(x_i)|_{x_i = 0} = w(x_{i+1})|_{x_{i+1} = 0}, \qquad \text{(A5.2)}$$

$$\exp(\lambda)\, \phi(x_i)|_{x_i = 0} = \phi(x_{i+1})|_{x_{i+1} = 0}, \qquad \text{(A5.3)}$$

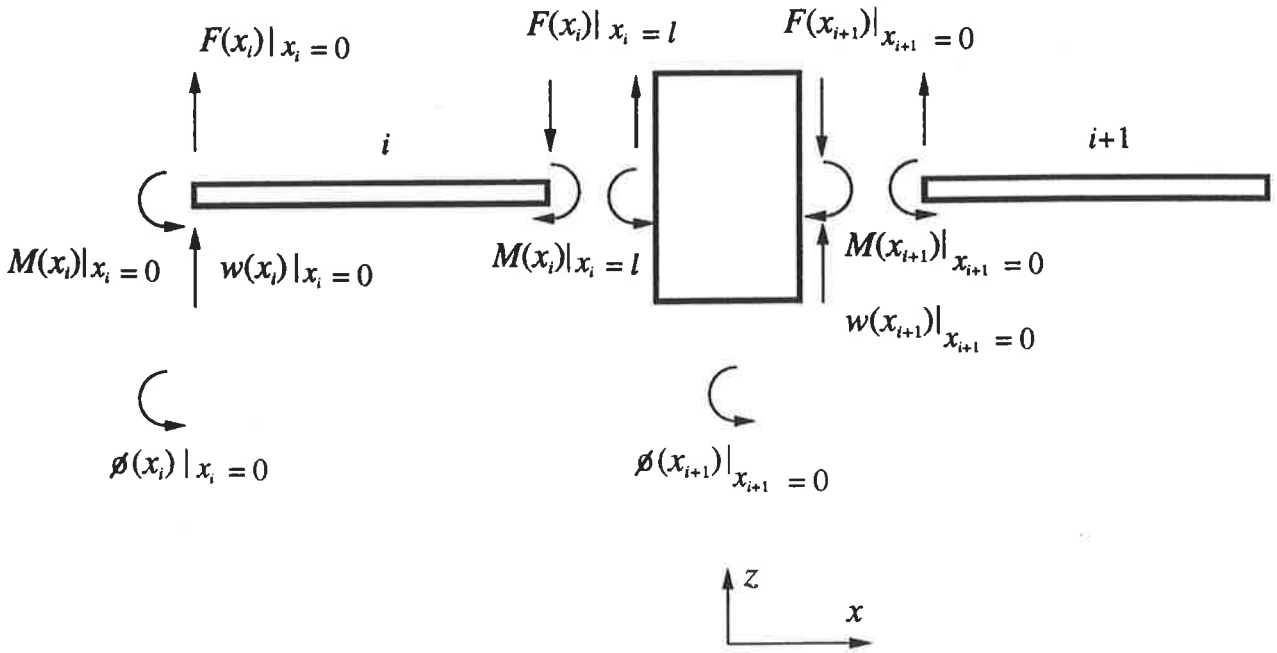

Figure A5.1 Forces and displacements at an arbitrary junction of a plate with periodic beam stiffeners.

$$\exp(\lambda)\, F(x_i)|_{x_i=0} = F(x_{i+1})|_{x_{i+1}=0}, \tag{A5.4}$$

$$\exp(\lambda)\, M(x_i)|_{x_i=0} = M(x_{i+1})|_{x_{i+1}=0}, \tag{A5.5}$$

where ϕ, F and M are the plate rotation, junction force and junction moment respectively (see equations (A1.18), (A1.22) and (A1.23) in Appendix 1 respectively for expressions of these quantities).

The quantities on the right hand side of equations (A5.2) - (A5.5) can be expressed in terms of element i by the compatibility and equilibrium requirements at the junction. Consider first the compatibility requirements:

$$w(x_{i+1})|_{x_{i+1}=0} = w(x_i)|_{x_i=l}, \tag{A5.6}$$

$$\phi(x_{i+1})|_{x_{i+1}=0} = \phi(x_i)|_{x_i=l}. \tag{A5.7}$$

The equilibrium of forces and moments at the junction must allow for the torsional, bending and inertia effects of the beam. As a result of beam bending in the y - z plane (see Figure 3.1), the plate force F is augmented by the shear force of the beam. Summation of forces in the z-direction gives:

$$F(x_i)|_{x_i=l} - F(x_{i+1})|_{x_{i+1}=0} - \partial F_b/\partial y = -\rho A\omega^2 w(x_i)|_{x_i=l}, \tag{A5.8}$$

where $\partial F_b/\partial y = EI_x\, \partial^4 w(x_i)/\partial y^4|_{x_i=l}$,

and ρ, A, E, I_x are the density, cross sectional area, elastic modulus and second moment of area of the beam respectively.

The variation in plate rotation in along the y - axis causes the beam to twist and results in a torsional moment. Consider the equilibrium of moment about a line parallel to the y - axis and passing through the beam centroid:

$$M(x_i)|_{x_i = l} - M(x_{i+1})|_{x_{i+1} = 0} - \partial M_b/\partial y = - I_c \omega^2 \phi(x_i)|_{x_i = l}, \tag{A5.9}$$

where $\partial M_b/\partial y = - GJ \, \partial^2\phi(x_i)/\partial y^2|_{x_i = l}$,

and G, J, I_c are the shear modulus, torsional constant and second moment of inertia per unit length of the beam respectively.

Eliminating the quantities that relate to element $i + 1$ from equations (A5.2) - (A5.9) and expressing $w(x_i)$, $\phi(x_i)$, $F(x_i)$ and $M(x_i)$ in terms of the wave amplitudes $A_1 ... A_4$:

$$\sum_{m=1}^{4} A_m \exp(k_m l) = \exp(\lambda) \sum_{m=1}^{4} A_m, \tag{A5.10}$$

$$\sum_{m=1}^{4} A_m k_m \exp(k_m l) = \exp(\lambda) \sum_{m=1}^{4} A_m k_m, \tag{A5.11}$$

$$\sum_{m=1}^{4} (k_m^2 - I_c \omega^2 k_m/D - GJ k_y^2 k_m/D + \mu k_y^2) A_m \exp(k_m l) = \exp(\lambda) \sum_{m=1}^{4} (k_m^2 + \mu k_y^2) A_m, \tag{A5.12}$$

$$\sum_{m=1}^{4} (k_m^3 + \rho A \omega^2/D - EI_x k_y^4/D + (2 - \mu) k_y^2 k_m) A_m \exp(k_m l) = \exp(\lambda) \sum_{m=1}^{4} (k_m^3 + (2 - \mu) k_y^2 k_m) A_m. \tag{A5.13}$$

where D and μ are respectively the flexural rigidity and Poisson's ratio of the plate elements. Equations (A5.10) - (A5.13) can be expressed in matrix form:

$$\Lambda\,[A_m] = \exp(\lambda)\,[A_m], \tag{5.14}$$

where Λ is a 4 × 4 matrix and $[A_m]$ is a column vector. Equation (A5.14) represents a standard eigenvalue problem. The four eigenvalues exist in two pairs, one of each pair being the reciprocal of the other, indicating propagation of waves in the positive and negative directions.

REFERENCES

Abramowitz, M. and Stegun, I. A., 1972. *Handbook of mathematical functions*. Dover.

Allwright, D. J., Blackmore, M., Brazier-Smith, P. B. and Woodhouse, J., 1994. Vibration transmission through symmetric resonant couplings. *Philosophical Transactions of the Royal Society of London, Series A*, **346**, 511-542.

Beranek, L. L., 1971. *Noise and Vibration Control*. McGraw-Hill.

Bies, D. A. and Hamid, S., 1980. *In-situ* determination of loss and coupling loss factors by the power injection method. *Journal of Sound and Vibration* **70**, 187-204.

Blakemore, M., Myers, R. J. M. and Woodhouse, J., 1992. The statistical energy analysis of a cylindrical structure. *Proceedings of the Second International Congress on Recent Developments in Air- and Structure-borne Sound and Vibration, Auburn University, U.S.A.*

Bolotin, V. V., 1984. *Random vibrations of elastic systems*. Martinus Nijhoff Publishers.

Brillouin, L., 1946. *Wave propagation in periodic structures*. New York: Dover.

Buiten, J., 1976. Experiments with structure-borne sound transmission in ships. *Proceedings of the.International Symposium on Shipboard Acoustics, Elsevier*.

Clarkson, B. L. and Pope, R. J., 1981. Experimental determination of modal densities and loss factors of flat plates and cylinders. *Journal of Sound and Vibration* 77, 535-549.

Clarkson, B. L. and Ranky, M. F., 1984. On the measurement of the coupling loss factor of structural connections. *Journal of Sound and Vibration* **94**, 249-261.

Conn, R. B., 1976. Acoustics and ship design. *Proceedings of the International Symposium on Shipboard Acoustics, Elsevier.*

Cowper, G. R., 1966. The shear coefficient in Timoshenko's beam theory. *Journal of Applied Mechanics* **33**, 335-340.

Craven, P. G. and Gibbs, B. M., 1981. Sound transmission and mode coupling at junctions of thin plates, part 1: representation of the problem. *Journal of Sound and Vibration* 77, 417-427.

Cremer, L., 1948. The propagation of structure-borne sound. *Department of Scientific and Industrial Research Report No.*1, *Series* B.

Cremer, L., Heckl, M. and Ungar, E. E., 1973 and 1988. *Structure-borne sound.* Berlin: Springer-Verlag.

Fahy, F. J., 1970. Energy flow between oscillators: special case of point excitation. *Journal of Sound and Vibration* **11**, 481-483.

Fahy, F. J., 1974. Statistical energy analysis - a critical review. *The Shock and Vibration Digest* **6**, 14-33.

Fahy, F. J. and Lindqvist, E., 1976. Wave propagation in damped, stiffened structures characteristic of ship constructions. *Journal of Sound and Vibration* **45**, 115-138.

Fahy, F. J. and Mohammed, A. D., 1992. A study of uncertainty in applications of SEA to coupled beam and plate systems, part 1: Computational experiments. *Journal of Sound and Vibration* **158**, 45-67.

Fahy, F. J., 1994. Statistical energy analysis: a critical overview. *Philosophical Transaction of the Royal Society of London, Series A*, **346**, 431-447.

Fukuzawa, K. and Yasuda, Ch., 1979. Studies on structure-borne sound in ship. *Proceedings, INTER-NOISE 79, Warszawa.*

Fuller, C. R., 1981. The effects of wall discontinuities on the propagation of flexural waves in cylindrical shells. *Journal of Sound and Vibration* **75**, 207-228.

Gibbs, B. M., and Tattersall, J. D., 1987. Vibration energy transmission and mode conversion at a corner junction of square section rods. *Journal of Vibration, Acoustic, Stress, and Reliability in Design*. **109**, 348-355.

Hansen, C. H. and Pope, L, D., 1982. Response of a cylindrical machine casing to oscillatory bearing forces. *Journal of Sound and Vibration*. **80**, 179-192.

Harari, A., 1977. Wave propagation in cylindrical shells with finite regions of structural discontinuity. *Journal of the Acoustical Society of America* **162**, 1196-1205.

Hart, F. D. and Shah, K, C., 1971. Compendium of modal densities for structures. *NASA CR-1773*.

Heckl, M., 1961. Wave propagation on beam-plate systems. *Journal of the Acoustical Society of America* **33**, 640-651.

Heckl, M., 1962. Vibration of point driven cylindrical shells. *Journal of the Acoustical Society of America* **34**, 1553-1557.

Heckl, M., 1964. Investigation on the vibrations of grillages and other simple beam structures. *Journal of the Acoustical Society of America* **36**, 1335-1343.

Herlufsen, H., 1984. Dual channel FFT analysers. *B & K Technical Review. Nos.* 1 & 2.

Hodges, C. H., Power, J. and Woodhouse, J., 1985a. The low frequency vibration of a ribbed cylinder, part 1: theory. *Journal of Sound and Vibration* **101**, 219-235.

Hodges, C. H., Power, J. and Woodhouse, J., 1985b. The low frequency vibration of a ribbed cylinder, part 2: observations and interpretation. *Journal of Sound and Vibration* **101**, 237-256.

Hodges, C. H. and Woodhouse, J., 1986. Theories of noise and vibration transmission in complex structures. *Reports on Progress in Physics* **49**, 107-170.

Horner, J. L. and White, R. G., 1991. Prediction of vibration power transmission through bends and joints in beam-like structures. *Journal of Sound and Vibration* **147**, 87-103.

Horner, J. L., 1993. Prediction of vibration power transmission in frameworks. *Proceedings of the 4th International Congress on Intensity Techniques, Senlis, France.*

Hsu, K. H., Nefske, D. J. and Akay, A., 1987. Statistical energy analysis. *NCA-Vol.3. The American Society of Mechanical Engineers.*

Hwang, Chintsun and Pi, W. S., 1973. Investigation of vibration energy transfer in connected structures. *NASA CR - 124456.*

Hynnä, P., Klinge, P and Vuoksinen, J., 1995. Prediction of structure-borne sound transmission in large welded ship structures using statistical energy analysis. *Journal of Sound and Vibration* **180**, 583-607.

Irie, Y. and Takagi, S., 1978. Structure-borne noise transmission in steel structures like a ship. *Proceedings, INTER-NOISE 78, San Fransisco.*

Janssen, J. H. and Buiten, J., 1973. On acoustic designing in naval architecture. *Proceedings, INTER-NOISE 73, Copenhagen.*

Keane, A. J., 1988. Statistical energy analysis of engineering structures. *Ph. D. thesis, Brunel University.*

Keane, A. J. and Price, W. G., 1989. Statistical energy analysis of periodic structures. *Proceedings of the Royal Society of London, Series A*, **423**, 332-360.

Keswick, P. R. and Norton, M. P., 1987. A comparison of modal density measurement technique. *Applied Acoustics* **20**, 137-153.

Lalor, N., 1989. The experimental determination of vibrational energy balance in complex structures. *Proceedings, SIRA Conference, Stress and Vibration: Recent Development in Industrial Measurement and Analysis, London, Paper No.* 108429.

Lalor, N. 1990. Practical Considerations for the measurement of internal and coupling loss factors on complex structures. *ISVR Technical Report No.* 182.

Langley, R. S., 1990. A derivation of the coupling loss factor used in statistical energy analysis. *Journal of Sound and Vibration* **141**, 207-219.

Langley, R. S. and Heron, K. H., 1990. Elastic wave transmission through plate/beam junctions. *Journal of Sound and Vibration* **143**, 241-253.

Langley, R. S., 1991. An elastic wave technique for the free vibration of plate assemblies. *Journal of Sound and Vibration* **145**, 261-277.

Langley, R. S., 1994a. Elastic wave transmission coefficients and coupling loss factors for structural junctions between curved panels. *Journal of Sound and Vibration* **169**, 297-317.

Langley, R. S., 1994b. On the modal density and energy flow characteristic of periodic structures. *Journal of Sound and Vibration* **172**, 491-511.

Langley, R. S., 1994c. On the forced response of one-dimensional periodic structures: vibration localization by damping. *Journal of Sound and Vibration* **178**, 411-428..

Langley, R. S., 1995. Wave transmission through one-dimensional near periodic structures: optimum and random disorder. *Journal of Sound and Vibration* **188**, 717-743.

Leissa, A. W., 1969. Vibration of plates. *NASA Special Report* 160.

Leissa, A. W., 1973. Vibration of shells. *NASA Special Report* 288.

Love, A. E. H., 1927 *A treatise on the mathematical theory of elasticity*. Cambridge University Press.

Lu, I. T., Bertoni, H. L. and Chen, H. Y., 1992. Coupling of plate waves at joints. *Journal of the Acoustical Society of America* **92**, 510-526.

Lyon R. H. and Eichler, E., 1964. Random vibration of connected structures. *Journal of the Acoustical Society of America* **36**, 1344-1354.

Lyon, R. H. and Scharton, T. D., 1965. Vibrational energy transmission in a three-element structure. *Journal of the Acoustical Society of America* **38**, 253-261.

Lyon, R. H., 1975. *Statistical energy analysis of dynamical systems: theory and applications.* MIT Press. Cambridge, Massachusetts.

Lyon, R. H., 1986. In-plane contribution to structural noise transmission. *Noise Control Engineering Journal* **26**, 22-27.

Lyon, R. H. and DeJong, R. G., 1995. *Theory and application of statistical energy analysis.* Butterworth-Heinemann.

McLachlan, N. W., 1955. *Bessel functions for engineers.* Oxford.

Mead, D. J., 1971. Vibration response and wave propagation in periodic structures. *Transactions of the American Society of Mechanical Engineers, Journal of Engineering for Industry* **93**, 783-792.

Mead, D. J. and Pujara, K. K., 1971. Space-harmonic analysis of periodically supported beams: response to convected random loading. *Journal of Sound and Vibration* **14**, 525-541.

Mead, D, J., 1973. A general theory of harmonic wave propagation in linear periodic systems with multiple coupling. *Journal of Sound and Vibration* **27**, 235-260.

Mead, D. J., 1975a. Wave propagation and natural modes in periodic systems: I. Mono-coupled systems. *Journal of Sound and Vibration* **40**, 1-18.

Mead, D. J., 1975b. Wave propagation and natural modes in periodic systems: I. Multi-coupled systems, with and without damping. *Journal of Sound and Vibration* **40**, 19-39.

Mead, D. J. and Parthan, S., 1979. Free wave propagation in two-dimensional periodic plates. *Journal of Sound and Vibration* **64**, 325-348.

Mead, D. J. and Bardell, N. S., 1986. Free vibration of a thin cylindrical shell with discrete axial stiffeners. *Journal of Sound and Vibration* **111**, 229-250.

Mead, D. J. and Bardell, N. S., 1987. Free vibration of a thin cylindrical shell with periodic circumferential stiffeners. *Journal of Sound and Vibration* **115**, 499-520.

Miller, D. K. and Hart, F. D., 1967. Modal density of thin circular cylinders. *NASA CR* - 897.

Moore, J. A., 1990a. Vibration transmission through frame or beam junctions. *Journal of the Acoustical Society of America* **88**, 2766-2776.

Moore, J. A., 1990b. Frame junction vibration transmission with a modified frame deformation model. *Journal of the Acoustical Society of America* **88**, 2777-2788.

Nilsson, A. C., 1976. Wave propagation in simple hull-frame structure of ships. *Journal of Sound and Vibration* **44**, 393-405.

Nilsson, A. C., 1977. Attenuation of structure-borne sound in superstructures on ships. *Journal of Sound and Vibration* **55**, 71-91.

Nilssen, A. C., 1978. Reduction of structure-borne sound in simple ship structures: results of model tests. *Journal of Sound and Vibration* **61**, 45-60.

Ødegaard Jensen, J., 1976. Calculation of structure-borne noise transmission in ships, using the statistical energy analysis approach. *Proceedings of the International Symposium on Shipboard Acoustics, Elsevier.*

Ødegaard Jensen, J., 1978. Calculation of structure-borne sound in plate structures by the application of 'Statistical Energy Analysis'. *Proceedings, NAM 78, Odense.*

Plunt, J., 1980a. Method for predicting noise levels in ships, part 1: noise level prediction methods for ships, based on empirical data. *Report* 80 - 06, *Chalmers University of Technology, Göteborg, Sweden.*

Plunt, J., 1980b. Method for predicting noise levels in ships, part 2: prediction of structure-borne sound transmission in complex structures with the SEA method. *Report* 80 - 07, *Chalmers University of Technology, Göteborg, Sweden.*

Pollard, J. S., 1992. Measurement of cylinder/plate coupling loss factors and associated problems. *Noise Control Engineering Journal* **39**, 109-117.

Ranky, M. F. and Clarkson, B. L., 1983. Frequency averaged loss factors of plates and shells. *Journal of Sound and Vibration* **89**, 309-323.

Sablik, M. J., 1982. Coupling loss factor at a beam L-joint revisited. *Journal of the Acoustical Society of America* **72**, 1285-1288.

Sablik, M. J., Beissner, R. E., Silvus, H. S. and Miller, M. L., 1985. Statistical energy analysis, structural resonances, and beam networks. *Journal of the Acoustical Society of America* **77**, 1038-1045.

Sawley, R. J., 1969. The evaluation of a shipboard noise and vibration problem using statistical energy analysis. *ASME Symposium on Stochastic Process in Dynamical Problems, Los Angeles.*

Schlesinger, A., 1995. Transmission of elastic waves from a cylinder to an attached flat plate. *Journal of Sound and Vibration* **186**, 761-780.

Smith, P. W., 1955. Phase velocities and displacement characteristics of free waves in a thin cylindrical shell. *Journal of the Acoustical Society of America* **27**, 1065-1072.

Swift, P. B., 1977. The vibrational energy transmission through connected structures. *Ph. D. thesis, University of Adelaide.*

Szechenyi, E., 1971. Modal densities and radiation efficiencies of unstiffened cylinders using statistical methods. *Journal of Sound and Vibration* **19**, 65-81.

Timoshenko, S., Young, D. H. and Weaver Jr., W., 1974. *Vibration problems in engineering.* John Wiley & Sons, Inc.

Thrane, N., 1984. The Hilbert Transform. *B & K Technical Review, No.* 3.

Tratch, J., 1985. Vibration transmission through machinery foundation and ship bottom structure. *M. S. thesis, Massachusetts Institute of Technology.*

Wöhle, W., Beckmann, Th. and Schreckenbach, H., 1981. Coupling loss factors for statistical energy analysis of sound transmission at rectangular structural slab joints, part 1. *Journal of Sound and Vibration* 77, 324-334.

LIST OF PUBLICATIONS ORIGINATED FROM THIS THESIS

Tso, Y., and Norwood, C., 1995. Vibratory power transmission through three-dimensional beam junctions. *Journal of Sound and Vibration* **185**, 595-607.

Tso, Y. and Hansen, C., 1995. Wave propagation through cylinder/plate junctions. *Journal of Sound and Vibration* **186**, 447-461.

Tso, Y. and Hansen, C., 1995. A investigation of the coupling loss factor for a cylinder/plate structure. *Accepted for publication in the Journal of Sound and Vibration.*

Tso, Y. and Hansen, C., 1996. The transmission of vibration through a coupled periodic structure. *Submitted to the Journal of Sound and Vibration.*